An Ab Initio Study Of The Origin Of p-type Doping In ZnO Using Group-V Elements

by Abdusalam Mohamed Saleh Gsiea

A thesis submitted to Newcastle University for the degree of Doctor of Philosophy. March 2011.

Dedicated to

My family and my parents those help me to came to finish my study.

Acknowledgements

First of all I would like to thank God for everything. There are many people I would like to thank for their help during my PhD study. First is Jon Goss for his regular guidance, motivation, understanding, assistance and for looking after me especially when going to the conferences. Patrick Briddon for his lectures, motivation and manful development of AIMPRO, and his wonderful smile just has made me more trust.

To my colleagues and friends in Newcastle University for regular discussion on all things physics, or other things.

Most especial thank to my family (my wife and son), and my parent for encouraging me to finish my study.

Abstract

Zinc oxide is a transparent semiconductor with a direct wide band-gap $3.4\,\text{eV}$ and large exciton binding-energy of 60 meV, that combine to make ZnO a promising material for possible applications such as optoelectronic devices, lasers and light emitting diodes. Recently, the difficulty in obtaining high quality p-type ZnO has attracted much attention.

Considerable effort has been made to obtain p-type ZnO by doping with the group-V elements N, P, As, and Sb, with the anticipation of replacing oxygen atoms in the ZnO lattice. However, experimentally these dopants can produce both p-type and n-type conductivity. Here the results of first principles density functional theory calculations performed using the AIMPRO code are presented. By evaluating the relative energies of substitution on the oxygen and zinc sub-lattices, it is possible to predict the most likely forms of doping centres that might be achieved depending both upon the dopant species and whether the ZnO is grown under oxygen or zinc rich conditions.

As a general trend, it is found that dopants tend to be stabilised in environments where covalent bonds with oxygen can be formed, such as substitution on the zinc sub-lattice. The doping properties of the group-V elements can be best understood by not considering the dopant atoms individually, but as a part of an atomic group such as phosphate and nitrate ions either substituting for host atoms, or lying in interstitial sites. The preferential formation of dopant-oxygen bonds leads to a revision of the zinc-vacancy based model for p-type doping (such as P-$(V_{Zn})_2$ complexes) to structures involving interstitial oxygen.

Contents

List of Figures

List of Tables

Publications and Conferences

List of Publications

1. K. M. Etmimi, M. E. Ahmed, P. R. Briddon, J. P. Goss, and **A. M. Gsiea**, Nitrogen-pair Paramagnetic Defects in Diamond: a Density Functional Study, *Phys. Rev. B* **79**, 205207 (2009).

2. K. M. Etmimi, J. P. Goss, P. R. Briddon and **A. M. Gsiea**, A density functional theory study of models for the N3 and OK1 EPR centres in diamond, *J. Phys.: Condens. Matter*

   22, 385502 (2010).

3. K. M. Etmimi, J. P. Goss, P. R. Briddon and **A. M. Gsiea**, Density functional studies of muonium in nitrogen-aggregate containing diamond: the MuX centre, *J. Phys.: Condens. Matter* **21**, 364211 (2009).

List of Conferences

1. AIMPRO meeting 2010, 19 - 22 April 2010, University of Nottingham, Nottingham, UK.

2. Postgraduate Research Conference 2010, 13 - 14 January 2010, School of Electrical, Electronic & Computer Engineering, Newcastle University, Newcastle upon Tyne, UK.

3. Postgraduate Research Conference 2009, 21 - 22 January 2010, School of Electrical, Electronic & Computer Engineering, Newcastle University, Newcastle upon Tyne, UK.

4. AIMPRO meeting 2008, 10 - 12 December 2008, Institute of Materials Jean Rouxel, Nantes, France.

Chapter 1

Introduction

1.1 The problem: the formation of p-type, semi-conducting ZnO

ZnO is an ionic material made up from Zn^{+2} and O^{-2}. It is a transparent, semi-conductor with a direct, wide band-gap ($3.4\,eV$) and large exciton binding energy ($60\,meV$) that makes ZnO a promising material for possible applications such as optoelectronic devices, high efficiency lasers operable at room temperature and light emitting diodes [1–4]. It can be degenerately doped n-type and free electron concentrations in excess of $10^{21}cm^{-3}$ are achievable [5]. Indeed, ZnO exhibits n-type conductivity even without any intentional doping: possible sources of donors have been suggested to be native defects such as the oxygen vacancy [6], or extrinsic defects such as hydrogen [7,8].

In contrast, the growth of p-type ZnO has proved to be difficult. The difficulty in obtaining p-type ZnO is mainly attributed to the unintentional n-type doping. Very recently, doping problems have attracted much attention and thereby considerable efforts have been made to obtain p-type ZnO by doping with group-V elements (N, P, As and Sb) as traditional p-type dopants. Amongst these group-V elements, N is possibly the most popular p-type dopant [9,10], and high hole carrier concentrations

from N impurities (10^{17}–10^{19} cm^{-3}) have been achieved experimentally [10,11].

However, theoretical studies show that there is a difficulty in explaining the p-type activity as nitrogen substituting for oxygen at room temperature [12–15].

Perhaps some clues can be taken from the nature of the molecular source of nitrogen used to dope the material. For example, some experimental work reports obtaining p-type ZnO films using NO gas [16–18] as the oxygen source and nitrogen dopant. However, nitrogen-doped ZnO films produce n-type conduction when using an N$_2$ or NH$_3$ [17,19]. This may point to a more complex, **molecular** doping effect, rather than the traditional doping where a group-VI element is replaced by a group-V, or a group-II by a group-I.

Molecular doping may be further supported by atomistic simulations that show the doping efficiency of N acceptors is limited by the compensation effect by the N$_2$ complex, which behaves as a double donor [20].

However, the location of the group-V impurities in the ZnO lattice is still a matter of debate. Recent x-ray emission experiments [17] have been interpreted as suggesting that p-type ZnO does not reflect N substitution of O, but something more complex, perhaps involving N$_2$ species. In addition, experiments using an emission channelling technique seem to verify that the majority of arsenic atoms occupy Zn sites [21] in p-type material. Also, p-type ZnO with a high carrier concentration (3.3×10^{20} cm^{-3}), a hole mobility of 12.1 cm^{2}V^{-1}s^{-1}, and with a low resistivity (1.6×10^{-2} Ω cm) has been achieved with antimony doping and the X-ray photo-electron spectroscopy shows here too that the majority of group-V atoms reside on the Zn site [22].

Temperature and composition effects also provide useful information as to the nature of the acceptors and donors formed in group-V doped ZnO. There can be a change of the type of conductivity from p-type to n-type upon annealing, which can be attributed to the evaporation of oxygen gas from the samples, correlated with the formation of native donors. Furthermore, whether the material is zinc rich or zinc lean during growth can have a strong influence over the electrical conduction [23].

Where p-type conduction is achieved, say in P-doped ZnO, a widely held model

for the origin of the shallow acceptor state is a combination of the triple-donor config-uration of P on a zinc site combined with two zinc-vacancies, [24, 25] since each V_{Zn} behaves as a double acceptor [24]. Such a centre would naturally be most favourable in oxygen-rich (zinc-lean) conditions, but suppressed in zinc-rich conditions, which is as observed. A natural explanation for the efficacy of phosphorus-based p-type doping may be envisaged to be based on these centres.

An alternative native defect which yields a double-acceptor level is the oxygen-interstitial [26, 27]. This defect also acts as a donor as the interstitial O atom may either be in a non-bonded anion state, or chemically react with the lattice where it forms an O_2 molecule on the O-site which is thought to be a donor.

1.2 Methodological approach

The subject of this thesis is the proposition of alternative mechanisms for the for-mation of p-type ZnO based upon the use of group-V elements. In so doing, a wide range of both donor and acceptor defects have been examined so that the relative probabilities of their formation can be estimated.

However, to reach a conclusion as to which of the many possible combinations of intrinsic centre with one or more group-V impurities is lowest in energy, and therefore most likely, one needs a quantitative approach. In this thesis, the approach adopted is based upon the standard quantum-mechanical method for such problems: density functional theory.

Indeed, the existing modelling performed for the electrical activity of group-V elements in ZnO is mostly based upon similar methods to those used here [20, 25, 27–35]. Although there are some challenges in the application of density functional theory to the electronic structure of ZnO and defects therein, not least of which is the underestimate of the band-gap, the properties of point defects obtained from the modelling generally agrees well with experiment. For example, the O–H vibrational modes obtained using infra-red absorption spectroscopy for complexes made up from

hydrogen trapped at a zinc-vacancy are reproduced well by theory [36].

Therefore, the strength of the computational framework can be exploited to make predictions regarding the likely structures that should be present in group-V doped material. More specifically in so doing, the modelling provides specific spectroscopic targets, such as vibrational modes, for experiment to look for.

1.3 Thesis structure

The thesis is divided into three parts: theory and AIMPRO modelling, application, conclusions and future work. Each part is divided into chapters and a summary of the content of each chapter is provided below, along with general references that might be helpful to the reader.

1.3.1 Part I - Theory and Method

Part I outlines the methodology employed in order that the semiconductor problem of interest can be understood.

Chapter 2 - Theory

This chapter involves an overview of many-body quantum mechanics and approximations used to solve the associated Schrödinger equation. This follows the development from methods such as Hartree-Fock to those of density functional theory. The key approximations used are also outlined, including the local density approximation for exchange-correlation and pseudo potentials used to eliminate the need to simulate the core electrons that do not participate in the formation of chemical bonds.

Chapter 3 - `AIMPRO`

Based upon the fundamental approximations highlighted in Chapter 2, there are additional approximations in their application. In addition, one can determine, amongst other things, the properties of defects in crystalline solids. In Chapter 3, the various

mathematical approximations are explained, such as basis sets and the treatment of the Brillouin zone. This chapter also outlines how the experimental observables such as vibrational modes and electrical levels are estimated.

1.3.2 Part II - Application

This part includes the results of *ab initio* calculations which have been obtained through the use of the modelling package, `AIMPRO`. These results are discussed in the context of experimental observations, and conclusions drawn as to the likely role of group-V elements in p-type doping.

Chapter 4 - Native defects

Since many of the defects of interest involving the group-V dopants are complexes with native defects (self-interstitials and vacancies), in this chapter a study of the properties of native defects is presented. In particular, their energies, geometries and electrical levels are reviewed, and where appropriate compared with values from the literature.

Chapter 5 - Nitrogen Doping ZnO

This chapter presents a study of the role of nitrogen as a dopant in ZnO to produce p-type material. The structure, electrical levels and vibrational modes of nitrogen-related defects are presented. The relative role of molecular groups which are internally covalently bonded to the conventional nitrogen acceptor on an oxygen site forms the focus of the discussion in this case.

Chapter 6 - Phosphorus, Arsenic and antimony doping ZnO

The final application chapter focuses on the possibility of other group-V doping such as phosphorus, arsenic and antimony, may act as p-type dopants in ZnO are presented. Again, the role of covalent bonding in these centres is shown to be important.

1.3.3 Part III - Conclusions

Chapter 7 - Summary

In the final chapter the general conclusions are presented and some possible future avenues of research in these subjects are suggested.

1.4 Abbreviations

The following abbreviations have been used within this thesis.

Abbreviation	Definition
AIMPRO	*Ab Initio* Modelling PROgram.
DFT	Density Functional Theory.
HF	Hartree-Fock theory.
BZ	Brillouin Zone.
LDF	Local Density Functional.
LDA	Local Density Approximation.
MP	Monkhorst-Pack.
NEB	Nudged Elastic Band.
PL	Photoluminescence.
EPR	Electron Paramagnetic Resonance
XPS	X-Ray Photoelectronic Spectroscopy
IR	Infrared

1.5 Notation

The following notations have been used throughout this thesis.

Notation	Definition
E_g^{ks}	Kohn-Sham Energy Gap.
E_{GS}	Ground State Energy.
Q	Charge State.
E_{kin}	Kinetic Energy.
V_{ext}	External Potential.
E_{xc}	Exchange Correlation Energy.
U_H	Hartree Energy.
V_{eff}	Effective Potential.
T	Temperature.
E_v	Valance band top.
E_b	Binding Energy.
RT	Room Temperature.

Part I

Theory and Method

Chapter 2

Theory

2.1 introduction

The task to be addressed in the simulation of collections of atoms is essentially one of quantum mechanics. The equations of motion of electrons in the fields of a set of nuclei can be treated in a number of ways, but those termed *ab initio* techniques are methods used to solve the Schrödinger equation without the use of any experimental input (*ab initio* means from first principles). All these particles interact with each other under Coulomb electrostatic forces. Only in a few cases, such as the hydrogen atom is a complete analytic solution available, and this becomes very complicated when the number of particles in the system increases, solids, for example, which consist of considerable arrays of atoms. There are many complexities underlying the application of these techniques to different classes of system.

2.2 The Schrödinger Equation for a many-body problem

The aim of an *ab initio* method is to find the solution to an approximation to the many-body Schrödinger equation for the system being studied.

The Schrödinger equation for a single particle in three dimension is

$$\left[-\frac{\hbar^2}{2m}\nabla^2 + V(\vec{r}) \right] \psi(\vec{r}) = E\psi(\vec{r}) \tag{2.1}$$

where

$$-\frac{\hbar^2}{2m}\nabla^2 + V(\vec{r}) = \hat{H} \tag{2.2}$$

so

$$\hat{H}\psi(\vec{r}) = E\psi(\vec{r}) \tag{2.3}$$

where $\psi(\vec{r})$ is the wave function for the particle eigenstates, E is the total energy, and $\hat{H}$ is the Hamiltonian for one particle. The Hamiltonian for a system of N non-interacting particles is

$$\hat{H} = \sum_i^N \hat{H}_i \tag{2.4}$$

where

$$\hat{H}_i = -\frac{\hbar^2}{2m_i}\nabla_i^2 + V_{ext}(\vec{r_i}) \tag{2.5}$$

where ∇_i^2 is the standard, three dimensional second derivative with respect to position for particle i, and

$$\hat{H}_i\psi(\vec{r}) = \sum_i -\frac{\hbar^2}{2m_i}\nabla_i^2\psi(\vec{r}) + V_{ext}(\vec{r_i})\psi(\vec{r}) = E_i\psi(\vec{r}) \tag{2.6}$$

where the external potential due to the nuclei is V_{ext}, $\psi(\vec{r_i})$ contains all of the ground state information about the system, including the potential from the electron density of the other particles. In general, for an interacting system the wave function depends on 3N electronic degrees of freedom, and the Schrödinger equation is extremely hard to solve. We need to find the ground state energy for a system composed of N interacting fermions, in particular electrons. The Hamiltonian is:

$$\hat{H} = \hat{T}_e + \hat{T}_n + \hat{V}_{ee} + \hat{V}_{nn} + \hat{V}_{en} \tag{2.7}$$

where $\hat{T}_e$ represents the kinetic energy of the electrons, $\hat{T}_n$ represents the kinetic energy of the nuclei, and there are three types of interaction, represents by the three

terms $\hat{V}_{nn}$, $\hat{V}_{ne}$, and $\hat{V}_{ee}$ which are between nuclei-nuclei, nuclei-electrons, and between electrons. That leads to an equation which is extremely difficult to solve:

$$\hat{H}\Psi = E\Psi \tag{2.8}$$

where

$$\begin{aligned}
\hat{H} &= \sum_i -\frac{1}{2M_i}\nabla_i^2 + \frac{1}{2}\sum_{i\neq j}\frac{Z_i Z_j}{|R_i - R_j|} + \sum_k \frac{1}{2}\nabla_k^2 \\
&+ \frac{1}{2}\sum_{k\neq l}\frac{1}{|r_k - r_l|} - \sum_{k,i}\frac{Z_i}{|r_k - R_i|}
\end{aligned} \tag{2.9}$$

where (R, r) are the positions of nuclei, and electrons. We have used atomic units $\hbar = e = m = 4\pi\epsilon_0 = 1$. The first and third terms represent the kinetic energy of the nuclei and the electrons. All other interactions are Coulomb in nature (nucleus-nucleus, electron-electron and electron-nucleus, respectively). To simplify equation (Eq. 2.9) two main approximations can be used to simplify the Hamiltonian to give a soluble problem. The first approximation replaces the final term of (Eq. 2.9) by a pseudo potential (see Sec.3.3). The second approximation considers that the electrons respond fast compared to the ion cores. This leads to the Born-Oppenheimer approximation [37].

2.3   Density functional theory

Density functional theory (DFT) is a quantum mechanical theory based on the conception of the single electron density as a fundamental variable. Density functional theory is a popular method and has been used in computational physics and computational chemistry calculations to investigate the electronic structure, principally the ground state of many-body systems. Density functional theory calculates the total energy of an electron gas in the presence of a background potential $V_{ext}(\vec{r})$ [38]. Density functional theory describes the system in terms of the electron density, rather than the many-body wave function, for a system consisting of N electrons. The most widely used approximation is the Local Density Approximation (LDA) [38], which approximately treats the exchange-correlation energy of an inhomogeneous system.

2.3.1 Hohenberg-Kohn theorem

For a system of N interacting electrons in a non-degenerate ground state, the density $n(\vec{r})$ uniquely determines the potential $V_{ext}(\vec{r})$, up to an arbitrary constant (Hohenberg and Kohn [38,39]). To prove this Hohenberg and Kohn theorem for non-degenerate ground states, consider two trial wave functions Ψ_1 and Ψ_2 at the same density, but arising from different external potentials, V_1 and V_2. The variational principle gives

$$E_1 = \langle\Psi_1|H_1|\Psi_1\rangle < \langle\Psi_2|H_1|\Psi_2\rangle \tag{2.10}$$

clearly

$$H_1 = H_2 + (V_1 - V_2) \tag{2.11}$$

so this gives

$$E_1 \leq \langle\Psi_2|H_2 + V_1 - V_2|\Psi_2\rangle \tag{2.12}$$

$$E_1 < E_2 + \langle\Psi_2|V_1 - V_2|\Psi_2\rangle \tag{2.13}$$

$$E_1 < E_2 + \int n(r)[V_1 - V_2]dr \tag{2.14}$$

interchanging symbols $1 \leftrightarrow 2$ gives (since both Ψ_1 and Ψ_2 have been assumed to have the same charge density)

$$E_2 < E_1 + \int n(r)[V_2 - V_1]dr \tag{2.15}$$

or

$$E_1 > E_2 + \int n(r)[V_1 - V_2]dr \tag{2.16}$$

(Eq. 2.14) and (Eq. 2.16) are contradictory.

Hence it is impossible for systems with different potentials to give the same $n(\vec{r})$. This means that V, and the energy, can be written as a functional of $n(\vec{r})$.

The second Hohenberg-Kohn theorem states that the true ground state charge density is that which minimises the total energy.

$$E[n] = \min_{\Psi\to n}\langle\Psi|\hat{H}|\Psi\rangle \tag{2.17}$$

$$\min_{\Psi\to n}\langle\Psi|\hat{H}|\Psi\rangle = \min_{\Psi\to n}\langle\Psi|\hat{T} + \hat{V}_{ee}|\Psi\rangle + \int d^3r V_{ext}(\vec{r})n(\vec{r}) \tag{2.18}$$

where all wave functions are constrained to yield $n(\vec{r})$, Hohenberg-Kohn introduced a universal functional, defined as:

$$F[n] = \min_{\Psi \to n} \langle \Psi | \hat{T} + \hat{V}_{ee} | \Psi \rangle \tag{2.19}$$

$F[n]$ is universal, that is, same for all electronic structure problems. The ground state energy is:

$$E_{GS} = \min_{n} E[n] = \min_{n} \left[F[n] + \int d^3 r V_{ext}(\vec{r}) n(\vec{r}) \right] \tag{2.20}$$

where the search is over all N-electron densities. The minimum energy density is then the exact ground state density. Finally the Euler-Lagrange variational equation for this problem is:

$$\frac{\delta F}{\delta n(\vec{r})} + V_{ext}(\vec{r}) = \mu \tag{2.21}$$

where μ is the chemical potential. $F[n]$ is unknown, and depends on the electron-electron interactions.

2.3.2 Kohn-Sham formulation

We proceed by considering a non-interacting system in an unknown potential $v_s(\vec{r})$ chosen so that its electron density is the sum as the real system. The kinetic energy of such a system is given by:

$$T_s[n] = \min_{\Psi \to n} \langle \Psi | \hat{T} | \Psi \rangle \tag{2.22}$$

Now we will rewrite $F[n]$ as

$$F[n] = T_s[n] + U[n] + E_{xc}[n] \tag{2.23}$$

where $U[n]$ is the Hartree energy for Coulomb interactions, defined by

$$U[n] = \frac{1}{2} \int d^3 r \int d^3 \acute{r} \frac{n(\vec{r}) n(\vec{\acute{r}})}{|\vec{r} - \vec{\acute{r}}|} \tag{2.24}$$

and $E_{xc}[n]$ is the exchange-correlation energy. The potential in the Kohn-Sham equation is then:

$$v_s(\vec{r}) = v_{ext}(\vec{r}) + \frac{\delta U[n]}{\delta n(\vec{r})} + v_{xc}[n](\vec{r}) \tag{2.25}$$

where $v_{xc}[n](\vec{r})$ is the exchange-correlation potential, defined by

$$v_{xc}[n](\vec{r}) = \frac{\delta E_{xc}[n]}{\delta n(\vec{r})} \tag{2.26}$$

This must then be approximated. Kohn and Sham [40] using this approach derived the equations

$$\left\{ -\frac{1}{2}\nabla^2 + v_{ext}(\vec{r}) + \int d^3\acute{r}\frac{n(\vec{\acute{r}})}{|\vec{r} - \vec{\acute{r}}|} + v_{xc}[n](\vec{r}) \right\}\psi_i(\vec{r}) = \varepsilon_i\psi_i(\vec{r}) \tag{2.27}$$

now known as the KS equations.

2.3.3 Local Density Approximation

The Local Density Approximation (LDA) is an approximation for the exchange-correlation energy functional in density functional theory (DFT). It is based on the exchange-correlation energy of a homogeneous electron gas, for which the kinetic and exchange energies can be calculated analytically, and the correlation part accurately approximated. The exchange-correlation functional for an inhomogeneous system is then defined within the LDA [41] as:

$$E_{xc}[n(r)] = \int d^3 rn(\vec{r})\varepsilon_{xc}^{unif}(n(\vec{r})) \tag{2.28}$$

where $\varepsilon_{xc}^{unif}(n)$ is the exchange-correlation energy per electron in a homogeneous electron gas with density n. The LDA is a common and simple approximation for this functional, it is local in the sense that the electron exchange and correlation energy at any point in space is a function of the electron density at that point only [42]. To facilitate development of this, the exchange-correlation $E_{xc}[n]$ function can be separated into two parts as:

$$E_{xc}[n(r)] = E_x[n(r)] + E_c[n(r)] \tag{2.29}$$

For a non-spin polarised system, with density [n(r)], it is easily shown that [43]

$$E_x[n] = -\frac{3}{2}\left(\frac{3}{8\pi}\right)^{\frac{1}{3}}n^{\frac{4}{3}} \tag{2.30}$$

CHAPTER 2. THEORY

This can be extended [44] to a spin polarised system $E_{xc}[n_\uparrow, n_\downarrow]$ thus:

$$E_x\left[n_\uparrow, n_\downarrow\right] = -\frac{3}{2}\left(\frac{3}{4\pi}\right)^{\frac{1}{3}}\left[n_\uparrow^{\frac{4}{3}} + n_\downarrow^{\frac{4}{3}}\right] \tag{2.31}$$

The second term in equation (Eq. 2.29), $E_c[n(r)]$, is significantly more complicated to find. There are many methods used to treat this problem numerically, like the parameterised functionals of Perdew and Zunger (PZ) [45], Vosko-Wilk-Nusair [46], and Perdew and Wang [47]. The parameters come from a fit to expressions derived in the low electron density regime [45] and high electron density regime [48]. The LDA approximation is successful for inhomogeneous systems when the charge density is slowly varying. On the other hand the LDA leads to an underestimate of the band-gap largely due to self-interaction. For example in the LDA the ZnO band-gap is $\sim$ 1.4 eV, where the experimental band-gap for ZnO is 3.4 eV.

2.3.4 Generalised Gradient Approximation

The generalised gradient approximation (GGA) improves upon the LDA by adding a new factor F_{xc} to the equation (Eq. 2.28). The exchange-correlation is treated numerically in the formalism of Perdew, Burke and Ernzerhof (PBE) [49], and Patton, Porezag, and Pederson [50] in the form.

$$E_{xc}[n(r)] = \int d^3 r n(\vec{r})\varepsilon_{xc}^{unif}F_{xc}(n_\uparrow, n_\downarrow, |\nabla n_\uparrow|, |\nabla n_\downarrow|) \tag{2.32}$$

This tends to improve binding energies, bond lengths, atomisation energies, energy barriers, and structural energy differences at least for small molecules. However the band gap underestimate is still not fixed. For defects in bulk semiconductors, the GGA does not consistently produce better results than LDA, so the work in this thesis applies the LDA to ZnO.

Chapter 3

The Modelling Package `AIMPRO`

3.1 Introduction

`AIMPRO` is a computer modelling package which uses density functional theory with
a choice of different functionals, pseudo potentials and simulation techniques for ex-
perimental observables. The electrons (more correctly the Kohn-Sham functions) are
expanded using a Gaussian orbital basis set [51]. This combination of techniques is
successful for describing the many semiconductor properties, and generally gives good
results when compared with experiment.

3.2 Boundary conditions

Boundary conditions are fundamental in the solution for any set of differential equa-
tions. Two kinds of boundary conditions can be employed in `AIMPRO`: the first cor-
responds to non-periodic systems, which is suitable for molecules and clusters; the
second applies periodic boundary conditions, which is particularly suitable for crys-
talline systems. Only periodic boundary conditions have been used for calculations in
this thesis.

3.2.1 Periodic boundary conditions

This boundary condition describes a solid crystalline system, where the a unit cell is effectively repeated infinitely in all directions. Periodic systems can eliminate the problems of surface termination and associated defect-surface interaction. However, other problems are introduced: as a consequence of repeating the unit cell, a defect will also be repeated and this introduces defect-defect interaction, necessitating the use of large numbers of atoms to avoid spurious effects. In particular, the supercell must be chosen large enough so that these interactions do not have a significant influence on the properties being studied, which in the case of doping may be characterised as a combination of electronic interactions (the direct overlap of electron states between supercells), electrostatic interactions, and elastic interactions due to the displacements of atoms in the vicinity of a point defect not decaying to zero within the supercell.

The modelling of ZnO as applied in this thesis is made up of linear combinations of the primitive units for bulk ZnO. The primitive cell for ZnO is a hexagonal lattice with a basis of four atoms. Table 3.1 shows the parameters of the cell used in this study. Most calculations presented are based upon the 192 atom supercell, with both smaller and larger cells being used as tests for convergence.

In particular, it should be noted that because of the relatively long-range perturbation of the lattice for many doping centres, the 72-atom supercells are not sufficient for some calculations of formation energies. In some cases, structures that are obtained to be stable in this supercell size are completely unstable in those with longer lattice vectors, i.e. the errors due to the small cell size may be qualitative as well as quantitative.

3.2.2 Brillouin Zone Sampling

Many observables are calculated in the supercell approach require integrals the Brillouin zone. For example, the total energy and electron density can be expressed in

Table 3.1: Details of lattices of the primitive unit cell of Wurtzite ZnO, and the supercells used in the simulation of point defects. The lattice vectors are expressed in the normal Cartesian form with components in the directions $(\vec{i}, \vec{j}, \vec{k})$, and a and c are the hexagonal lattice constants.

No. of atoms	Composition		Lattice Vectors	
4	Zn_2O_2	$a(1,0,0)$	$-\frac{a}{2}(1,\sqrt{3},0)$	$c(0,0,1)$
72	$Zn_{36}O_{36}$	$3a(1,0,0)$	$-\frac{3a}{2}(1,\sqrt{3},0)$	$2c(0,0,1)$
192	$Zn_{96}O_{96}$	$4a(1,0,0)$	$-\frac{4a}{2}(1,\sqrt{3},0)$	$3c(0,0,1)$
400	$Zn_{200}O_{200}$	$5a(1,0,0)$	$-\frac{5a}{2}(1,\sqrt{3},0)$	$4c(0,0,1)$

the form:

$$E_{tot} = \frac{1}{V_{BZ}} \int_{1st\ BZ} E(k)d^3k \tag{3.1}$$

$$n(r) = \frac{1}{V_{BZ}} \int_{1st\ BZ} n_k(r)d^3k \tag{3.2}$$

where V_{BZ} is the volume of Brillouin zone $(2\pi)^3/\Omega$. These integrals are very computationally expensive to evaluate as the functions $E(k)$ are time consuming to find in any but the most simple systems. Since in practice the electron wave-vector, $\vec{k}$, dependence of the electron energies is not known analytically, a strategy has to be adopted to perform these integrals *numerically*: integrals are approximated using sums over finite grids of k-points.

$$E_{tot} \approx \sum_i E(k_i)w_i \tag{3.3}$$

in which w_i is a weighting to ensure that the integral reflects the symmetry and internal structure of the Brillouin zone. The question then arises as to the most efficient set of k_i, or what is the fewest number of electronic structures that needs to be obtained in order to obtain an integral which is sufficiently accurate.

There are some methods for choosing single k-points which consider the simplest case to give the mean value of the function, such as that of Baldereschi [52]. Another single-point approximation commonly used is to neglect the k-dependence entirely, by evaluating the electronic structure only for the null electron wave vector. Since the Brillouin zone centre is always labelled as Γ, this approximation is termed the Γ-point approximation, which works best for large systems where band-structure folding means that electron dispersion is accommodated at this point.

A further method introduces a *set* of special k-points and takes the average over the Brillouin zone [53, 54]. Another method, which has proved extremely successful and has therefore been widely adopted, was proposed by Monkhorst and Pack [55] which is the method use in the results presented in this thesis.

In brief, the Monkhorst-Pack scheme uses a uniformly spaced mesh of k-points over the Brillouin zone. The density of this mesh can be easily varied to test the accuracy (and convergence) of an integral over the Brillouin zone. For a typical supercell used for the simulation of point defects, the lattice vectors are chosen such that they all have approximately the same length. In a cell that can be described as being approximately cubic, and which has approximately isotropic contents, the number of k-points rapidly increases with the sampling density. For example, increasing the sampling mesh from two points in each reciprocal lattice direction to three points, increases the number of k-points (neglecting symmetry) by a factor of more than three. Since the time of a calculation scales linearly with the number of k-points, the meshes used in practice must be chosen carefully.

For bulk ZnO, taking the 72-atom supercell (table 3.1), the energy was calculated for a range of sampling schemes. The *absolute* variation in energy is shown in table 3.2.

The impact of sampling has been tested in an additional way. For a sample 72 atom supercell containing a P-related defect centre (chapter 4, 5 and 6), the energy difference between $2 \times 2 \times 2$ and $4 \times 4 \times 2$ is $0.1 \, \text{meV}$ per atom.

It should be noted that energy differences tend to converge more rapidly with sampling than absolute energies, so that in general formation energy differences (which

Table 3.2: Relative total energy per atom (meV) for a 72-atom supercell of bulk ZnO as a function of sampling scheme. The zero of energy is taken from the energy with a sampling mesh of $4 \times 4 \times 3$.

Mesh:	Γ	$2 \times 2 \times 2$	$3 \times 3 \times 2$	$4 \times 4 \times 3$
Relative energy:	29.69	0.14	0.05	0.00

are shown extensively in the applications chapters) are most likely to be converged to an even better degree than the absolute errors highlighted here, at least in terms of the dependence upon the sampling.

3.3 Pseudo potentials

The pseudo potential approximation is an attempt to replace the complicated effects of the core electrons of an atom and its nucleus with an effective potential, so that the Schrödinger equation contains a modified effective potential term instead of the Coulomb potential term for core electrons. Within modern density functional theory, the majority of the pseudo potentials used in electronic-structure calculations are generated from all electron atomic calculations. Pseudo potentials are designed on the basis of division of the atom into two regions $r_c \geq r$ which defined as the core region near the nucleus, and $r \geq r_c$ defined as the as the valence region, which determines the chemical and physical properties of the material and is responsible for atoms bonding. Fig. 3.1 shows that the electron wave functions near the nucleus oscillate and are rapidly changing, while becoming non-oscillatory and smooth further away from the core $r \geq r_c$. Outside the core the pseudo wave function should be virtually identical to the electron wave function.

$$\Psi^{ps} = \Psi^r \tag{3.4}$$

when $r \geq r_c$ and the potentials should also agree, $V_{ps} = V$.

CHAPTER 3. AIMPRO
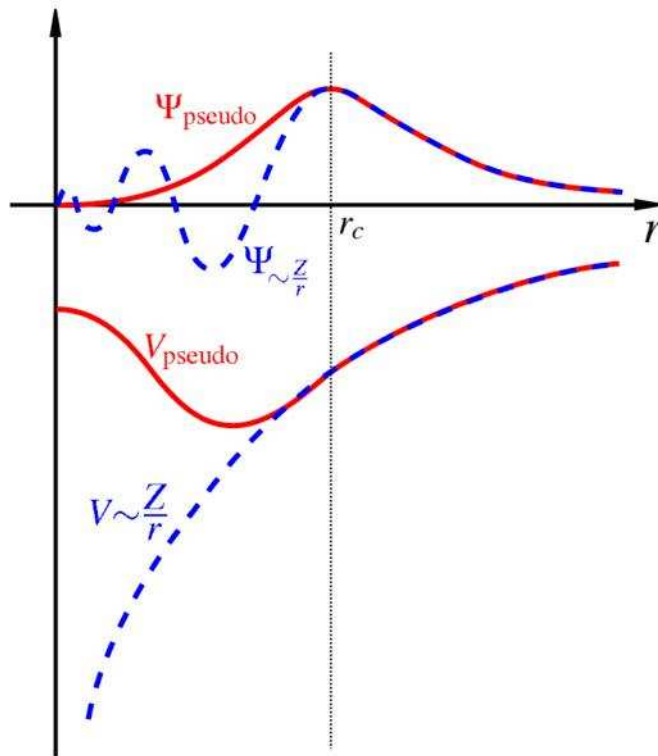
Figure 3.1: Schematic diagrams illustrating the concept of the pseudo-wave function (top) and the pseudo-potential (bottom) utilised to replace core electrons. The cut-off radius r_c indicates the defined region at which point the systems must match. The pseudo wave function and potential are plotted with a full red line whilst the true all-electron wave function and core potential is plotted with the dotted blue line.

Many kinds of pseudo potential have been developed, but the formalism used throughout this work is that of Troullier and Martins (TM) [56].

3.4   Basis Sets

It is normal for density-functional simulations to represent some of the key variables, and in particular the electron functions (i.e. the Kohn-Sham functions) in terms of a

basis. The more freedom a basis has, the more accurately it may be able to represent the functions, but the more computational cost must be paid. For electronic structure calculations, the two common types of basis sets are plane waves and Gaussian type orbitals.

The former have two advantages. First, they are by construction solutions to a periodic potential (i.e. they are solutions in Bloch's theorem), and since they also automatically form an orthogonal set, the number of basis functions can be systematically varied to obtain a converged result (provided CPU and memory constraints allow). However, very large basis sets are required to represent localised states such as those seen molecules and defects.

Gaussians have the advantage of phenomenologically representing localised states, but the computational exploitation of them is less straight forward than is the case for plane waves. Importantly, since they do not form an orthogonal set, they cannot be methodically converged, and one has to take care to choose basis sets that accurately represent the system of interest. However, the computational advantages of the Gaussian approach out-weigh the disadvantages, and it is this type of function that is employed in AIMPRO. They have the form:

$$\phi(r - R_i) = (x - R_{ix})^{n_1}(y - R_{iy})^{n_2}(z - R_{iz})^{n_3}e^{-\alpha(r-R_i)^2} \tag{3.5}$$

where n_1, n_2 and n_3 are integers. $\sum n_i = 0, 1, 2, ...$ correspond to the conventional labelling of the the orbitals like s-, p-, d-, ... which may be further extended to generate in higher order basis functions[1].

The values of α dictate the widths of the functions in real space, and these are chosen to span the usual length scales associated with bonding and crystal lattices involving the associate atomic species. For example, the basis sets used to represent O and Zn in ZnO are optimised so that they yield a minimum in total energy for bulk ZnO. Similar procedures are used in the determination of the exponents for the impurity species.

---

[1]Note, this construction actually generates combinations of angular momenta. For example, for $\sum n_i = 2$, one term is of the form $x^2 + y^2 + z^2$, which is spherically symmetric and therefore s-like.

A short-hand notation for a basis set has been adopted, where the highest orbital angular momentum included in the basis for increasing exponent is listed. For example, *ddpp* corresponds to a set of *s*-, *p*- and *d*-Gaussians for the smallest and second smallest exponents, plus *s*- and *p*-Gaussians for the second largest and largest exponents. Typical values for the smallest exponent is of the order of 0.1. The largest exponent is typically in the range of 5–10.

For the results presented in this thesis, the basis used for the modelling of Wurtzite ZnO are given in table 3.3

Table 3.3: Parameters defining the basis sets used to represent the Kohn-Sham functions in this study. The notation is defined in the text. The exponents, α_i, are listed, and have units of a.u.$^{-2}$.

Atomic species	No. functions	Basis	Exponents				
Zn	*ddpp*	28	0.18953	0.80047	3.38071	14.27813	
O	*ddpp*	28	0.27500	0.85964	2.68718	8.40000	
N	*ddpp*	28	0.21810	0.78062	2.79396	10.00000	
P	*ddppp*	32	0.26647	0.66950	1.68210	4.22625	10.61838
As	*ddpp*	28	0.25431	0.60307	1.43010	3.39131	
Sb	*ddpp*	28	0.16788	0.36410	0.78967	1.71266	
S	*ddpp*	28	0.16338	0.50666	1.57124	4.87266	
Se	*ddpp*	28	0.13746	0.42427	1.30957	4.04211	

It is obviously of great importance that the computational framework can correctly model bulk ZnO before one can have confidence in the properties of defects and dopants in this material. The combination of basis sets for Zn and O yields an average error of $\sim 0.6\%$ and $\sim 0.3\%$ in the two lattice constants, *a* and *c* compared to experiment: the equilibrium lattice constants are calculated to be $a = 3.269\,\text{Å}$ and

$c = 5.189\,\text{Å}$, respectively, which are in good agreement with experimental value of $a = 3.249\,\text{Å}$ and $c = 5.204\,\text{Å}$. In addition there was a $\sim 7\%$ in the bulk modulus compared with experimental value for the Zinc-Blende structure.

Finally, as an indication of the convergence of the basis, the band-structure was calculated using *ddpp* basis sets for both Zn and O yielding a value of $1.4\,\text{eV}$ (figure 3.2). With a larger, *dddp* basis, the change in the band-structure is very small, such that if the two calculations are plotted on the same axes, they cannot be visually distinguished.
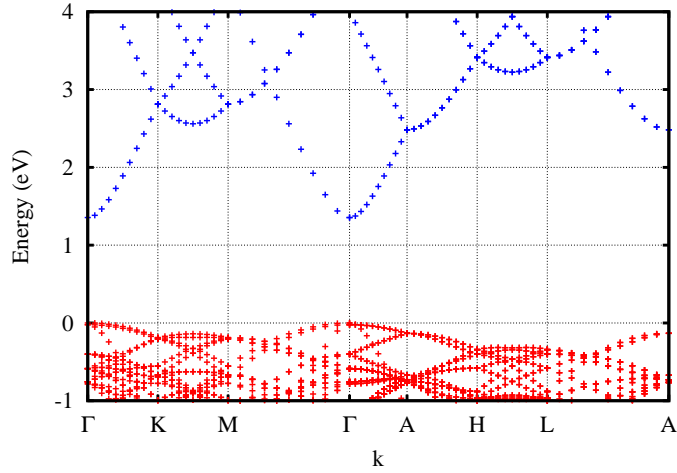
Figure 3.2: Plot of band structure of bulk w-ZnO. Occupied (empty) bands are shown as red and blue crosses, respectively.

Fig. 3.2 shows the band-structure calculated for bulk Although this band-gap is converged with respect to basis, this calculation highlights one of the main problem associated with functionals: the underestimation of the band-gap due to self-interaction. Since the band-gap is calculated to be $1.4\,\text{eV}$, whereas in experiment it is $3.4\,\text{eV}$, it seems highly likely that such an error may strongly affect, for example, the calculation of electrical levels. The impact of the underestimate is discussed in section 3.9. However, it is noted that one solution to this problem might be the use of the alternative fundamental approximations, such as screened exchange [57]. Although this has not been available for the current simulations it is the subject of future work, as described

in chapter 7.1.

A second part of the basis occurs in the representation of the charge density. Since periodic boundary conditions are used, it is possible to Fourier transform the charge density and then represent it efficiently using a convergable plane wave basis. In this way matrix elements of the Hamiltonian are determined using a plane wave expansion of the density and Kohn-Sham potential [58] with, in the current calculations, a cutoff energy of 150 Ry.

As with the choice of Gaussian basis for the Kohn-Sham functions, the plane-wave basis must be chosen carefully to ensure that the physical system is modelled sufficiently accurately. However, since this is a relatively minor component of the calculation in terms of the computational time, one normally selects a relatively large value. Indeed, the choice of 150 Ry yields a well converged total energies with respect to the charge density basis at an absolute level.

3.5 Self-Consistency methods

Self-consistency has a key role in *ab initio* electronic structure calculations to solve the Kohn-Sham equations (Eq. 2.27). Self-consistent methods attempt to ensure that the output charge density $n_r(r)$ obtained from the Kohn-Sham potential V_{ext} is the same as the input charge density $n_i(r)$ used to generate V_{ext} within a certain numerical tolerance $R = n_0(r) - n_i(r)$. The obvious strategy is to start with an initial guess for the charge density, which is generally taken from a superposition of neutral atomic species for the same system. Self-consistent calculations can proceeding mixing $n_i(r)$ and $n_0(r)$ and using the result as input to the next cycle, attempting to decrease R at every step [59].

3.6 Structural Optimisation

After obtaining a solution of the Kohn-Sham equation using a self-consistent method, forces between atoms can be found analytically and used to determine the lowest energy structure for a system of atoms. The force on any atom (a) in the system in the direction (l) is given by the following equation:

$$f_{la} = -\frac{\partial E}{\partial R_{la}} \tag{3.6}$$

where R_{la} is the position of atom a, and l is the direction of the force (x, y or z). This derivative is found analytically [60]. In order to find the lowest energy for a system once the forces are known, the conjugate gradient method [61, 62] is used. Structures are optimised until the change in energy between iterations is less than 10^{-5}Ha, and forces are below 10^{-3}a.u.

3.7 Calculation of Diffusion Barriers

An important problem in condensed matter physics and theoretical chemistry is the understanding of the energetics of the diffusion of a defect atom through a lattice, or the reorientation of a defect centre. The atoms that make up the system move along continuous paths between two states which are stable (or metastable). This system is most likely to move along the paths with the lowest intermediate energy maximum. This path is called the minimum energy path (MEP), the structure with the highest energy along this path is called a saddle point and its energy is an important quantity in the study of transition processes. There are many approximation methods that use local information to find the saddle point between the end points. An efficient and reliable method for finding an approximate minimum energy path is the nudged elastic band (NEB) method [63–66].

The migration calculations are implemented within AIMPRO via use of the successful nudged elastic-band method (NEB). There are many variations on the NEB method, including the climbing image nudged elastic band. Nudged elastic band is

used to find a saddle points and minimum energy paths between two known stable structures. The method works by optimising a number of intermediate images along the reaction path. These images are moved according to the force acting on them perpendicular to the path and an artificial spring force keeping the images spaced along the MEP. The highest energy image gives a good estimate of the transition state. The climbing image is a small modification to the NEB method in which the highest energy image is driven up to the saddle point. This image does not feel the spring forces along the band. Instead, the true force at this image along the tangent is inverted. In this way, the image tries to maximise its energy along the band, and minimise in all other directions. When this image converges, it will be at the exact saddle point. Because the highest image is moved to the saddle point and it does not feel the spring forces, the spacing of images on either side of this image will be different. It can be important to do some minimisation with the regular NEB before this method is used, both to have a good estimate of the reaction co-ordinate around the saddle point, and so that the highest image is close to the saddle point. If the maximum energy image is initially very far from the saddle point, and the climbing image was used from the outset, the path would develop very different spacing on either side of the saddle point.

3.8 Vibrational modes

A molecule or a defect in a solid has special patterns of vibration in which each atom vibrates with a different amplitude but with the same frequency. These are called normal modes and are important because they can be observed using infrared (IR) absorption or through Raman scattering experiments. Modes are IR-active if the change of the bond length causes a change in electric dipole, while Raman active modes rely on changes in the polarisability.

The vibration modes calculations throughout this thesis are implemented within `AIMPRO` via the use of the quasi harmonic frequency, which is very close to experiment

for all atoms other than hydrogen (where errors of say 100 cm^{-1} may result from this approximation). The force constants for the dynamical matrix are obtained by displacing the selected atoms in the x, y and z directions by 0.1a.u., and calculating the forces on all atoms. The second derivative of the energy with respect to the displacement is then obtained by a finite difference formula using the analytical forces.

The ability to calculate vibrational frequencies is very valuable as they are sensitive to structure and a comparison of calculated with experimental values can be a powerful tool in characterisation. An example of this as in (Chapter 5).

3.9 Formation Energies and Electrical Levels

Several important quantities can be obtained from density functional theory. Firstly, the formation energy of a defect, which is one of the most important factors in its solubility and stability. Secondly, electrical levels of defect, which the lowest energy charge state of the system change associated with a defect, which can explain the conductive properties, and optical transitions of the material. Thirdly, the binding energy of a complex defect in the same structure.

3.9.1 Formation Energy

The formation energy is defined for the defect system as a function of the chemical potentials of the atomic species of the material and electrons. The chemical potential (μ_x) of the species (x) is defined as the derivative of the Gibbs free energy with respect to the number of particles of the species (N_x):

$$\mu_x = \frac{\delta G}{\delta N_x} \tag{3.7}$$

$$G = E + PV - TS, \tag{3.8}$$

where E is the internal energy, P is pressure, V is volume, T is the temperature, and finally S is the entropy. The species in this equation could be atoms and/or electrons. For solid-state situations, the PV term is very small and can be neglected, and TS

is typically small for moderate temperatures (say up to around room temperature). Neglecting these terms, the formation energy may be expressed as:

$$E^f(X,q) = E^{tot}(X,q) - \sum_i n_i\mu_i + q(E_v(X,q) + \mu_e) + \chi(X,q), \qquad (3.9)$$

where $E^{tot}(X,q)$ is the total energy of system X in charge state q. n_i is number of atoms, μ_i denotes the chemical potential of atomic species, $E_v(X,q)$ is the energy of the valance-band top, and μ_e is the electron chemical potential, defined as zero at the valence band top.

In ZnO, the chemical potentials of components μ_O and μ_{Zn} are related by $E(\mathrm{ZnO}) = \mu_O + \mu_{Zn}$ where $E(\mathrm{ZnO})$ is the energy per bulk formula unit in ZnO. The range of possible values for μ_O and μ_{Zn} is related to the requirement for ZnO to be stable relative to decomposition into its elemental constituents, so that the zinc-rich limit is taken from zinc-metal, and for oxygen-rich limit μ_O is taken from the O_2 molecule. The heat of formation for ZnO in this way is calculated to be $3.9\,\mathrm{eV}$, while experimentally it is $3.61\,\mathrm{eV}$ [67].

For the dopants there is a relative formation energies *per impurity atom* are independent of the impurity chemical potential, but for the reference state of nitrogen-based centres is derived by comparison with N_2 molecule as a lower limit for N. For the phosphorus-based centres is derived by comparison with P_4O_6, and therefore linked to μ_O.

3.9.2   The Electrical levels

The electrical levels are one of the most important properties of defects, as they strongly influence the electrical and optical properties of the material. Electrons can transfer from one band to the other by means of carrier generation and recombination processes. The band gap and defect states created in the band gap by doping can be used to design semiconductor devices such as solar cells, diodes, transistors, laser diodes, and others. One method to calculate electrical levels is the formation energy approach, which compares the formation energies of charged and neutral defects. The

donor level is the chemical potential at which the formation energies of neutral and positive charge states are equal:

$$\mu_e(0/+) \quad \text{when} \quad E^f(X, 0) = E^f(X, +) \tag{3.10}$$

The acceptor level is the chemical potential at which the formation energies of negative and neutral charge states are equal:

$$\mu_e(-/0) \quad \text{when} \quad E^f(X, -) = E^f(X, 0) \tag{3.11}$$

The effect upon the electrical levels arising from the periodic boundary condition, $\chi(X, q)$ in Eq. 3.9, is a complicated and controversial quantity to estimate. In this study, a simple approach is adopted of focusing on the larger differences between the formation energies of different structures, rather than the specific values of the donor and acceptor levels. The total energies are corrected using the Lany and Zunger model [68], and to take into account the underestimation of the band gap, a term is added which is proportional to the number of electrons in any conduction-band-like level [25, 27] of $2\,\text{eV}$ per electron arising from a simple addition of the difference between the calculated and experimental band-gaps.

When comparing the absolute formation energies, and in particular in the important cases of comparison between like-systems, such as band-like donors, or comparison between the models for p-type doping, these corrections largely cancel. Amongst the calculated electrical levels, based upon the marker-method philosophy [51], relative locations of two donor systems, or two acceptor systems might be expected to be reasonably reliable at a quantitative level.

3.9.3 Binding energy

The Binding energy is the energy required to dissociate a complex into separate parts. A bound system has a lower potential energy than its constituent parts; this is what keeps the system together. The usual convention is that this corresponds to a positive binding energy. In general, binding energy represents the energy which must be

provided to overcome the forces which hold an object together. The binding energy of a structure formed from two primary defects A and B, is defined as the difference in formation energies

$$E^b(A, B) = E^f(A) + E^f(B) - E^f(A, B) \tag{3.12}$$

This formula expresses the binding energy in terms of the total energies, each of which can be found using a total energy calculation using `AIMPRO`.

Part II

Application

Chapter 4

Native Defects

4.1 Introduction

Experimentally, there is no conclusive evidence regarding a dominant role for native defects in as-grown ZnO [7, 69–71]. However, there is substantial evidence based on calculations of diffusion of native defects, the anticipated impact upon electrical conductivity and Hall Effect measurements which can be interpret as native defects being the predominant defects causing the unintentional electrical conductivity. Regardless of their role in electrical conduction, photoluminescence observations of bulk ZnO commonly show green and blue luminescence, both of which have been widely attributed to native defects [72–74].

Understanding the behaviour of native defects is critical to the successful application of any semiconductor material, especially in compound materials. These defects often affect, directly or indirectly, the doping efficiency, growth of the material, and subsequent device specification. Oxygen vacancies, V_O, zinc interstitials, Zn_i, oxygen interstitial, O_i, and zinc vacancies, V_{Zn} are the primitive forms of native defects in ZnO. Oxygen vacancies and zinc interstitials have been suggested as the source of the commonly observed unintentional n-type conductivity in as-grown ZnO, while oxygen interstitials and zinc vacancies are potential sources of p-type ZnO [13, 20, 75].

Perhaps more importantly in the context of intentional doping with impurities,

there is a significant possibility that combinations of dopants with native defects may affect conduction mechanisms. It is critical to have a good understanding of the structure and electronic properties of these native defects so that their interaction with dopants can be viewed in a broader context.

In this chapter the structure and properties of the simple forms of native defects are presented, as obtained using AIMPRO.

4.2 Results

4.2.1 The oxygen vacancy, V_O

Based upon simple ionic arguments, the native defect V_O might well be expected to be a source of compensation in p-type ZnO doped with group-V impurities. V_O may be envisaged as a host oxygen atom, in the -2 oxidation state, being removed from the lattice. The electrons that would normally be bound to the now missing O atom can be viewed as coming from the four neighbouring Zn sites, half an electron from each. These electrons are still present, at least for an uncharged defect, so the two additional electrons that would have been at the O site mean that V_O is expect to act as a (double) donor. Fig. 4.1 shows the relaxed structure of V_O.

In the neutral charge state the four neighbouring Zn atoms shift inwards by around 10%, forming a pair of Zn–Zn bonds. In the case of the $+1$ and $+2$ charge states, the four neighbouring Zn atoms shift in the opposite direction, i.e. breathe outwards by 3% and 23% respectively. The structures obtained using AIMPRO are in excellent agreement with other theoretical studies [27, 76, 77].

The origin of the different structures may be viewed as a chemical reconstruction in the neutral charge state, and this large geometric effect has an impact upon the electrical properties. The charge-dependent formation energies (Fig. 4.2) indicate a $(0/+2)$ level around $E_v + 1.0\,\mathrm{eV}$, too deep for the production of n-type ZnO. The oxygen vacancy is a deep, negative-U donor, where the $1+$ charge state is never thermodynamically the most stable charge state for any value of the electron chemical
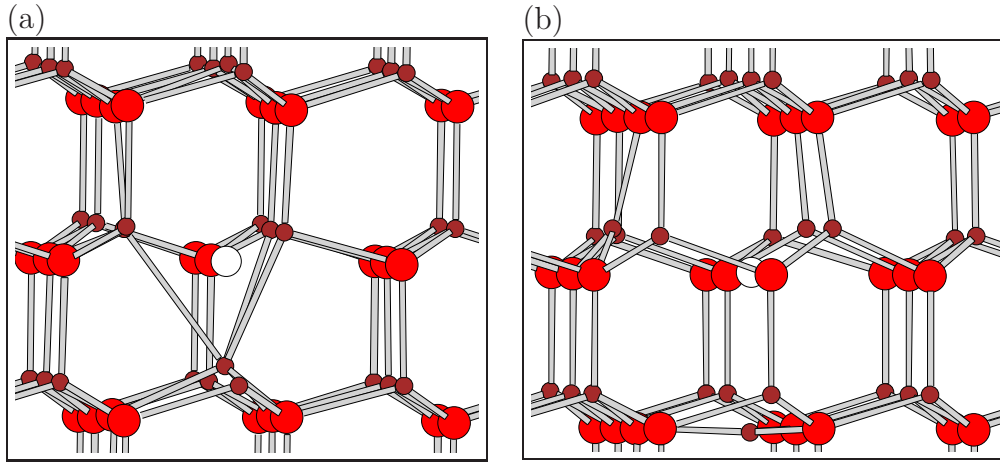
Figure 4.1: Schematics of V_O in (a) the neutral charge state, and (b) the positive (+2) charge state. Red and brown Colours indicated oxygen and zinc atoms, respectively. The white circles indicate the vacated oxygen sites. Vertical and horizontal axes are $[0001]$ and $[01\bar{1}0]$ directions, respectively.

potential. Then, when the Fermi energy is above the $(0/+2)$ level, the defect is in the neutral charge state. When the Fermi energy is below the $(0/+2)$ level, the defect has a charge of $+2e$. The negative-U nature of this centre is a result of the chemical reconstruction in the neutral charge state: indeed, negative-U centres are typically characterised by large structural changes with charge state. It is noted that, in addition to the structural agreement, the donor level is in excellent agreement with the transition level of $E_v + 1.0\,\text{eV}$ of previous calculations [78–80].

The current calculation indicates that neutral V_O has a relatively low formation energy of $\sim 1\,\text{eV}$ under Zn-rich conditions, which is in good agreement with other theoretical calculations [68, 79–81]. In addition, the formation energy is lower in p-type ZnO. This is consistent with the model that under such conditions, V_O centres are formed during growth, compensating the acceptor species and preventing the formation of highly conductive material.

It is worth noting that previous calculations suggest that V_O has relatively high migration barrier of 2.4 eV [27]. This would imply that V_O undergoes little diffusion

at room temperature, but that annealing to higher temperatures may result in the movement of these double donors, and possibly their direct interaction with other defects in the lattice, such as candidate acceptors.
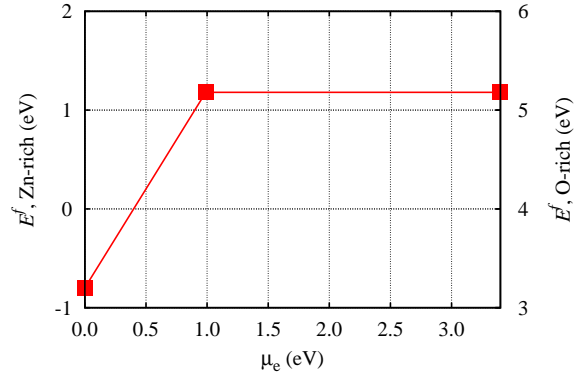
Figure 4.2: Plot of E^{f} *vs.* μ_e for V_O in ZnO calculated using the 192 atom supercell.

4.2.2 Zinc Interstitial Zn_i

Zinc interstitials might, in principle, be another of the sources of the common, unintentional n-type conductivity in as-grown ZnO.

It is understood that there are two main sites for zinc interstitials in the Wurtzite structure: Zn_i at the tetrahedral interstitials site, Zn_i, tet as shown in Fig. 4.3(a), and zinc at the octahedral interstitial site, Zn_i, oct, as shown in Fig. 4.3(b). The difference between the tetrahedral and octahedral interstitial sites can be understood by considering a view of the Wurtzite structure along the hexagonal axes. There are open, six-member channels in the structure, and a location within one such channel approximately equidistant from six oxygen sites is the octahedral interstitial location. In contrast, the tetrahedral location is along a c-axis column occupied by host atoms, so that viewed along the hexagonal axis, the tetrahedral site is eclipsed by host atoms. In fact the tetrahedral site can be viewed as a site along the c-axis projected from a

CHAPTER 4. NATIVE

host site away from the associated host bond, such that it is approximately equidistant from four host oxygen atoms.

It is found that Zn_i, oct is more stable than Zn_i, tet by 1.2 eV, in the +2 charge state, which is in reasonable agreement with previous calculations for this defect centre [27]. Placing the zinc interstitial at an octahedral site induces a noticeable local lattice relaxation, particularly in terms of a strong interaction between the Zn atom and three of the nearest neighbour O atoms. For the additional Zn ion, the six surrounding Zn atoms are moved outward by 0.2Å, the ionic Zn_i-Zn bond distance being calculated to be between 2.36Å and 2.73Å. This is smaller than the value of 2.66Å and 2.81Å for bulk Zn metal (which is hcp in structure and therefore has neighbours at different distances).
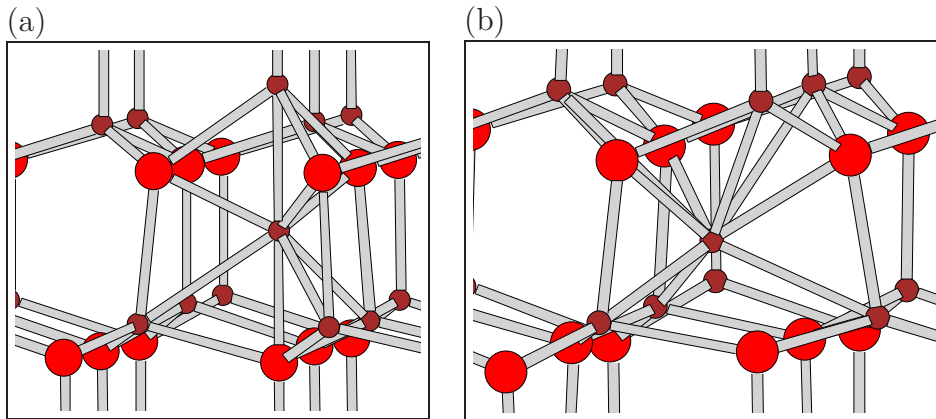
Figure 4.3: Schematics of Zn_i in ZnO (a) at tetrahedral site Zn_i, tet (b) octahedral site Zn_i, oct. Colours and axis are as in Fig. 4.1.

Zn interstitials have a relatively high formation energy in n-type material and are expected to rapidly diffuse with a low migration barrier of about 0.57 eV [27]. The charge-dependent formation energies in the current calculations, plotted in Fig. 4.4, indicate a (0/+2) level above the conduction-band minimum). It is therefore found that the zinc interstitial behaves a shallow donor, which is in agreement with the interpretation of some experimental observations [70,82], although its thermodynamic stability might well be questioned.

CHAPTER 4. NATIVE

Based upon the calculated energy of formation and migration barrier, Zn inter-
stitials are not expected to be stable in pure ZnO at room temperature [83], and are
thus unlikely to be responsible on their own for unintentional n-type conductivity
under equilibrium conditions. On the other hand, the zinc interstitial can diffusion
relatively freely due to its low barrier, and thus may cause it to find other sites such as
V_O to form Zn_O or be attracted Coulombically to with negatively charged impurities
which can form a complex with sufficiently high binding energy. This interaction may
provide a mechanism to play a role in the unintentional n-type conductivity of ZnO
5.3.5.
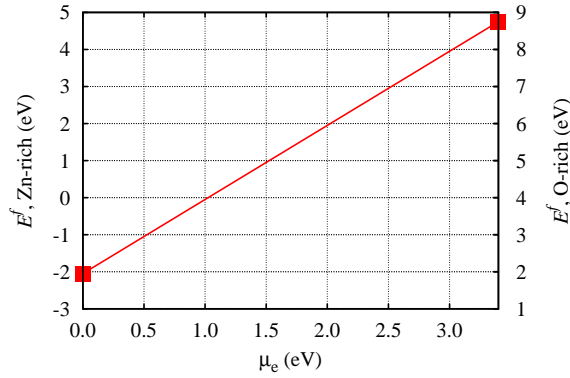
Figure 4.4: Plot of E^f *vs.* μ_e for Zn_i defects in ZnO calculated using the 192
atom supercell.

4.2.3 Oxygen Interstitial O_i

As with the zinc interstitial, there are two type of non-bonded oxygen interstitial
O_i sites in the w-ZnO: O_i at tetrahedral O_i, tet or octahedral site O_i, oct. It is
found in these calculations that O_i, tet is unstable and relaxes into a split-interstitial
configuration as shown in Fig. 4.5(a), $(O_2)_O$.

In this case, the O-O bond length was calculated as 1.46Å, which is in good
agreement with other theoretical calculations 1.46Å [77], and the experimental value of
1.49Å for gas phase O_2^{2+}. Oxygen at the octahedral site O_i, oct is shown in Fig. 4.5(b),
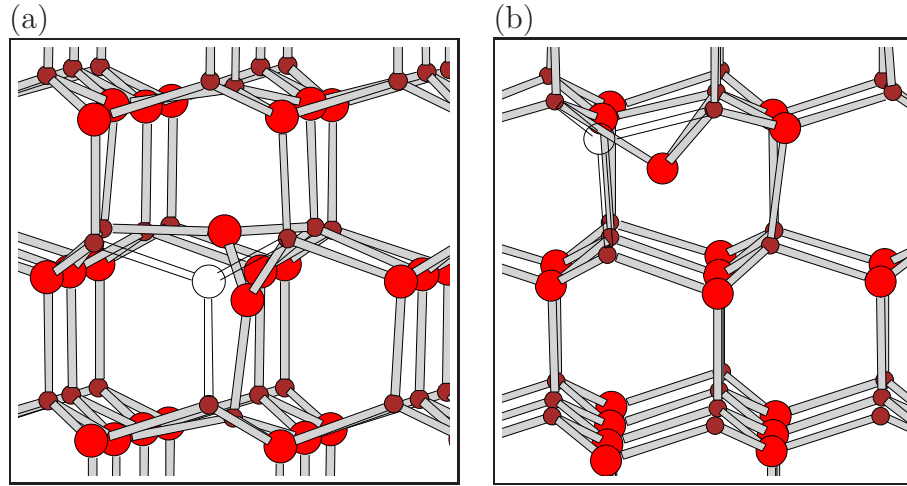
Figure 4.5: Schematics of O_i in ZnO (a) starting from the tetrahedral site O_i, tet, and (b) the octahedral site O_i, oct. Colours and axis are as in Fig. 4.1. Atoms and bonds that would otherwise obscure the structure of the interstitials are shown in outline for the sake of clarity.

which introduces states in the band-gap that could accept two electrons. For the neutral charge state the total energy for O_i, oct is higher by $1.66\,\mathrm{eV}$ than that of the $(O_2)_O$, while O_i, oct site is lower in energy for negative charge states. This is in good agreement with other theoretical calculations [20, 27, 84]. The Zn-O_i, oct distance calculated to be 2.19Å, somewhat greater than the 1.98Å for the host Zn–O bond-length.

The charge-dependent formation energies, Fig. 4.6, indicate a $(0/+1)$ level around $E_v + 0.3\,\mathrm{eV}$, and therefore will not contribute to n-type conduction in ZnO. The electrical level of the split-interstitial are derived from anti-bonding $pp\pi^*$ state from a molecular orbital of the isolated O_2 molecule. This explains the O–O bond length for split interstitial which longer than the O_2 molecule.

Oxygen at the octahedral site introduces states in the band-gap that can accept two electrons, so transition levels of O_i, oct $(0/-1)$ and $(-1/-2)$ are located at $0.5\,\mathrm{eV}$ and $1.4\,\mathrm{eV}$ above the valance-band maximum, respectively. These levels are derived from the empty partially $2p$ orbitals of O_i.

CHAPTER 4. NATIVE
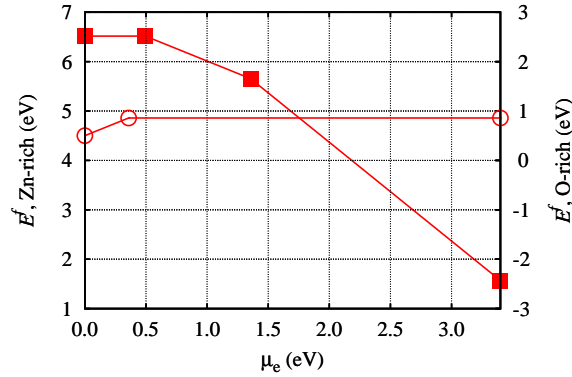
Figure 4.6: Plot of E^f *vs.* μ_e for O_i, oct ($\blacksquare$), O_i, tet (O). The energy is calculated using the 192 atom supercell.

Previous calculations have determined that oxygen interstitials have a relatively low migration barrier: $0.9 \, \text{eV}$ for O_i^0 (split) and $1.1 \, \text{eV}$ for O_i^{2-} (oct) [27]. If such species are present in the material, they may reduce the concentration of V_O donors even at modest temperatures. Alternatively they may be electrostatically attracted to impurities and form a complex with, for example, group-V elements. This interaction may provide a mechanism to play a role in the p-type conductivity of ZnO, as shall be presented in section 5.3.9.

4.2.4 Zinc Vacancy V_{Zn}

The relaxed structure of V_{Zn} for the neutral charge state is shown in Fig. 4.7(a). The oxygen atoms around the zinc vacancy shift outward by about 3% with respect to the equilibrium ZnO bond length. For the negative charge state, $(V_{Zn})^{-1}$, there is a similar relaxation. However, for $(V_{Zn})^{-2}$ there is a much more substantial relaxation. Based upon the location of the ideal site of the zinc at that has been removed, in the fully ionised form the the 'V–O' distance is calculated to be 1.98Å in the a,b-plane, but 2.57Å in c-direction, as shown in Fig. 4.7(b).

Fig. 4.8 shows a plot including the formation energies (Eq.3.9) of V_{Zn} in ZnO. This yields a double acceptor level, in line with previous calculations [24, 27, 84, 85].

(a) (b)
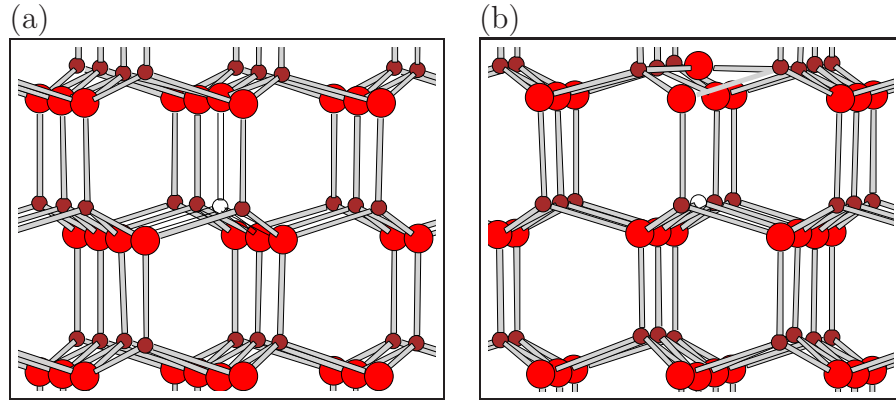
Figure 4.7: Schematics of V_{Zn} in ZnO (a) at neutral charge state (b) in (-2) charge state. Colours and axis are as in Fig. 4.1.
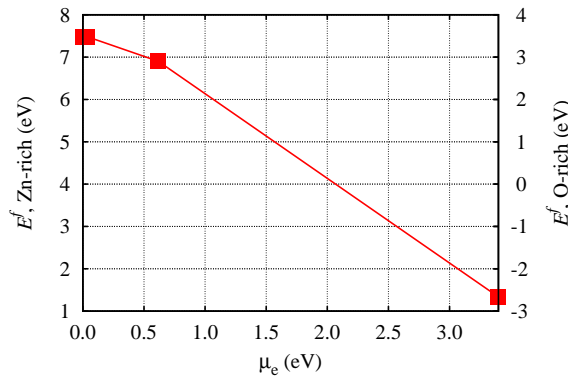
Figure 4.8: Plot of E^f *vs.* μ_e for V_{Zn} defect in ZnO. The energy is calculated using the 192 atom supercell.

The $(0/-1)$ transition level is located around $E_v + 0.1\,\text{eV}$ and the $(-1/-2)$ transition level around $E_v + 0.6\,\text{eV}$ above the valance band top, both of which are also in good agreement with other theoretical calculations [27, 84, 86].

Neutral V_{Zn} centres have a very high formation energy, being about $3.5\,\text{eV}$ in the neutral charge state even under under O-rich conditions. In n-type material the formation energy is lower. However, the equilibrium concentration might be expected to be low, and in which case they will not play a role in p-type conductivity of ZnO, as sometimes has been suggested [25, 29, 87].

4.2.5 Zinc antisite Zn_O

Finally, the zinc antisite defect is reviewed. This consists of a zinc atom substituting for an oxygen host atom. The relaxed structure of Zn_O for the $+2$ charge state is shown in Fig. 4.9.
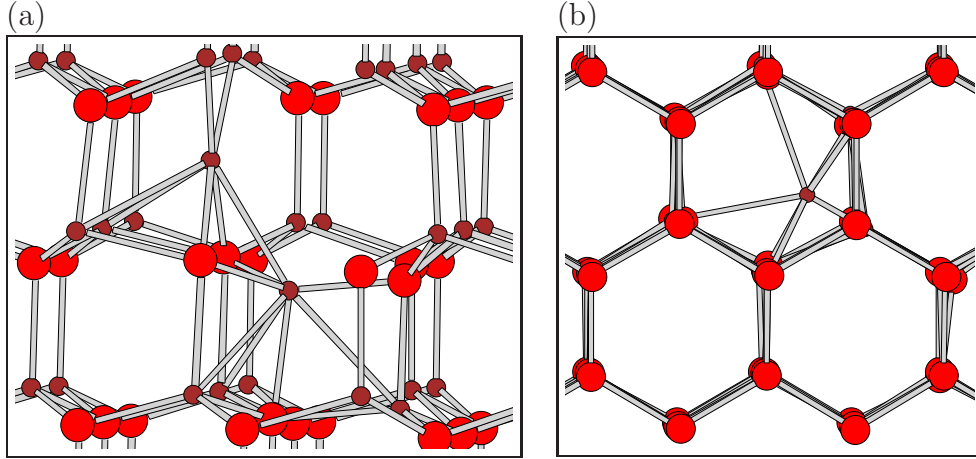
Figure 4.9: Schematics of Zn_O in ZnO. Colours are as in Fig. 4.1. (a) and (b) show views along $[2\ \bar{1}\ \bar{1}\ 0]$ and along the hexagonal axis, respectively.

After optimisation, in the $+2$ charge state structure the Zn_O–O distance is calculated to be 2.20Å, which is larger than the host Zn–O bond length by about 10%. As ZnO is a hexagonal material, there are two different Zn_O–Zn distances: three Zn_O–Zn distances are calculated to be 2.4Å, and another two Zn_O–Zn distance of 2.80Å. These values are in good agreement with other theoretical calculations [27,77].

Fig. 4.10 shows a plot of the formation energies (Eq.3.9) of Zn_O in ZnO. Only the $+2$ charge state is thermodynamically stable in the band-gap. Perhaps more significantly, although the zinc antisite has a high formation energy in n-type, O-rich material, they would be highly favourable in Zn-rich, p-type material. Such centres, being shallow double-donors must be considered to be a plausible compensation centre.
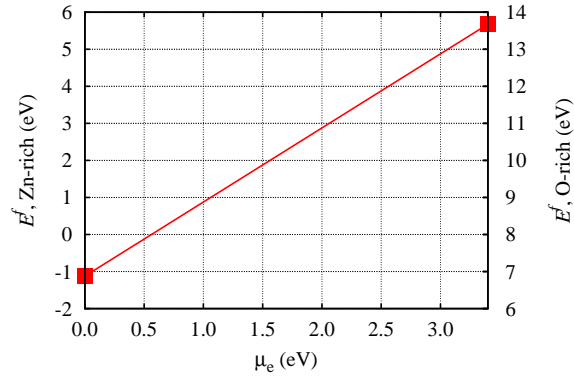
Figure 4.10: Plot of E^f *vs.* μ_e for Zn$_O$. The energy is calculated using the 192 atom supercell.

4.3 Summary

To facilitate comparison between the various forms, the results of the formation energies for native defects are summarised in Fig 4.11.

As one might expect, in oxygen-rich material, V_{Zn} and O_i centres dominate. Both act as acceptors, but as O_i can chemically react with the lattice to form covalent bonds with host oxygen, this can also be a donor. Under equilibrium conditions, a combination of O_i and V_{Zn} would be expected to yield compensated material. The chemistry resulting in the covalent bond in the neutral charge state of O_i is an important qualitative effect that shall be seen to be significant in the case of impurity doping.

In Zn-rich material, V_O, Zn_i and perhaps surprisingly, the Zn antisite is favoured. All of these centres are donors, but in the cases of the antisite and Zn_i the donor levels are shallow. Although it is inadvisable to rely upon these energies exclusively, the calculations here, and from previous reports, are consistent with the potential role for native defects as shallow donors to generate n-type conductivity in as-grown material.

(a)

(b)
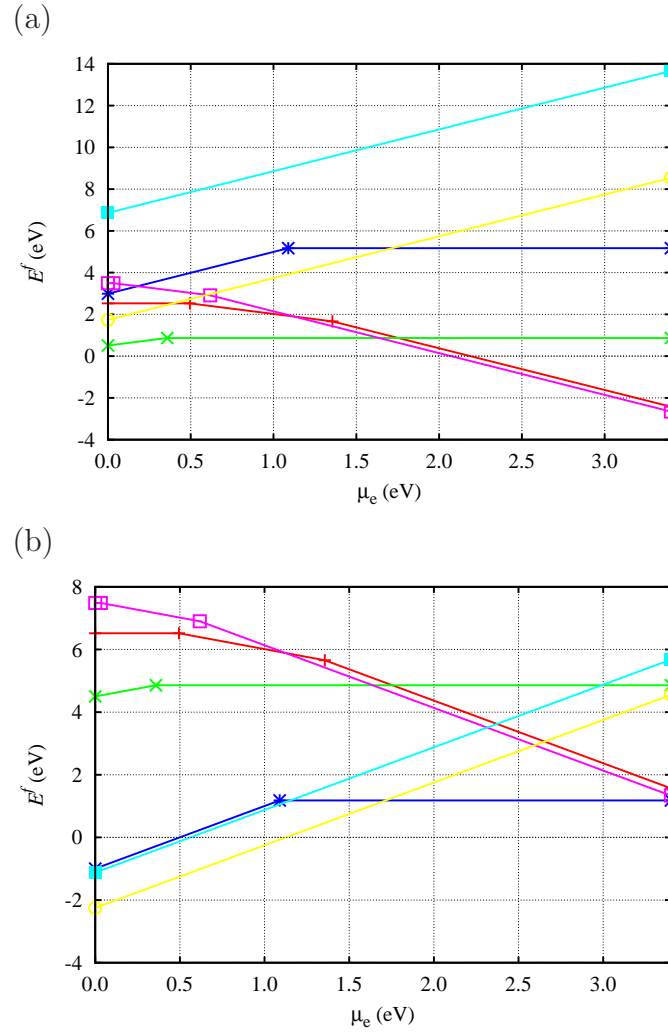
Figure 4.11: Plot of E^f *vs.* μ_e for the native defects for ZnO. The energy is calculated using the 192 atom supercell: $V_O(*)$, $O_i(\text{split})(x)$, $O_i(\text{Oct})(+)$, $Zn_i(\text{Oct})(O)$, $Zn_O(\blacksquare)$, $V_{Zn}(\square)$. (a) Oxygen-rich conditions (b) Zinc-rich conditions

Chapter 5

Nitrogen Doping ZnO

5.1 Introduction

Nitrogen, having one fewer valence electron than oxygen, is a natural choice for the production of p-type ZnO by formation of nitrogen substitution on the oxygen sub-lattice, N_O. There are several ways to prepare zinc oxide thin-films where nitrogen impurities are introduced with the aim to obtain p-type conductivity. These include chemical vapour deposition [88], metal organic chemical vapour deposition (MOCVD) [89], pulsed laser deposition [90], molecular beam epitaxy [11], and sputter deposition [91]. Each method produces a different set of challenges with respect to its use in the manufacture of semiconductor electronic devices, including growth temperature (thermal budget), cost and resulting film quality including crystallinity and stoichiometry. There are many sources of nitrogen and oxygen containing molecular groups that are used for the preparation of these films including NH_3, N_2O, N_2, NH_4NO_3, NO, NO_2, and Zn_3N_2. Encouragingly, based upon these standard growth techniques and source materials in some cases there has been success in getting films of p-type conductivity [11, 18, 92–96]. However, the conductivity obtained is not uniformly good, with carrier type, concentrations and mobilities depending not only upon the details of the growth species, but also upon growth temperature and any subsequent thermal treatments.

For example, typically where ammonia (NH_3) is used as the nitrogen source, the resulting ZnO is n-type, where it is thought that a combination of hydrogen and oxygen vacancy defects (see Chapter 4) act as donors, the role of NH_3 being to cause a reduction in the oxygen concentration in the samples and increase the concentration of shallow hydrogen donors [97], rather than insertion of electrically active nitrogen within the lattice. Even so, experimentally it has been shown that both N_2 and NH_3 dopant sources do lead to increased nitrogen incorporation [19, 97–100]. It is thought that nitrogen diatomic molecule dopants, N_2, are very easily incorporated within the the ZnO thin films, and as it is difficult to break the N–N triple bond, they do not dissociate and therefore do not produce any N_O acceptors. Instead they may actually lead to additional n-type conductivity by N_2 molecules either inserting as interstitial species or substituting for oxygen, generating a modified oxygen vacancy (the N_2 electron states lie deep in the host valence band) [101, 102].

Perhaps significantly, many experimental studies have indicated that the use of NO, NO_2, or a mixture of these species can be activated, to produce p-type material [18, 103]. Experimental investigations have also produce evidence that doping with a high level of oxygen is more successful in producing p-type material with nitrogen [95], as well as other group-V dopants: phosphorus [23, 93, 104] and arsenic [96]. In oxygen rich conditions it is the zinc substitutions that may be more significant, or the suppression of the formation of donors based upon the oxygen vacancy may be key.

Independent of the origin of the doping problems, it is the reproducibility and thermal stability of nitrogen doping that leads to key challenges in its use in real devices applications. For example, the important issue for optoelectronic devices is how to fabricate both high-quality p-type and n-type ZnO films to manufacture p-n junction based photo-diode or LED structures; it is relatively easy to dope the material to produce high quality n-type ZnO [19], but the challenge is how to dope p-type, and it is this that forms the central question in this study. This chapter aims to explain the mechanism of interaction between the nitrogen containing structures combined with host species that may occur within the film, and proposes why there

is success in producing p-type material in some cases and failure in others. For each defect made up from nitrogen atom(s) both with and without native defects (zinc and oxygen vacancies, zinc and oxygen interstitials), the structure (atomic geometry), electronic, electrical and for selected defects vibrational properties will be presented in this chapter.

Before the results of the current calculations are presented, first previous theoretical data pertaining to N-containing defects in ZnO will be reviewed in section 5.1.1, followed by a more detailed review of the key experimental observations in section 5.1.2.

5.1.1   Theoretical background

According to many recent first-principles density-functional based calculations [13–15, 20] when nitrogen substitutes for a host O-site (N_O), unfortunately it does not yield a shallow acceptor level, but instead is a hyper-deep acceptor with an ionisation energy of 1.6 eV calculated by screened exchange and hybrid density functionals, which include different fractions of Fock exchange and range separation in the hybrids [15], or a deep level at $E_v + 0.4$ eV [13, 14, 20], depending upon the specific type of theory used. On the other hand first-principles density functional calculation with the MBPP code and LDA-PP of dopant elements at grain boundaries in ZnO, suggested that N_O *is* a shallow acceptor [32]. The consensus seems to be that N_O is not a good candidate for p-type ZnO.

Independent of the detailed location of the acceptor level, nitrogen acceptors may be electrically compensated via the formation of complexes such as with oxygen vacancies (V_O), zinc interstitials (Zn_i), and other N-based defects such as interstitial nitrogen molecules [13, 20, 30]. As explained in Chapter 4, V_O is a deep, negative-U double-donor, where the $+1$ charge state is thermodynamically unstable [20, 76, 77].

First-principles calculations also show that Zn_i are shallow donors but with a high formation energy in n-type ZnO [77], but a low migration barrier of 0.57 eV [27]. Nitrogen molecules (N_2) on the O site are suggested to be an important compensating double donor as well [20, 30]. Finally, other native defects such as zinc vacancies (V_{Zn})

and oxygen interstitials (O_i) are reported to be acceptors [27, 86], so combinations of N_O acceptors with these centres may result in stabilisation of an shallow acceptor level.

Finally, the N_O acceptor may undergo a chemical reaction with a nearby oxygen site, forming a double donor [13]. This is one of the well known AX centres, which are characteristic of the removal of electrons from the standard ionic arrangement because they are taken up in the formation of new covalent bonding. It will be shown in this chapter that the formation of covalent bonds is an important route to the formation of thermodynamically stable, N-containing point defects.

5.1.2   Experimental background

There are many techniques used in the experimental investigation of semiconductors which reveal different types of data regarding the activity and structure of dopants. Amongst them are electron paramagnetic resonance (EPR), optical-detected magnetic resonance (ODMR), X-ray photo-electron spectroscopy (XPS), X-ray diffraction (XRD), photoluminescence (PL) and vibrational mode spectroscopy (Raman and IR-absorption). In addition, films can be electrically contacted and through current-voltage and capacitance-voltage characterisation the electrical properties of the material can be obtained including carrier concentrations (and types), electrical levels and carrier mobilities.

Amongst the experimental observations, there is some evidence to support the candidacy of nitrogen for p-type doping [11, 18, 92–96].

EPR is a potent methodology for defects that possess a net electron spin. It can not only determine absolute concentrations, it is chemically sensitive in the event that defects are constituted from atomic species with nuclear spins, such as nitrogen, and can reveal symmetry and even the nature of the electron states. EPR studies of N-doped ZnO have produced dominant centres which are interpreted as being molecular nitrogen and isolated nitrogen acceptors on the oxygen site (N_O) in single crystals of ZnO where the samples have been grown with N_2 gas source [105]. At low temperature,

the EPR spectrum assigned to the molecular species has a hyperfine interaction where the principle direction is parallel to the hexagonal c-axis, the centre being assigned to N_2^{-1} molecules substituting for O-site. Upon annealing in the 600–800°C, EPR data also indicates that there is an increase in the number of nitrogen acceptors, possibly suggesting a conversion from one form of N defect to simple substitutional N, under the assumption that this is the dominant acceptor. In addition, ODMR [106] has been reported that shows that there are defect centres seen in N-doped material where N-related EPR is seen, which is in a spin triplet ($S = 1$) state.

PL data can also be used to determine useful microscopic information about the state of N in doped films. However, just as the paramagnetic resonance is limited to detection of unpaired electron spins, PL may be viewed as suffering from two critical problems. First, as luminescence is a competitive process, it is the most efficient emitters in the sample that are the centres that seen in practice, even if they are not the dominant structures. Secondly, in most cases it is not trivial to determine the chemical nature of the emitting centre, although by careful variation in the isotopic concentrations of chemical species in the materials, the presence of specific chemical constituents can be inferred. Where PL emission corresponds to energies close to free exciton emission, the depth of the states associated with the emission defects can be determined. In such a way, experiment suggested that nitrogen produces an acceptor level lies between $E_v + 100\,\mathrm{meV}$ and $E_v + 300\,\mathrm{meV}$ after nitrogen doping followed by annealing at $520\,°\mathrm{C}$ in an O_2 ambient [14, 107–110]. The PL peak at $3.22\,\mathrm{eV}$ is attributed to a donor–acceptor transition with acceptor ionisation energy of $195\,\mathrm{meV}$, and the acceptor suggested to be nitrogen [111]. The connection with nitrogen dissolved in the lattice is not unambiguous. Some research indicates that the acceptor level between $E_v + 100\,\mathrm{meV}$ and $E_v + 130\,\mathrm{meV}$ may be related to stacking faults of undoped ZnO [112, 113].

A blue-green defect-related emission has been explained within the context of transitions involving self-activated centres formed by a double ionised zinc vacancy and an ionised interstitial zinc [114], oxygen vacancies [13, 73, 115, 116], or donor-acceptor

pair recombination involving an impurity acceptor, and/or interstitial oxygen. The broad photoluminescence emission centred at around 1.6 eV, and red emission around 1.9 eV can be observed in ZnO:N and has been attributed to N-related defect states. Also in N-doped material is a green emission band in the range from 2.1–2.4 eV in p-type ZnO:N. It will be shown in this chapter that one possible explanation for this may be due to combinations of native defects compensating N-related acceptors.

IR absorption measurements on N-doped ZnO show several peaks significantly higher in frequency than the one-phonon maximum of the ZnO host. Recent X-ray photo-electron spectroscopy (XPS) experiments [117] found evidence for N-pairs as the spectrum exhibits a peak corresponding to the energy of free N_2 molecules. IR absorption and Raman spectroscopy measurements on N-doped ZnO show several peaks in the frequency range of 335–995 cm^{-1} [118], as well as high frequency 1800–2000 cm^{-1} characteristic of covalent bonds involving low mass species [119]. Indeed, the higher vibrational frequencies are close to those of free diatomic molecules such as N_2 and NC, and significantly higher than the phonon frequencies of the ZnO host.

Finally, it is important to reflect upon how conclusive the evidence is for the substitution of oxygen by nitrogen. Perhaps the most commonly quoted evidence comes from X-ray techniques. X-ray absorption near-edge spectroscopy (XANES) and photo-electron spectroscopy (XPS) have been interpreted as indicating that the nitrogen atoms incorporate substitutionally at the O sites, N_O, to act as acceptors [101, 117, 120] because the peak position at 395.8 [120] is in line with the N-peak in N–metal systems in the 396-397 eV range [121] and in Zn_3N_2. Additional XPS peaks at 403–406 eV and 399.5 eV have been interpreted as being related to N–O and N–N molecular species when nitrogen incorporation ZnO at low temperature [117, 120, 121]. Although peak positions are usually very good indicators of the state of a given chemical species in XPS, the technique is not a proof. The position of the x-ray peak indicates the energy required to remove an electron from the core state, and therefore is a reflection of the confining potential and/or oxidation state of the defect. In principle, two different types of environment may give rise to very similar emission

energies, and one should view the assignment of chemical environment from XPS as indicative and not a proof.

The experimental evidence for the state of N in ZnO has, unfortunately, not led to a detailed understanding of the state of N in these films. It is then the role of atomistic modelling in the light of the experimental evidence to develop a model for the most likely state of N in ZnO as a function of growth conditions and source species. In the following section, the results of AIMPRO simulations of N associated with both the oxygen and zinc sub-lattices, and where possible the properties are compared with experiment.

5.2 Result

The presentation of the results is divided into sections. First, in section 5.3, the defects most closely related with the oxygen sub-lattice are presented. Then, in sections 5.4 and 5.5 those defects associated with the Zn sub-lattice and interstitial to the ZnO lattice are presented. Finally, all N-defects examined are reviewed together, and some overall conclusions are drawn in section 5.6.

5.3 Nitrogen associated with the oxygen lattice

The covalent radius of nitrogen is almost equal to that of the the oxygen atom [122], so most researchers initially focused on nitrogen substitution of this element. According to the x-ray absorption spectroscopy, based upon the emission energy corresponding to N in Zn_3N_2, it was verified that N occupies the O substitutional site [123]. Since nitrogen has one fewer valence electron than the oxygen atom it replaces, it is expected that N_O will be an acceptor, and indeed this is what is found.

5.3.1 Nitrogen substituting for an O site, N_O

There are at least four different gases, N_2, NO, NO_2 and N_2O, that can be used as a source for nitrogen doping of ZnO. The N_2 and N_2O gases contain pairs of N atoms that can be incorporated directly into the growth surface to form $(N_2)_O$ or other stable structures containing a nitrogen molecule. However, this is not considered to be the best option because additional energy must be supplied to break the N-N bonds before isolated N_O can be formed. In contrast, alternative gases such as NO and NO_2 contain a single N atom which can be incorporated directly into the growth surface to form N_O defects, and O atoms as host atoms.

N_O was constructed to find the stable structures resulting from this substitutional, the type of conductivity, and the location of the states in the band-gap. The first characteristic to review is the geometry.

Structure Details
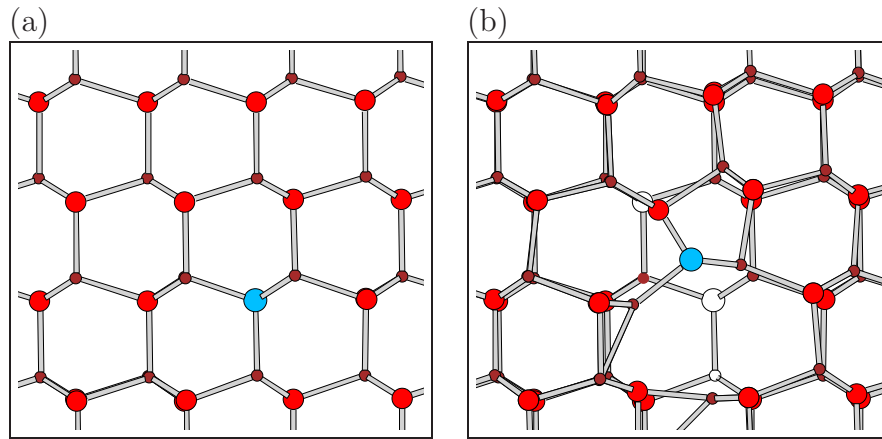
Figure 5.1: Schematics of the relaxed structures of N_O in (a) the neutral charge state and (b) the AX-structure stable in the positive charge state. Here brown, red and blue sites represent zinc, oxygen and nitrogen, respectively. The vertical and horizontal axes are [0001], and [01$\bar{1}$0]. In (b), the unrelaxed, ideal sites for the atoms involved in the reconstruction are shown in outline.

The stable structure obtained for neutral N_O is shown in Fig. 5.1(a). The nitrogen remains on-site and, resulting in an approximately tetrahedral defect, where the four Zn neighbours of N_O were found to lie at a distance of 2.0Å which is similar to the bond length of 2.18–1.94Å [15]. [1]

As N has one fewer valence electron than the O atom it replaces, it is expected that this centre can accept an additional electron and become negatively charged. The negative charge state, the relaxed geometry closely resembles that obtained for the neutral charge state, but with slightly shorter N–Zn "bonds" at 1.9Å which is close to the bond-length of 1.9Å found in previous calculations [15].

It is perhaps worthy to note that the N–Zn bond-lengths in both charge states where the N-atom remains on-site are shorter than the 2.0–2.3Å in Zn_3N_2, but close to the Zn–O bond-lengths of bulk ZnO.

In addition to the simple, on-site substitution, it is known [13] that upon removal of an electron there is a possible chemical interaction between the nitrogen atom and a next-nearest-neighbour oxygen atom. This substantial re-organisation of the bonding is termed the AX centre [13]. In addition to creating an N-O bond, an O-Zn bond is broken, as shown in the relaxed structure obtained using AIMPRO, Fig. 5.1(b). As ZnO is a hexagonal material, there are several distinct types of second-neighbour site by symmetry. It is found in this study that the more energetically stable structure is that shown in Fig. 5.1(b). The alternative structures where the N=O bond is in the basal plane is found in this study to be around 0.32 eV higher in energy. The approximately c-axis orientation as the most stable orientation is at odds with those of the first report [13].

In addition to the orientational energy variation for the AX^+ structure another key energy is the difference in energy between the on-site and the reconstructed AX forms in this charge state. Park *et al.* reported this to be just 0.13 eV in favour of

---

[1]Note, in hexagonal materials, the highest point group symmetry possible for a substitutional impurity is C_{3v}, with a set of three equivalent neighbours and one unique neighbour along the hexagonal axis. In the case of on-site N_O, the difference in the bond-lengths is less than 0.05Å.

the on-site form. In the current study where larger unit cells are used, the relative energy is found to be $0.5\,\mathrm{eV}$ based upon the energy difference between in basal-plane form of the AX^+ centre, and $0.2\,\mathrm{eV}$ in terms of the more stable form. The on-site $\mathrm{N_O}$ structure is therefore found to be the more stable form, even in the positive charge state, but the energies involved are relatively small.

The chemical reconstruction releases two electrons into the band-gap in the neutral charge state, although the AX-structure was found to be unstable in the neutral charge state, with the N-O bond spontaneously breaking to reform the on-site $\mathrm{N_O}$ structure.

The substantial structural rearrangement can be viewed as the formation of a N=O molecular group within the ZnO lattice, and the band-gap levels are highly characteristic of π^*-interactions. Thus, the energetic favourability can be correlated with the relatively more energetically stable covalent interactions that are gained relative to the most ionic interactions for the on-site structure. The neutral charge state is then not stable in the AX form because of the energy penalty of placing an electron either in the conduction band or a π^* molecular state.

Electrical levels
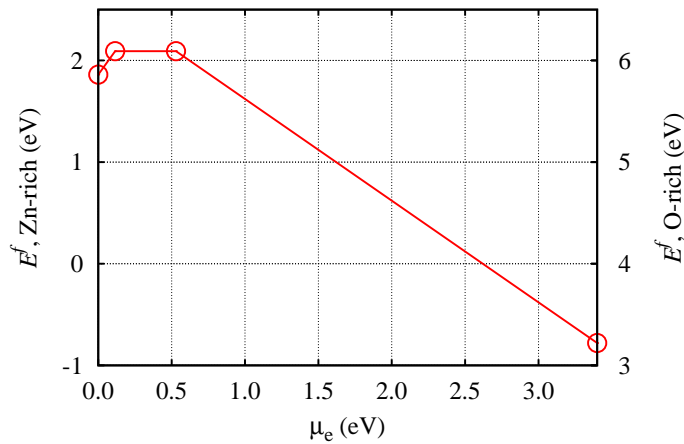
Figure 5.2: Plot of E^f *vs.* μ_e for $\mathrm{N_O}$ in ZnO calculated using the 192 atom supercell.
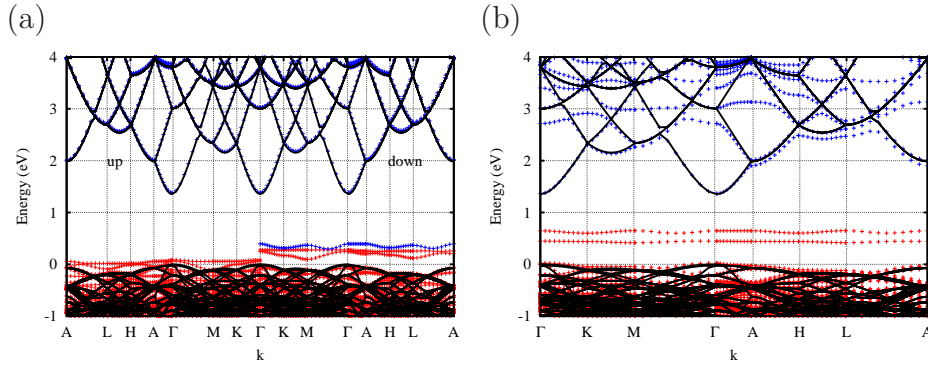
Figure 5.3: Band structures for (a) on-site N_O, and (b) the chemical recon-structed AX^{+1} structure, where the zero of energy is set to be the valance band top for bulk ZnO. Red and blue crosses indicate filled and empty bands, respectively, while black lines indicate the comparable bands of defect free ZnO.

Fig. 5.2 shows a plot of the electron chemical-potential dependent formation ener-gies (Eq. 3.9) of N_O in ZnO. As described in section 3.9, the formation energies can be used to yield an acceptor level, which is calculated at around $E_v + 0.53$ eV, which is in reasonable agreement with previous calculations using similar approaches [13, 14, 20]. This relatively deep level is at odds with the hyper-deep levels predicted in other calculations, as summarised in section 5.1.1 based upon different methods [15, 32]. Nevertheless, even the 0.4 eV estimate of the acceptor level is too deep to explain p-type conductivity seen in N-doped ZnO, and it seems a reasonable conclusion to draw that another source of holes is likely to be responsible for p-type doping. The donor level of N_O is calculated at around $E_v + 0.12$ eV which is close to the valance-band top.

The acceptor level of N_O is further illustrated in Fig. 5.3, which shows the band-structure along a high-symmetry directions in the Brillouin-Zone. There is an empty band following the valence-band top, consistent with the calculated location of the acceptor level determined using the formation energies. The positive charge state of the on-site structure may also be stable, but the donor level is close to the valence

band top in the calculations, and is therefore not of any practical importance.

Combining the formation energy and band structure data strongly suggests that nitrogen substitutional oxygen site is thermodynamically stable at neutral and negative charge states. The positive charge state, be it on-site or in the AX^+ form, may be of some interest as a metastable form of the centre, but more significantly, the reconstruction shall be shown in this thesis to become important where additional components to the defect are present.

5.3.2 N_O pairs, $(N_O)_2$

As mentioned above in section 5.3.1, there are many different gas species used in the introduction of nitrogen into ZnO films, including N_2, NO, NO_2 and N_2O. Some of these may be used as an oxygen source as well as a source of nitrogen defects in ZnO for electrical doping. Following the suggestion that N_O is favoured in n-type material [20, 31, 123, 124], the possibility of forming a complex of a pair of nearby N_O centres was considered.

It should be noted that as the number of components in complexes increases, the number of symmetrically distinct combinations that might be envisaged increases dramatically. In the study of N_O-pairs this is increased by there being additionally chemically nonequivalent structures, as will be discussed below. In an effort to provide some confidence that the structures obtained represent minima in the energy surface, the various chemically distinct arrangements found were relaxed independently in a range of charge and electronic spin states. Although it cannot be guaranteed that the approach has found all the energy minima, noting differences in energies obtained for orientationally distinct structures in the AX^+ are of the order of 0.3 eV, one may have confidence that the results presented in this section are accurate at least to this level of uncertainty

Structure Details

The relaxed structures of $(N_O)_2$ with different charge states are shown in Fig. 5.4.

(a)   (b)   (c)
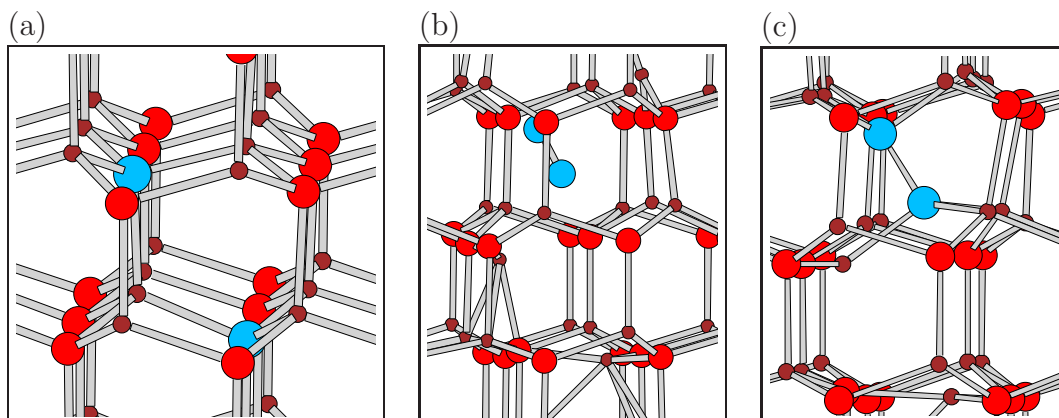
Figure 5.4: Schematics of $(N_O)_2$ in (a) the negative charge state -2 and (b) the positive charge state $+4$ (c) a metastable, AX-like form in the neutral charge state. Colours and axis are as in Fig. 5.1.

Amongst the geometries obtained from the various starting configurations, charge and spin states, relaxation of $(N_O)_2$ resulted in highly perturbed structures.

In the $+4$ charge state, the lowest energy structure obtained can be best described as an oxygen-vacancy associated with one of the sites and a nitrogen molecule, N_2, at the second. This structure is stable or metastable in other charge states, including the neutral. Then, for the molecule the nitrogen bond length was calculated to be 1.53Å in a neutral charge state, which is close to the value anticipated for a N–N single bond while it was 1.11Å in the $+4$ charge state of $(N_O)_2$ which shows an excellent agreement with the experimental value for a triple bond of 1.1Å in a gas-phase N_2 molecule. In the $+3$ charge state the N–N bond-length is slightly longer at 1.17Å, which is probably simply an effect of charging of the site containing the N_2, as a similar effect shall be shown to occur in a related centre in section 5.3.3.

The reconstruction between N atoms in N_O-pairs has a strong resemblance to that of the N_O AX centre (Fig. 5.4(c)) in the sense that there is a reconstruction involving the formation of strong, molecular covalent bonds in preference to ionic interaction, simultaneous with the tendency to form positive charge states. The AX-like form is not the most stable: instead a form structurally related to that in Fig. 5.4(b) is

$0.12\,\text{eV}$ lower in energy, with the V_O component being slightly different in line with what is known for isolated V_O in different charge states (see section 5.3.3).

It is therefore of no great surprise that N_O-pairs are found to preferentially adopt a different structure if they become negatively charged, since individual N_O centres in the negative charge state are close to tetrahedral and on-site. In the case of the $(N_O)_2$ defect where negatively charged, the reconstructed geometry was found to be unstable in the negatively charge state, with the N–N bond spontaneously breaking to form on-site the N_O-pairs. For example, in the -2 charge state of $(N_O)_2$, the N–Zn inter-nuclear distances are 1.90–1.96Å, which closely matches the structure of $(N_O)^-$, as described in section 5.3.1.

As shall now be shown, other charge states are not stable, so in the interests of brevity they shall not be described in detail here.

Electrical levels

As with N_O, the electrical properties of $(N_O)_2$ complexes can be understood through the calculation of the electron chemical potential dependent formation energies, Eq. 3.9.
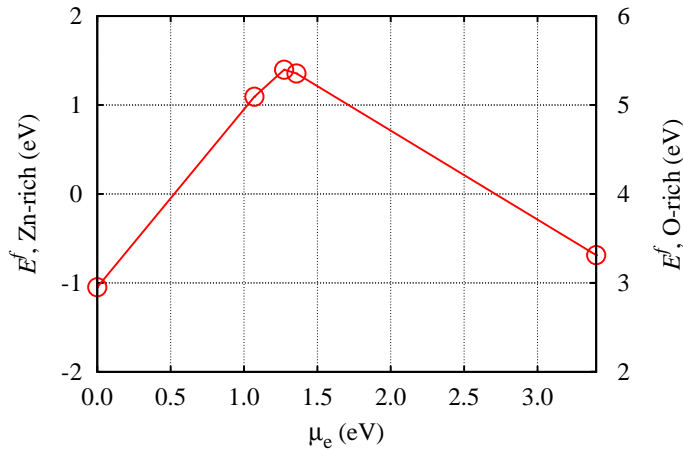
Figure 5.5: Plot of E^f per N atom *vs.* μ_e for $(N_O)_2$ defects in ZnO calculated using the 192 atom supercell.
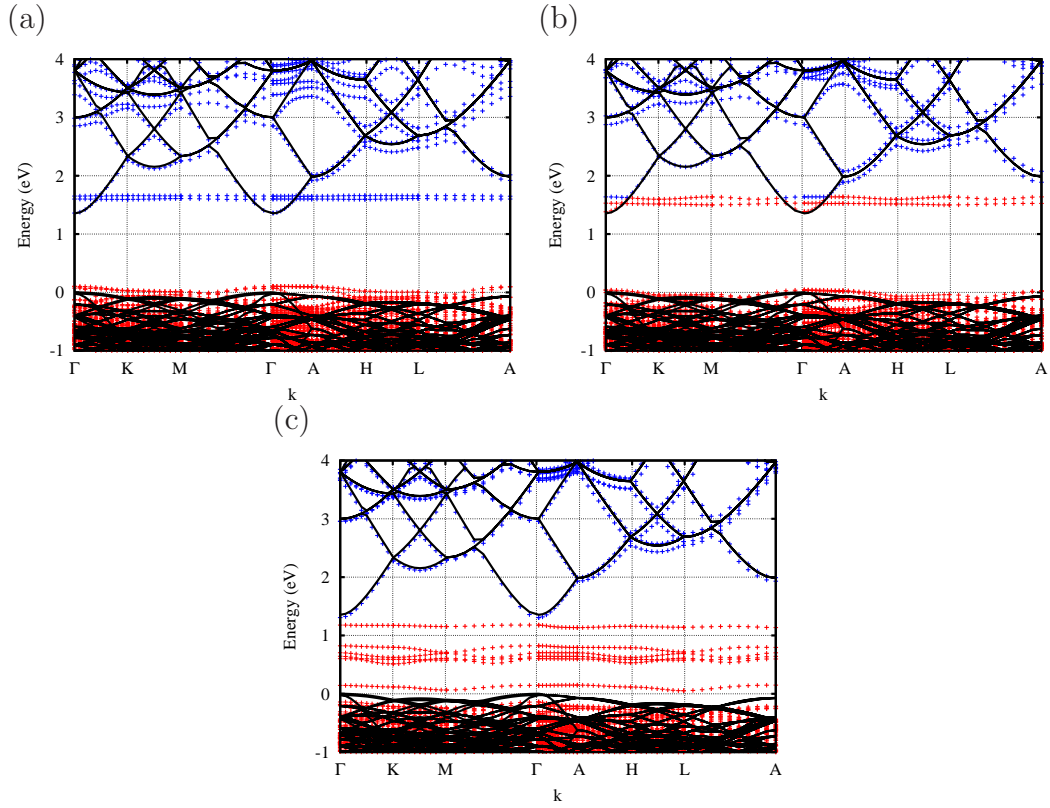
Figure 5.6: Plot of band structure of $(N_O)_2$ in the (a) +4 (figure 5.4(b)), (b) neutral (figure 5.4(c)), and (c) −2 (figure 5.4(a)) charge states.

Comparing the absolute values of the formation of N_O, Fig 5.2, with those calculated for the N_O-pairs, Fig. 5.5, it is clear that the formation energy of the paired defect is significantly lower per N-atom reduced compared to N_O in p-type material, but there is no significant energy impact for n-type material. In addition, $(N_O)_2$ is effectively a deep donor, and would be an energetically efficient compensating defect in material where N is mostly distributed on the oxygen sub-lattice. In equilibrium, therefore, the formation of N_O acceptors, even if they are poor candidates for p-type ZnO, will be expected to compete with the formation of $(N_O)_2$ donors, further reducing the probability of successfully producing p-type ZnO via such a route, due to compensation.

In addition to the lower absolute formation energies, as can be seen from Fig. 5.5,

$(N_O)_2$ is predicted to be a deep negative-U quadruple donor, where only the $+4$, $+3$, -1 and -2 charge states are thermodynamically stable, with the $+4$ and -2 charge states stable over the majority of the band-gap.

Figs. 5.6 and 5.5 show that the transition between donor and acceptor states is associated with the same kind of effects as for isolated N_O centred between the on-site and AX forms. In in the positive charge states the structures can be described as N_2 modified V_O centres neighbouring a second V_O centre, so that the associated band in the gap, and the electrical levels match broadly with those presented for the V_O centre in chapter 4. In the negative charge states, there is an acceptor level following the valence band (figure 5.6(c)) which corresponds to the on-site N_O centres.

Vibrational Modes

If the interaction of N_O centres leads to the formation of N_2 complexes, one might expect there to be a corresponding high-frequency vibrational mode to be resolved in IR and Raman spectroscopies.

However, amongst those calculated for $(N_O)_2$ in the neutral charge state (Fig. 5.4) a low frequency N–N stretch-mode was calculated at $602\,\mathrm{cm^{-1}}$. In material doped with N, there are several experimental Raman bands at around 510, 570 and $642\,\mathrm{cm^{-1}}$ where NO gas was used as the nitrogen source [118, 125]. Other peaks are seen where N_2 is used as a source [126], also lying in this relatively low-frequency spectral range, including peaks at 572 and $586\,\mathrm{cm^{-1}}$ These Raman peaks are not observed in undoped ZnO. Thus, combining the current calculations and the experimental observation, there may be a plausible argument that the formation of a relatively weak N–N interaction such as that seen in the neutral form of the $(N_O)_2$ complex might give rise to one of the many Raman peaks in this range.

However, there are some difficulties with making such an assignment. First, the neutral charge state of $(N_O)_2$ is thermodynamically unstable, although it may be possible that the chemical nature of the neutral centre is related to the source of the $580\,\mathrm{cm^{-1}}$ band. Secondly, the experimental data is rather unclear as to the nature of

the defects formed. Specifically, the presence of N in the vibrational centres is generally inferred from the use of nitrogen in the growth, rather than, say, fine structure consistent with the presence of ^{14}N and ^{15}N isotopes.

Finally, it has been noted that in the positively charged configuration, the N_2 component is structurally very similar to another defect which is presented in section 5.3.3. Given the computational cost of obtaining vibrational modes, those of the structures arsing from $(N_O)_2{}^{+4}$ have not been obtained. Given the clear chemical state of the N-pair, it is assumed that the vibrational properties only involve the N–N force constant.

5.3.3   N-molecule at an O site $(N_2)_O$

As stated before, N is added to the growth species using a wide range of chemical species. Those that contain N–N bonds, such as N_2 and N_2O, may be anticipated to be incorporated into the growing material while retaining the N–N bond. Indeed, it has been widely speculated that $(N_2)_O$ is a common compensating centre in as-grown N-doped ZnO [20, 98, 99, 127].

Structure Details

As with $(N_O)_2$, it is important to take into account that the relatively low symmetry (C_{3v}) of the oxygen site in the host lattice leads to a range of orientationally distinct possibilities when constructing the geometry of a N_2 molecular substitution at this site. By starting with a wide range of atomic configurations, a number of meta stable structures with small differences in total energy were obtained. The lowest energy relaxed structure is shown in Fig. 5.7.

The structure shown in the diagram can be considered as being related to one of the structures found for the substitutional pair, $(N_O)_2$, as described in section 5.3.2. The principal difference between $(N_2)_O$ and $(N_O)_2$ is simply that in the latter case there is an oxygen vacancy in the immediate environment, providing a strong electrical contribution to the properties of $(N_O)_2$. However, in contrast to the electrical
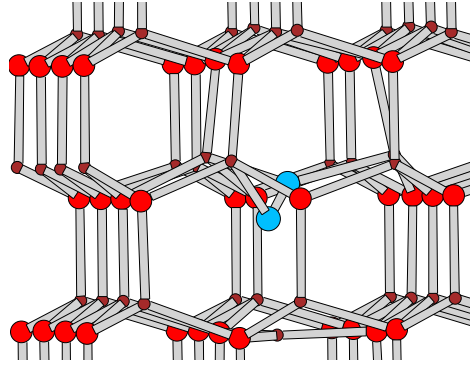
Figure 5.7: Schematic of the structure of $(N_2)_O$ in the neutral charge state. Colours and axis are as in Fig. 5.1.

impact there is only a modest geometric impact. In $(N_2)_O$, the N–N bond length was calculated to be 1.11Å where $(N_2)_O$ is in the overall $+2$ charge state, which is a value in good agreement with the experimental bond length of the free N_2 molecule, which is also 1.11Å, and also in agreement with previous calculations for $(N_2)_O$ [20, 75, 76] and for $(N_O)_2$ in the $+4$ charge state above. Since such a short bond is characteristic of a covalent interaction (a triple bond), the chemical interaction between the two N atoms is very strong compared to that between the nitrogen atoms and surrounding Zn neighbours. Indeed, Zn–N bonding is generally considered to be weak, so one can reasonably interpret the structure of $(N_2)_O$ as that of a modified V_O.

Electrical levels

Following on from the interpretation of the structure as being a modified V_O, one might anticipate that the electrical properties of $(N_2)_O$ parallel those of the native defect (see section 4.2.1). As with the previous centres, the electrical properties of $(N_2)_O$ have been examined by determining the electron chemical potential dependent formation energies in various charge states. Fig. 5.8 shows a plot of this data.

Surprisingly, the formation energies yield both donor and acceptor levels in the band-gap. The donor levels are located at $E_v + 1.6\,\text{eV}$ and $E_v + 1.9\,\text{eV}$ for $(0/+1)$ and $(+1/+2)$ transitions, respectively. These donor levels are in reasonable agreement
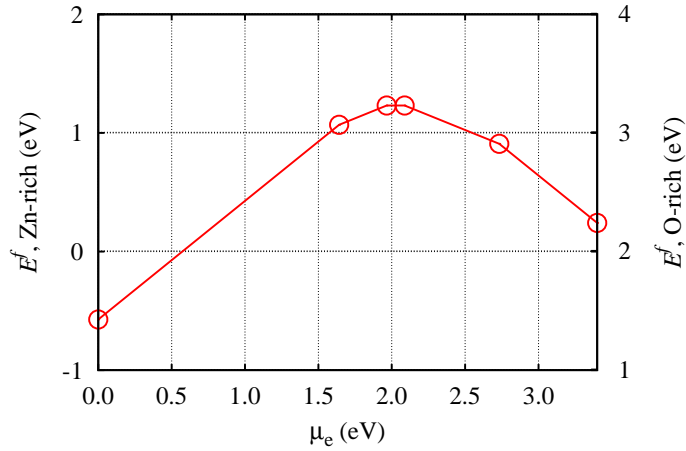
Figure 5.8: Plot of E^f per N atom *vs.* μ_e for $(N_2)_O$ defects in ZnO calculated using the 192 atom supercell.

with other calculations which place them both about $0.2\,\text{eV}$ higher in energy than those obtained for the current study with respect to the valence band top [30]. It is worthy of note that the previous calculations were performed using the much smaller 72-atom supercell, which may well be the source of the differences. Immediately, this is at variance to the levels of V_O which is a negative-U centre where the $+1$ charge state is thermodynamically unstable. However, this could be understood in that in the native centre there is a reconstruction between metal atoms, but the presence of the N_2 molecule in $(N_2)_O$ suppresses this effect.

However, the presence of negative charge states is more of a surprise. The acceptor levels are calculated to lie at $E_v + 2.1\,\text{eV}$ and $E_v + 2.6\,\text{eV}$ for $(-2/-1)$ and $(-1/0)$ transitions, respectively. The location of the acceptor levels corresponds to empty bands in the Kohn-Sham band-structure, as shown in figure 5.9. The origin of the negative charge states is resolved by examination of the localisation of the gap states. In the neutral charge state, there is a doubly occupied band in the band-gap which is mainly derived from the Zn atoms neighbouring the nitrogen molecule. In contrast, the empty levels are derived from $p\pi^*$ orbital localised on the nitrogen molecule.

However, one has to exercise some caution over the interpretation of the acceptor
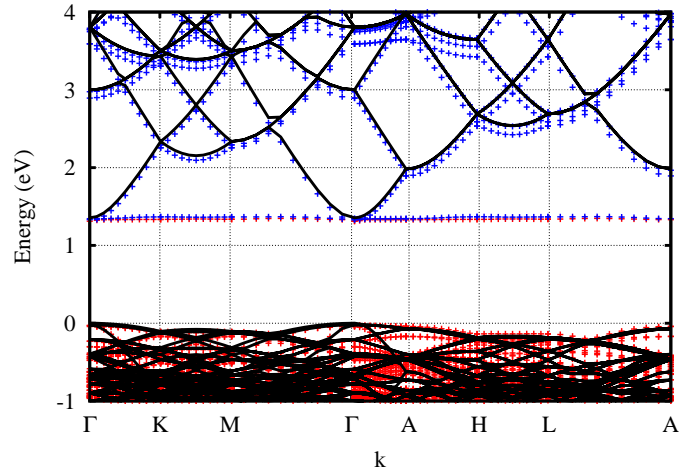
Figure 5.9: Plot of band structure of $(N_2)_O$ in ZnO. Symbols, lines and scales are as defined in figure 5.3

properties of $(N_2)_O$. In terms of band-structure, the electrical levels lie above the theoretical value of E_c, but within the experimental band-gap. However, if the predicted acceptor properties are correctly located within the band-gap, in as-grown N-doped n-type ZnO, the association of the $(N_2)_O$ centres with the n-type conduction must be incorrect.

Even if the acceptor levels are located above the conduction band minimum, the calculated donor levels lead to some difficulty in correlating the presence of $(N_2)_O$ with n-type conduction, as has previously been done [18, 98, 99, 128]. Both the first and second donor levels are predicted to be in the middle of the band-gap, similar to V_O for which there is independent experimental evidence of the deep nature of the donor level [13, 16, 116]. Even given the uncertainty in the calculations, based upon both the current and previous calculations it is unlikely that $(N_2)_O$ acts as a shallow donor.

Vibrational Modes

Since $(N_2)_O$ may be viewed chemically as being comprised from a simple molecular group, it may be fruitful to determine the associated vibrational frequencies that may

then be compared with experimental data. Amongst the local modes of $(N_2)_O$, there are values calculated at 1826, 1947 and 2240 cm^{-1} for neutral, +1 and +2 charge states, respectively, which all correspond to the N–N stretching mode along the N–N axis. These vibrational modes are in good agreement with other theoretical calculations for $(N_2)_O$ at 1537 cm^{-1}, 1852cm^{-1} and 2108cm^{-1} for neutral, +1 and +2 charge states, respectively [30]. The calculated modes are in notable agreement with IR peaks[2] from experiment at 1800, 1942 and 2100 cm^{-1} [129]. These IR features are not observed in the ZnO not doped with nitrogen.

5.3.4 N_O–V_O complexes

It has been speculated that N acceptors are compensated by native donor defects such as V_O, Zn_i, O_i and Zn_O, some of which are calculated to be relatively easily formed on the basis of free energies [13, 20, 75, 130]. Although combinations of all of these native donors with N_O have been considered for this thesis, in this section the focus is upon complexes of N_O with V_O.

Structure and binding energetics

As described in section 4.2.1, in isolated V_O centres the four neighbouring Zn atoms shift inwards by 10% in the neutral charge state, while in the case of +1 and +2 charge states it was found that the four neighbouring atoms shifted in the opposite direction by 3% and 23%, respectively, which is in excellent agreement with other theoretical studies [27,76,77]. Due to the μ_e dependence of $E^f(V_O)$, the formation of these centres is relatively high in n-type ZnO, and much lower in p-type ZnO. Therefore assuming that N_O gives rise to an acceptor level in the vicinity of the valence band top, during growth as N_O is incorporated the probability of the formation of compensating V_O centres is increased. However, another possibility is that it is even more preferable for

---

[2]Although the stretch mode of an isolate N_2 molecule is IR-inactive, when embedded in the ZnO matrix the equivalence of the N atoms is broken, and the stretch mode will in principle become IR-active.

the simultaneous incorporation of both N_O and V_O in close proximity.
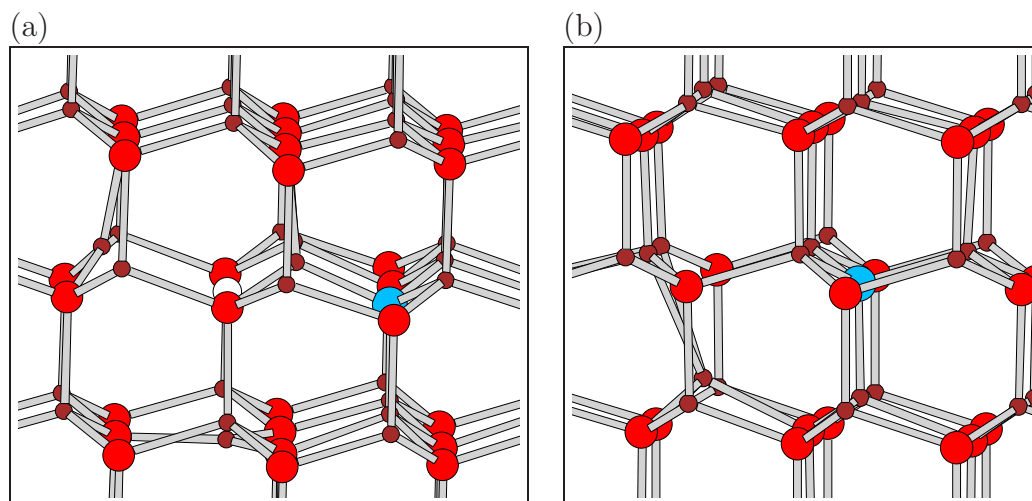
Figure 5.10: Schematics of $(N_O–V_O)$ in (a) the positive charge state, and (b) the negative charge state. Colours and axis are as in Fig. 5.1.

Fig. 5.10(a) shows the lowest energy relaxed structure obtained for $(N_O–V_O)$ in ZnO in both the neutral and positive charge states. In the vacancy component, the four neighbouring Zn atoms shift outwards by 19% in the case of neutral charge state, while in the case of -1 charge state it is found that the four neighbouring Zn-atoms shifted *inwards* by 2%. This is in qualitative agreement with the behaviour of V_O. In the negative charge state of $(N_O–V_O)$ there is evidence in terms of the inter-nuclear distances of the Zn–Zn reconstruction seen in the neutral charge state of V_O, which is lost upon the emission of two electrons.

It is also worth reflecting upon the structure in the vicinity of the N site. Noting that the proximity of the V_O centre lowers the local symmetry at the N-site so that all four N–Zn distances are in general different, the N–Zn distances are calculated to be between 1.85–1.96Å in both the neutral and positive charge states (which are structurally very similar), and 1.90–1.93Å in the negative charge state. These values, although broadly in line with the distances calculated for isolated N_O centres, also reflect the differences in the structures resultant from the relaxation afforded by the proximity of the V_O centre. However, as with N_O these distances are lower than the

N–Zn in bulk Zn_3N_2 which are 2.00-2.29Å, but close to the Zn–O bond-length of bulk ZnO.

Finally, although the structural details hints at some direct interaction between the two components, it is the binding energy (formation energy differences) that is key to the stability of the complex. The binding energies calculated from the formation energies individual defects for the reactions:

$$N_O^{1-} + V_O^0 \longrightarrow (N_O V_O)^{1-} \tag{5.1}$$

$$N_O^{1-} + V_O^{2+} \longrightarrow (N_O V_O)^{1+} \tag{5.2}$$

The binding energy of $(N_O\text{–}V_O)$ is just 0.1 eV for the overall negative charge state, and 0.4 eV in the overall positive charge state. This is in good agreement with previous calculations [76], but the small energies suggests that at growth temperatures, these complexes are unlikely to be thermally stable.

Electrical levels

As described above, V_O is a double donor $(0/+2)$ [27, 79–81, 131], with a donor in the upper part of the band-gap, and in section 5.3.1 it was shown that the acceptor level of N_O lies in the lower half of the band-gap. Therefore, combining these levels $(N_O\text{–}V_O)$ may be expected to give rise to a $(-/+)$ level (and possibly a $(+/+2)$ level), and indeed a $(-/+)$ level is what has been obtained.

Fig. 5.11 shows a plot of the electron chemical potential dependent formation energies (Eq. 3.9) calculated for $(N_O\text{–}V_O)$. $(N_O\text{–}V_O)$ is found to behave as a deep negative-U centre with a $(-1/+1)$ level in the lower half of the band-gap. The neutral charge state is thermodynamically unstable.

Finally, there is a second donor level for the $(N_O\text{–}V_O)$ complex, corresponding to a depopulation of the N_O acceptor level: in the $+2$ charge state the complex may be viewed as being $(N_O)^0\text{–}(V_O)^{+2}$. The location of the $(+/+2)$ level for $(N_O\text{–}V_O)$ is slightly closer to the valence band that the $(-/0)$ level of N_O, arising from a combination of the elastic and electrostatic interactions of the N_O and V_O components.
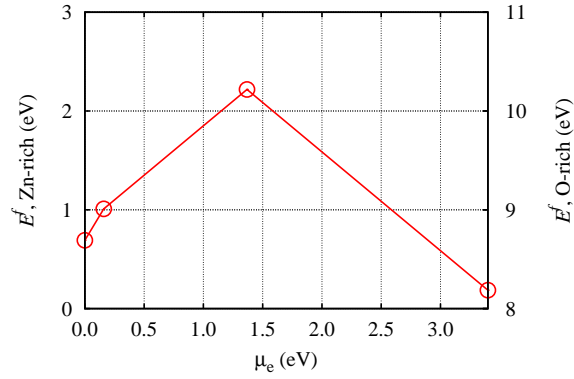
Figure 5.11: Plot of E^f *vs.* μ_e for $(N_O–V_O)$ in ZnO calculated using the 192 atom supercell.

(a) (b)
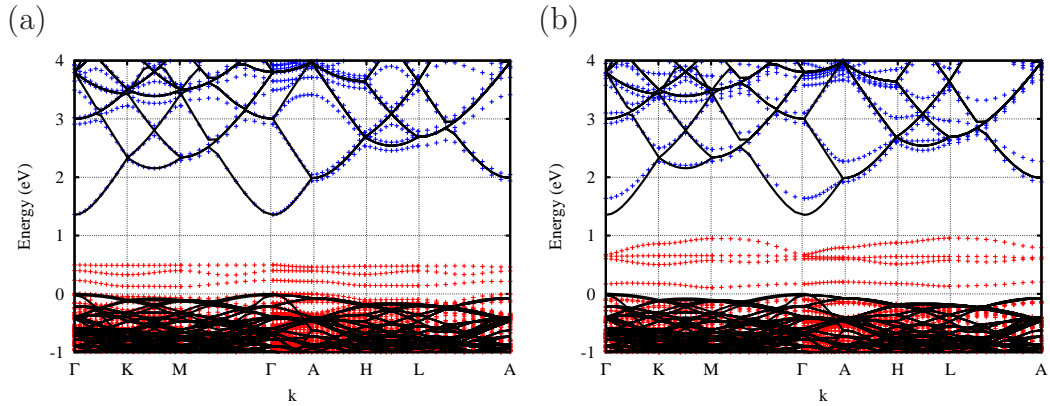
Figure 5.12: Plot of the band structure of $(N_O–V_O)$ in (a) the positive charge state and (b) the negative charge state. Symbols, lines and scales are as in Fig. 5.3

The one-electron band-structures, plotted in figure 5.12 for the positive and negative charge states, further illustrate the electrical properties of $(N_O–V_O)$. In the positive charge state there are three filled bands in the band-gap, and four filled bands in the band-gap at negative charge state.

Combining the formation energy and band structure data strongly suggests that the $(N_O–V_O)$ is thermodynamically stable in the $+2$, $+1$ and -1 charge states, yielding $(+2/+1)$, and $(+/-)$ transitions.

In summary, although the interaction is weak, as represented by the small binding energy, V_O is a potential compensation centre for the N_O acceptor.

5.3.5 (N_O–Zn_i) complexes

Another possible complex that may be formed in compensated N-doped ZnO may be envisaged to be a complex of N_O with the mobile Zn_i native defect, which, as reviewed in section 4.2.2, is a shallow donor [76, 130]. For p-type ZnO:N thin films there is a precedence for the emission from donor-acceptor pair recombination [18, 132].

Structure Details

The second native defect tested in a complex with N_O was the zinc interstitial, Zn_i. Noting that there are two types of zinc interstitial sites in the Wurtzite structure: Zn_i at the tetrahedral site, Zn_i, tet, shown schematically in Fig. 4.3(a), and zinc at the octahedral site, Zn_i, oct, shown schematically in Fig. 4.3(b). It is Zn_i, oct which is found to be more stable than Zn_i, tet for both neutral and positive charge states in the current study, in agreement with other simulations [27]. However, when combined with another defect component, the preferential site must be established.
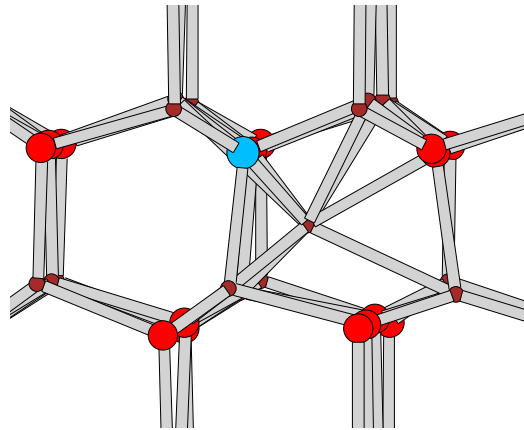
Figure 5.13: Schematics of $N_O Zn_i$ in the neutral charge state structure. Colours and axes are as in Fig. 5.1.

In addition, since Zn interstitials have a relatively high formation energy and are expected to rapidly diffuse with a low migration barrier of about $0.57\,\text{eV}$ [27]. Isolated Zn interstitials are not expected to be stable at room temperature [83], and are thus unlikely to be responsible for unintentional n-type conductivity under equilibrium conditions unless they are bound in deep structural traps. Since Zn_i is a double donor, a complex with a single acceptor such as N_O may be a candidate.

Indeed, the Zn_i native defect has been proposed [7, 20, 76, 133] for complexes involving N impurities that can be formed during growth of the material. Fig. 5.13 shows the lowest energy relaxed structure of the $(N_O–Zn_i)$ complex. As can be seen from the diagram, the preferred site for the interstitial species when closely associated with the N acceptor is in the Zn_i, oct form. The Zn_i–N inter-nuclear distance was calculated to be 2.03Å, which is the shortest distance interaction for the native defect atom, and smaller by 0.11Å than the Zn_i–O bond distances of 2.14Å. This may either reflect a chemical interaction or an ionic effect as in terms of the formal oxidation states of the N and O being -3 and -2, respectively.

The binding energy in neutral, $(N_O–Zn_i)^0$ and the ionised state, $(N_O–Zn_i)^+$, can be calculated relative to the most stable forms of the isolated components based upon their formation energies. In contrast to $(N_O–V_O)$, $(N_O–Zn_i)$ complexes have high binding energy of $2.22\,\text{eV}$, relative to N_O^{-1} and Zn_i^{+2}, which is in good agreement with other theoretical calculations [76], and low binding energy of $0.7\,\text{eV}$, relative to N_O^{-1} and Zn_i^{+1}. This low energy reflects the fact that Zn_i^{+1} is thermodynamically unstable. As shall be shown below, the $+1$ charge state of the complex is the only stable form of this complex, so reactions leading to other charge states are not relevant.

Although the pairing is bound, for it to be a good candidate for n-type doping, the strong interaction between the components must lead to appropriate electrical properties, which is the next topic.

Electrical levels

As reviewed in section 4.2.2, an isolated zinc interstitial in ZnO is found to introduce two electrons in a band above the conduction-band minimum, which is in good agreement with the calculations [76, 130]. This can simply be interpreted as when a Zn interstitial is inserted into the ZnO lattice, the $4s$ orbitals containing the two valence electrons is pushed up in energy due to the electrostatically confining potential of the nearby host atoms. The $4s$ level depopulates into the host conduction band. This shallow donor behaviour is in agreement with the interpretation of experimental observations [70, 82]. As described in section 5.3.1, N_O is a single acceptor, so might be expected to be converted to the single donor when reacted with a Zn_i double donor. By calculating the formation energies (Eq. 3.9) of $(N_O$–$Zn_i)$ indeed this is what is obtained, as shown in Fig. 5.14, where as with isolated Zn_i the donor level is located in the conduction band. The donor level is further illustrated in Fig. 5.15, which shows the band-structure of the complex along high-symmetry directions in the Brillouin zone of the 192 host-atom supercell. The bottom of the conduction band is occupied by an electron, consistent with a shallow donor level.
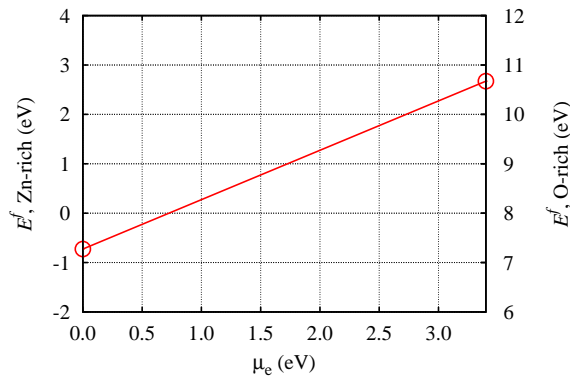
Figure 5.14: Plot of E^f *vs.* μ_e for the $(N_O$–$Zn_i)$ complex in ZnO calculated using the 192 atom supercell.

Combining the binding energies and electrical levels, it seems a plausible argument to ascribe n-type activity to these complexes. However, one should also take
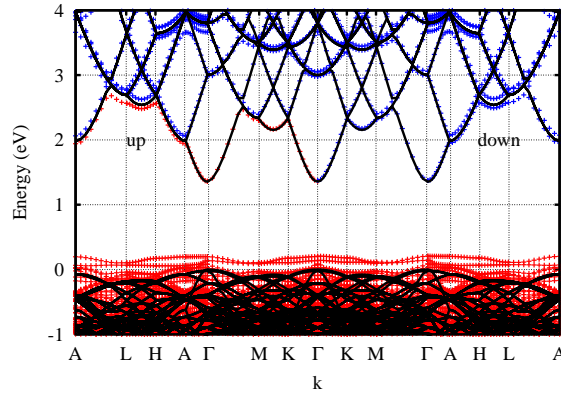
Figure 5.15: Plot of band structure of $(N_O–Zn_i)$ complex in the neutral charge state. Symbols, lines and scales are as defined in figure 5.3.

into account other aspects of the growth conditions. The substitution at an oxygen site and the insertion of a Zn interstitial are much more likely where material is grown under zinc-rich conditions, as can be seen by comparison of the absolute energy scales in figure 5.14. For p-type material, for example, the formation energy of $(N_O–Zn_i)$ is extremely favourable, driving the incorporation of donors to compensate the formation of N-related acceptors. This issue will be the subject of further discussion in section 5.6.

5.3.6 $(NO)_O$ defects

As with the zinc interstitial, there are two types of non-bonded oxygen interstitial sites in the ZnO: O_i at a tetrahedral, O_i, tet, or an octahedral site, O_i, oct (section 4.2.3). In contrast to the Zn interstitial O_i may also chemically react with the lattice to form a O_2 molecule at an oxygen site.

The chemical state of the oxygen interstitial has a big impact upon its electrical properties, since in the chemically reacted form electrons that are normally exchanged in the ionic bonding instead go into covalent bonding states within the oxygen pairs. Thus the non-bonded forms are acceptors and the reacted form is a donor (section 4.2.3). Since N–O chemistry is closely related to that of O–O interactions, it

may be anticipated that the interaction of O_i with N_O may lead to both bonded and non-bonded forms, with the former being electrically passive or even a hyper-deep donor.

In the case of a $(NO)_O$ centre one has also to keep in mind that this combination is compositionally identical to interstitial nitrogen nominally through the exchange of the two sites.

Structure Details

The complex of an oxygen interstitial O_i with a N_O acceptor was examined, starting with structures based upon both the non-bonded and bonded O_i geometries. The lowest energy structure is found to be that where the O_i and N_O share a single oxygen site. Such a structure can be viewed as a N–O molecule substituting for a host oxygen, $(NO)_O$. The most stable orientation is shown in Fig. 5.16. The connectivity of the N-O molecule often has strong influence on its physical and chemical properties and behaviour. A N-O molecule might have completely different chemical and physical properties if the atoms are connected differently or both in different positions and charge states.
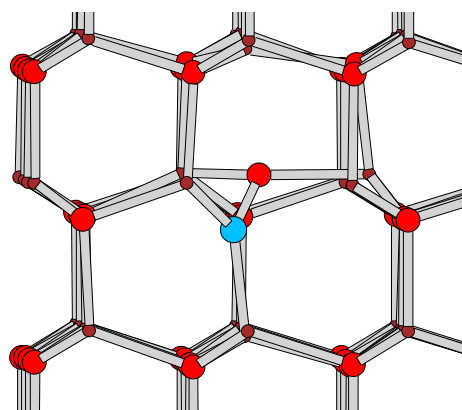
Figure 5.16: Schematic of $(NO)_O$ in the neutral charge state. Colours and axis are as in Fig. 5.1.

In the neutral charge state, the bond length of the N–O molecule to 1.35Å, which

is between the values of 1.20Å and 1.45Å corresponding to the 1.5 bond order interactions in NO_2 and the single N–O bond in NH_2-OH (hydroxylamine). It is considerably longer than the bond-length of a free NO molecule. In the overall +1 charge state the N–O bond-length decreased to 1.26Å, which is in reasonable agreement with the experimental value of a N–O bond in NO_2, where the bond-order is 1.5. The positive charge state is more stable in a spin polarised form with $S = 1$ compared to $S = 0$ by 0.7 eV, consistent with viewing the structure as being a composite of $(N=O)^-$ and $(V_O)^{+2}$. The ESR study of NO anions adsorbed on the surfaces of a range of materials found that they have an $S = 1$ ground state [134]. An NO molecule can either donate an electron (depopulating the π^* state) or accept an electron from a metal surface [135], so that electronically it resembles a neutral oxygen molecule.

It is perhaps worthy of note that NO species are sometimes used as the source of N in doped ZnO. In such a case, it seems plausible that NO molecules are incorporated into the lattice, resulting directly in the formation of $(NO)_O$ centres.

Electrical levels

Fig. 5.17 shows a plot of the electron chemical potential dependent formation energies using (Eq.3.9) for $(NO)_O$.

This yields a single electrical level in the band-gap, being a $(-/+)$ level calculated at around $E_v + 1.8$ eV, and the electrical levels of $(NO)_O$ are further illustrated in Fig. 5.18, which shows the band-structure along high-symmetry direction in the Brillouin-Zone. These results can be correlated with $(N_2)_O$, where the empty level is calculated to be around $E_v + 1.8$ eV, derived from $2\pi^*$ orbital for the (NO) molecule. These levels are above the theoretical value of E_c, but within the experimental band-gap, and the flat-band nature of these highly localised states is likely to be relatively less dependent upon the uncertainty in the position of the host conduction band energy.

Based upon the formation energies, $(NO)_O$ is thermodynamically stable at +1 and -1 charge states, the change in the charge state being related to the change in the
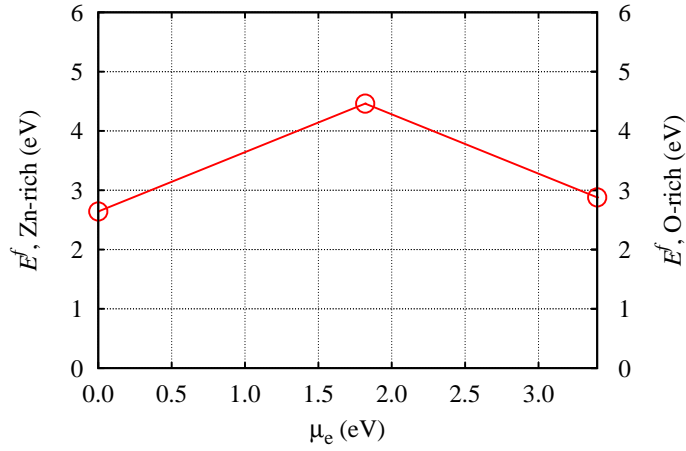
Figure 5.17: Plot of E^f *vs.* μ_e for $(N_O)_O$ defects in ZnO calculated using the 192 atom supercell.
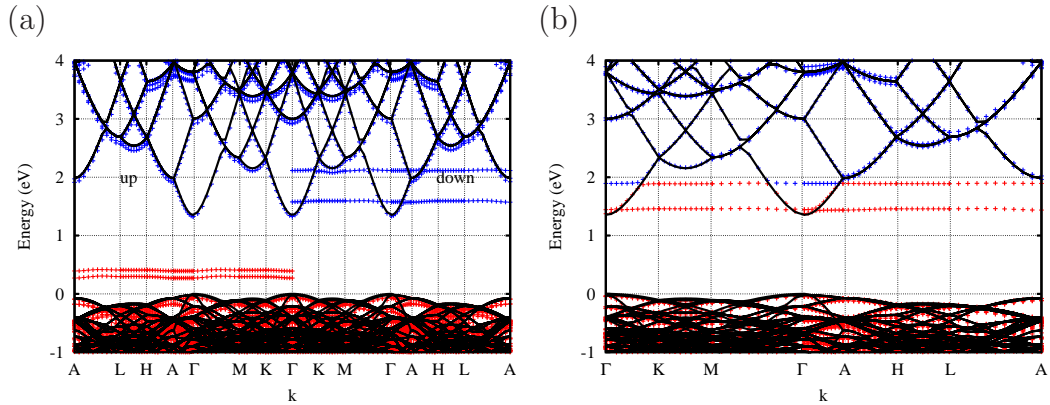
Figure 5.18: Plot of band structure of $(NO)_O$ in ZnO (a) the positive charge state with $S = 1$ and (b) the negative charge state. The zero of energy is set to be the valance band top for bulk ZnO. Red and blue circles indicate filled and empty bands, respectively.

number of electrons in the two p_π^* bands in the band-gap.

Vibrational Modes

As with those structures discussed above where N_2 are present, one would expect the $(NO)_O$ defect to give rise to vibrational modes characteristic of a N–O covalent bond. The vibrational modes of $(NO)_O$ are calculated to be 967 and $1461 \, cm^{-1}$ in the negative and positive charge state respectively, which is in excellent agreement with previous calculated values of 967 and $1462 \, cm^{-1}$ [30]. They are also in good agreement with experimental values for Raman peaks at 974 and $1410 \, cm^{-1}$, which are not observed in the undoped ZnO, but are seen in nitrogen doped ZnO [118, 136]. It is further noted that the local vibration mode of $1461 cm^{-1}$ is consistent with the lower end of the frequency range seen for the vibration of N-O molecules in contact with metal surfaces [135].

It should be noted that the presence of a vibrational mode in agreement with $(NO)_O$ is not necessarily conclusive evidence of its presence. There may be other defects which contain N–O covalent bonds which would be expected to give rise to frequencies in the same vicinity. Given that the positive charge state of $(NO)_O$ is anticipated to be EPR active a conclusive assignment could be made where there to be a correlation between EPR and vibrational spectroscopy.

5.3.7 $(NO_2)_O$ complexes

Taking the view that $(N_2)_O$ and $(NO)_O$ centres may form as a consequence of using N_2 and NO molecules as growth species, one may apply the same reasoning to other growth species. Many experiments have indicated that the doping of ZnO using NO and NO_2 molecules can result in the production of p-type carriers [16, 18, 31, 103]. It may be that a NO molecule combines with a host O-site in ZnO, or a direct insertion of a NO_2 molecules at an O site may occur. In this section the resulting defects are considered.

Structure Details

The structure is composed from the addition of a NO molecule to ZnO. The equilibrium structure can be described as insertion of nitrogen dioxide into an oxygen site in bulk ZnO. It is found that there are many metastable structures of an NO_2 molecule substituting for a host O-atom, and these distinct arrangements are separated by small energies. A NO_2 molecular substitution for an O-site is a single donor, characterised by the N being coordinated with two host oxygen atoms.
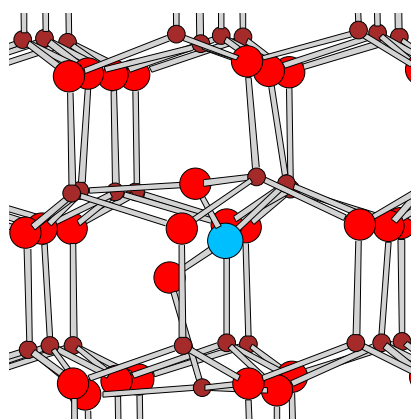
Figure 5.19: Plot of structure of the relaxed configuration of $(NO_2)_O$ in ZnO in the neutral charge state. Colours and axes are as in Fig. 5.1.

Fig. 5.19 shows the most stable structure for NO_2 substituting at an O-site. The N–O bond-lengths in the NO_2 core are calculated to be in the range of 1.30-1.33Å in the neutral charge state, which is typical of experimental values for N–O single bonds in nitrates [137]. In the event that the defect is positively charged, the N–O bond length was calculated to be in the range of 1.24-1.27Å, which is slightly longer than the experimental value for a bond of 1.21Å for nitrate ions (NO_3^{-1}) [137], where the N–O bonds are slightly stronger than single bonds.

The insertion of NO_2 displaces the neighbouring host Zn atoms (see figure 5.19). There is a substantial displacement of the four neighbouring Zn atoms away from the equilibrium host sites, with the smallest N–Zn inter-nuclear distance being 2.2Å in the neutral charge state. The oxygen atoms in the NO_2 molecule are nonequivalent

with one of them being more closely related to the nearby Zn atom than the other, as reflected in the differences in the N–O bond lengths above.

Electrical levels

The structure can be viewed as an NO_2 nitrite anion (NO_2^-) substituting for an oxygen ion (O^{-2}), so there is a deficit of electron capacity at the oxygen site for the four neighbouring Zn sites. Based upon such a description, one might expect the system to be a single donor.
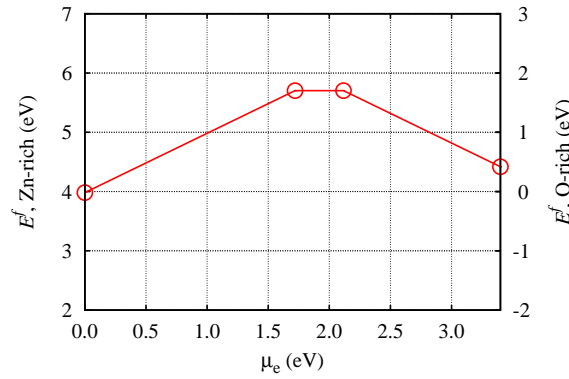
Figure 5.20: Plot of E^f *vs.* μ_e $(NO_2)_O$ defects in ZnO calculated using the 192 atom supercell.

Fig. 5.20 shows a plot of the formation energies (Eq.3.9) for $(NO_2)_O$. This yields deep states in the band-gap, the $(0/+)$ transition level located at $E_v + 1.6\,eV$. In addition, there is a $(-/0)$ transition level located at $E_v + 2.1\,eV$ in the band-gap. The acceptor level can be explained by considering the system as V_O and a nitrite group. In the overall negative charge state of $(NO_2)_O$, the vacancy is in the neutral charge state and the NO_2 group is in the negative charge state.

Again, some care has to be taken in interpreting the calculated electrical levels. Both the $(0/+)$ and $(-/0)$ levels lie above the theoretical value of E_c, but within the experimental value of the band-gap. The levels are in line with the existence of both filled and empty states resonant with the conduction band, as illustrated in Fig. 5.21.
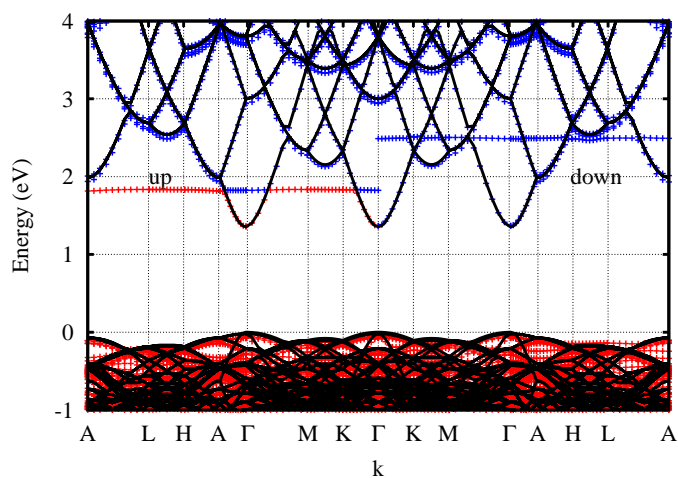
Figure 5.21: Plot of band structure of $(NO_2)_O$ in ZnO. Symbols, lines and scales are as defined in figure 5.3.

Thus, although there is some ambiguity as to the location the electrical levels, it is likely that the donor level is relatively deep, so that the contribution of this defect complex to n-type conduction is in some doubt.

5.3.8 $(NO_2)_i$ and $(NO_3)_O$ centres

Just as $(NO_2)_O$ may hypothetically arise from the association of NO source molecules with host oxygen, the associate of NO_2 source species [31] with host oxygen sites would yield a $(NO_3)_O$ centre. A NO_2 molecule might also be incorporated into the growth films to form an interstitial NO_2 species.

Structure Details

The simulations performed for this study are based upon a wide range of starting geometries including the insertion of NO_2 into different interstitial sites as well as the formation of a nitrate group (NO_3) substituting for a host oxygen atom. The relaxations indicate that there are many metastable structures for interstitial NO_2 molecules in ZnO based upon variations in orientation which result in very small

energy differences. This is a quality in common with the interstitial NO molecule (section 5.3.7).
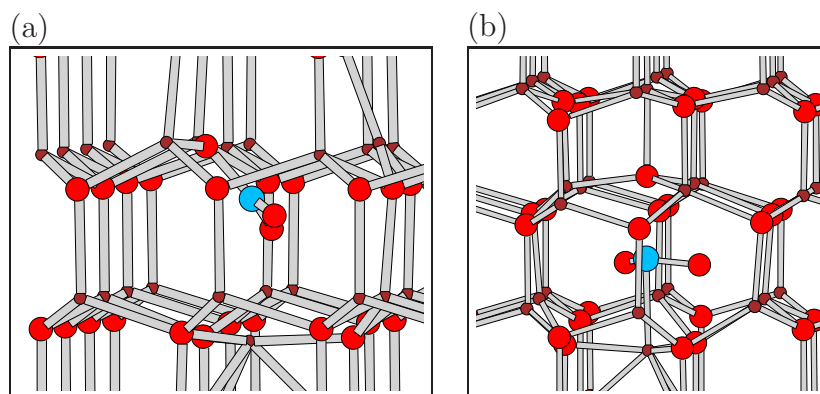
Figure 5.22: Schematic of the structure of (a) $(NO_3)_O$ in the positive charge state and (b) $(NO_2)_i$ in the negative charge state. Colours and axis are as in Fig. 5.1.

However, in the calculations, for specific charge states there are two significant relaxed geometries, as shown in Fig. 5.22. The first structure, being in the overall positive charge state, may be viewed as a negatively charged nitrate anion substituting for an O-site as shown in Fig. 5.22(a). In such an arrangement all species can adopt the natural oxidation states. The second structure may be viewed as insertion of the nitrite (NO_2) group into the lattice, breaking a host Zn–O bond, as shown in Fig. 5.22(b). (As will be shown below in section 5.3.9, this is a mode of interstitial molecule insertion that has been seen in previous studies of interstitial N_2 molecules [28]. The three N-O bond lengths are calculated to be 1.23Å for the +1 charge state, which is in good agreement with other calculations of 1.23Å [137] for the three N-O bonds for a free NO_3^- ion.

In the negative charge state, the structure is very different. A host Zn–O bond breaks, and the NO_2 group is inserted into the space this makes. As can be seen in figure 5.22(b), the displacement of the host atoms moves them to within around a host bond-length of other host atoms. The insertion of interstitial species has been

previously predicted for the inclusion of N_2 molecules as interstitial species [28].

Electrical levels

Fig. 5.23 shows a plot of the calculated μ_e-dependence of the formation energies (Eq. 3.9) of $(NO_3)_O$ in ZnO.
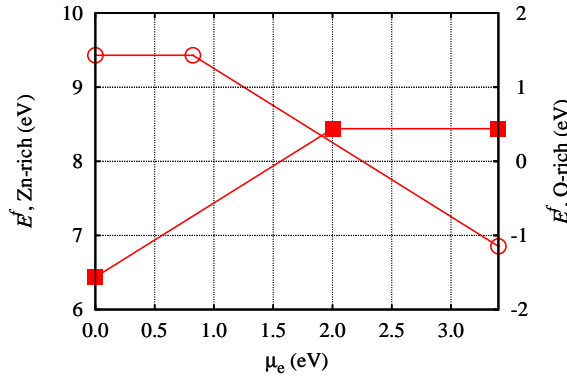
Figure 5.23: Plot of E^f *vs.* μ_e for (a) $(NO_3)_O(\blacksquare)$ (b) $(NO_2)_1$ (O). The structures in ZnO calculated using the 192 atom supercell.

Concomitant with the large change in structure, $(NO_3)_O$ acts as a negative-U centre with a $(-/+)$ transition level located about 2.0 eV above the valence band. It is perhaps worth noting that this is broadly consistent with the red PL commonly seen in material grown using N-dopants [13, 73, 114–116]. This point will be addressed further in section 5.6.

The electronic structures involved in the $(-/+)$ transition are further illustrated in Fig. 5.24, which shows the band-structure along high-symmetry direction in the Brillouin-Zone. The electron donated by the neutral $(NO_3)_O$ originates from a modified V_O, and the state into which the electron is accepted in $(NO_2)_i$ is localised on the NO_2^{-1} molecule.

The barrier to interconversion between the two forms has not been estimated. However, if barriers exist and this defect is really bi-stable, then the relevant electrical levels may not be those involving the equilibrium structures for each charge state.

CHAPTER 5. NITROGEN

(a)   (b)
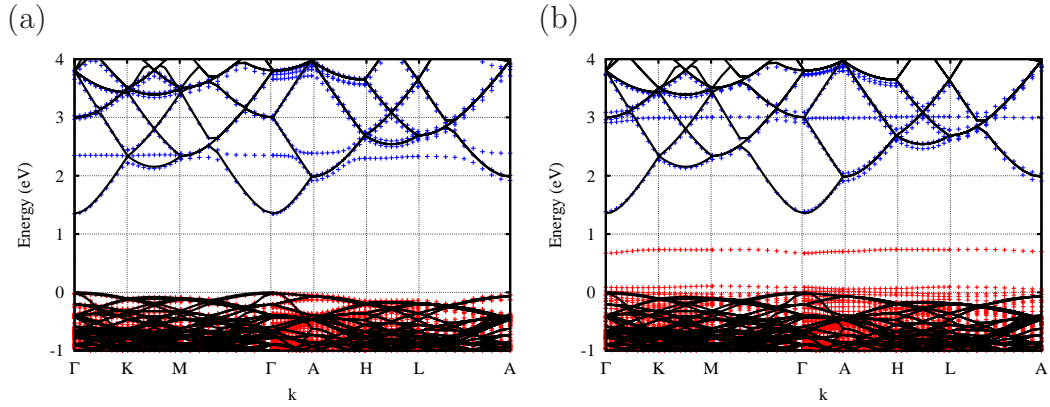
Figure 5.24: Plots of band structures for (a) $(NO_3)_O^+$, and (b) $(NO_2)_i^-$. Symbols, lines and scales are as defined in figure 5.3.

For example, the interstitial molecule in the negative charge state may loose an electron to form a neutral, metastable species, with a donor level predicted (figure 5.23) to be 0.9 eV above the valence band top. Similarly, there may be a metastable $(-/0)$ acceptor transition associated with the nitrate structure around 2.0 eV above the valence band top.

Nevertheless, given the very deep locations predicted for the donor and acceptor levels of this defect, it is not a good candidate for the production of either n-type or p-type material, although it is expected to readily form in O-rich conditions based upon the absolute formation energies.

5.3.9 $(NO3)_i$ and $(NO_4)_O$ complexes

As mentioned several times already, it is a potentially important observation that in many experiments where the source species for nitrogen doping involves N–O bonds, such as NO, NO_2 and NH_4NO_3 (ammonium nitrate), the resulting ZnO films may be activated to produce p-type carriers [16, 18, 31, 103, 103, 138]. The molecule group might be incorporated into the growing films as interstitial dopants, or even react with host atoms of ZnO.

In addition to the preceding molecular groups, the insertion of a complete nitrate

ion into the lattice might result in an interstitial object, $(NO_3)_i$, or react with the oxygen host to form an exotic $(NO_4)_O$ species. A superficial view of the chemistry by which such species might be formed may involve insertion directly of nitrate ions, or from the reaction of NO_2 source species with interstitial oxygen via reactions of the type:

$$NO_2 + O_i \longrightarrow (NO_4)_O \tag{5.3}$$

and

$$NO_2 + O_i \longrightarrow (NO_3)_i. \tag{5.4}$$

Structure Details

As with previous molecular groups, the structures composed from the addition of a single N atom and three additional oxygen atoms to ZnO were obtained in two ways. The first is simple insertion of the nitrate group into the lattice at a cage site. The second was the decoration of the structure obtained for $(NO_3)_O$, as described in section 5.3.8.

Relaxation of such starting configurations was found to result in two chemically distinct structures with practically the same total energies.

One configuration may be viewed as a modified nitrogen substitution for an O site, described as $(NO_4)_O$, depicted in Fig. 5.25(a). The nitrate group was found to preferentially insert itself into a Zn–O bond (similar to the structure of interstitial N_2 molecules), and this structure is shown schematically in Fig. 5.25(b).

The N-O bond lengths in $(NO_4)_O$ are calculated to be in the range of 1.34–1.37 Å which are in agreement with experimental value for a N-O single bonds in nitrates [137]. $(NO3)_i$ (Fig. 5.25(b)) involves a broken Zn–O bond, with the equilibrium structure having N-O bond lengths and angles calculated to be 1.25Å and 119°, respectively, which is in good agreement with the experimental values [137] of 1.21Å and 120° for the $(NO_3)^{1-}$ anion. The structures therefore reflect standard N-O chemistry, at least at a structural level.
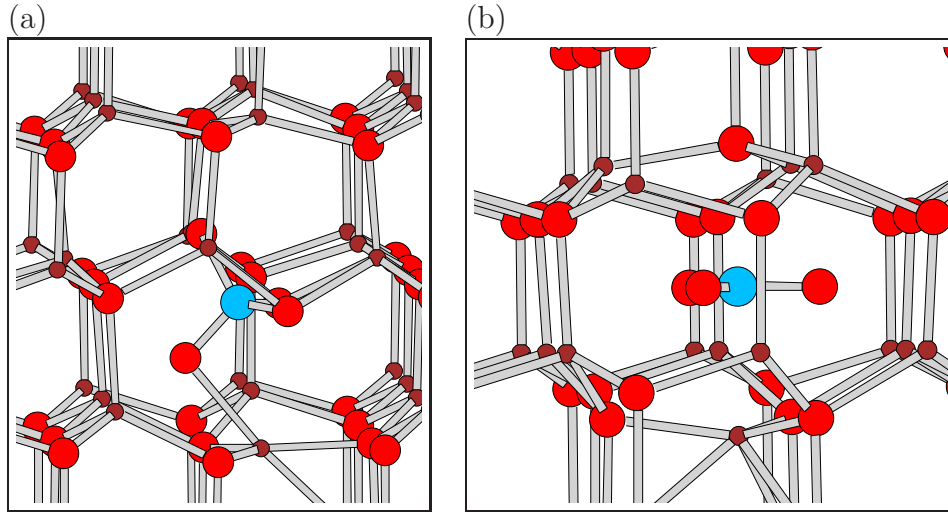
Figure 5.25: Schematic structures of (a) $(NO_4)_O$ and (b) $(NO_3)_i$ in ZnO. Colours and axis are as in Fig. 5.1.

The binding energies, as determined from the reactions,

$$(NO_2)_i^{1+} + O_i^{2-} \longrightarrow (NO_4)_O^{1-} \tag{5.5}$$

and

$$(NO_2)_i^{1+} + O_i^{2-} \longrightarrow (NO_3)_i^{1-} \tag{5.6}$$
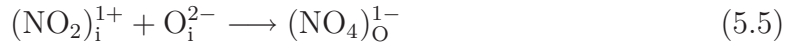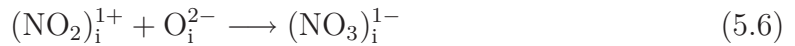
are 1.8 eV and 1.7 eV, respectively. Based upon the current data presented here, there are no reactions with smaller heats of reaction, so it seems reasonable to conclude that $(NO_4)_O^{1-}$ represents a thermodynamically stable species relative to likely dissociation products. The absolute formation energy will be discussed in comparison with other N-containing centres in section 5.6.

Electrical levels

Fig. 5.26 shows plots of the formation energies (Eq. 3.9) for $(NO_4)_O$ and $(NO_3)_i$. They both yield relatively shallow acceptor levels, around $E_v+0.20$ eV for $(NO_4)_O$ and $E_v+0.24$ eV for $(NO_3)_i$. These levels are in excellent agreement with one interpretation of bound-exciton photoluminescence from N-doped ZnO, suggestive of an acceptor levels at ~200 meV above E_v. [14, 107–110, 139].

(a)
(b)
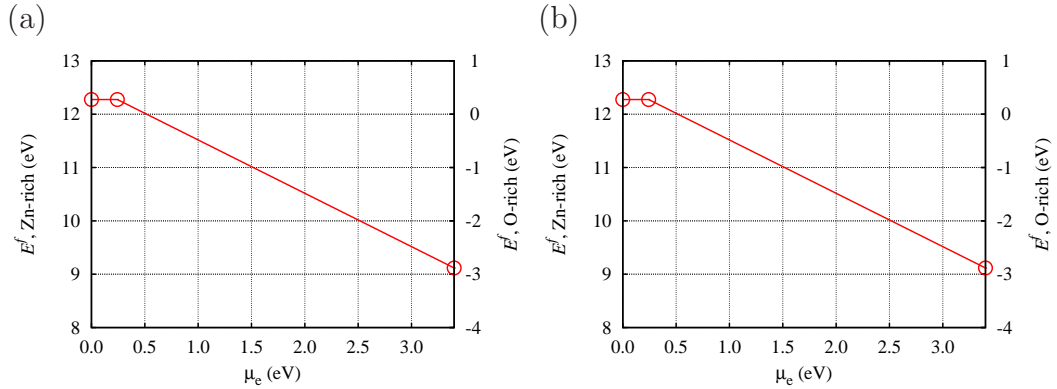
Figure 5.26: Plot of E^f *vs.* μ_e for (a) $(NO_4)_O$ and (b) $(NO_3)_i$ defects in ZnO calculated using the 192 atom supercell.

(a)
(b)
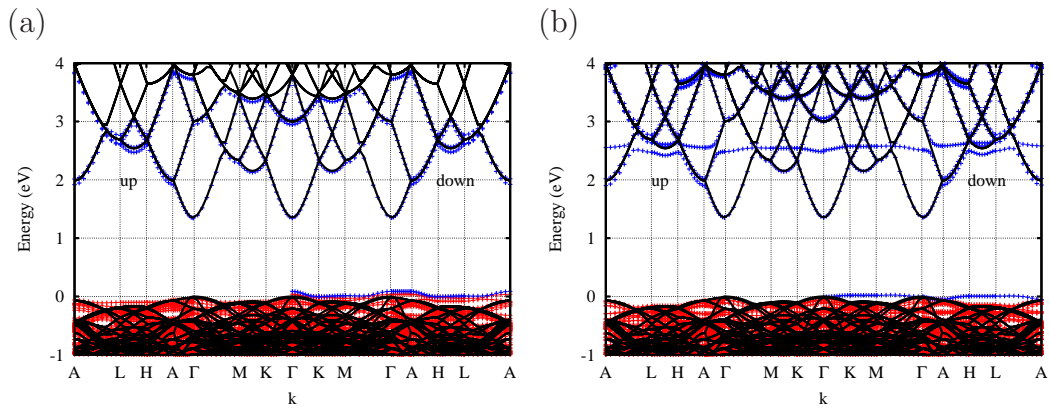
Figure 5.27: Plot of band structure of (a) $(NO_4)_O$ and (b) $(NO_3)_i$ in ZnO. The zero of energy is set to be the valance band top for bulk ZnO. red and blue circles indicates filled and empty bands, respectively.

The acceptor level of the both structures further illustrates in Fig. 5.27, which shows the band-structure along high symmetry directions in the Brillouin-Zone (BZ). Note the empty band close to the valance band top, consistent with the calculated acceptor levels.

To understand where is the empty stat came from and the location of the empty stat in band-gap, Fig. 5.28 shows the wave function distribution of the Kohn-Sham orbital of the empty level in the top of the valence band for the NO_3 molecule alone,
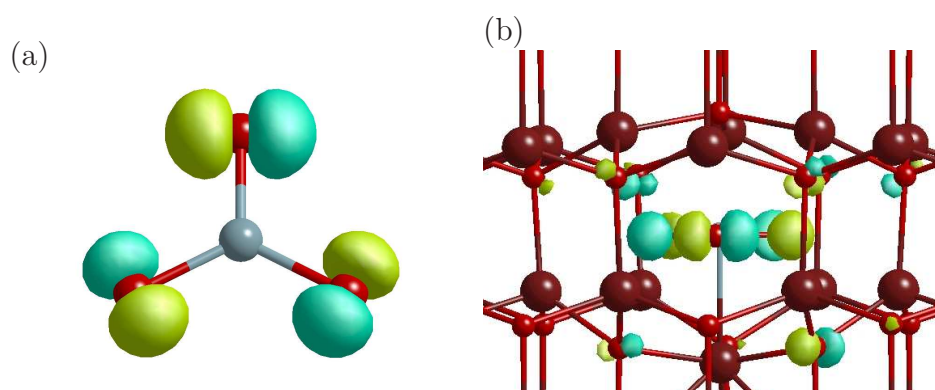
Figure 5.28: Plot of the wave function distribution of (a) (NO_3) molecule (b) the $(NO_3)_i$ defects in ZnO calculated using the 192 atom supercell.

and NO_3 defects in ZnO. Fig. 5.28(a) illustrates the wave function distribution of NO_3 molecule for the last empty orbital, and Fig. 5.28(b) illustrates the wave function distribution of the orbital in the valance band for $(NO_3)_i$ defects in ZnO. From Fig. 5.28 conclude that the molecule may grab electrons from the $2p$ orbital of the host oxygen atom.

Vibrational Modes

Finally, since both structures are based upon simple molecular groups, it may be fruitful to determine the vibrational frequencies that may be compared with experimental data, such as from PL.

Table 5.1: The local vibrational modes of $(NO_3)_i$ and $(NO_4)_O$ (cm^{-1}).

Defect						
$(NO_3)_i$	702	1071	1384	1392		
$(NO_4)_O$	703	731	929	974	989	1019

Amongst the local modes of $(NO_4)_O^{-1}$ and $(NO_3)_i^{-1}$, those calculated at 1019 and $1392\,cm^{-1}$ are in notable agreement with Raman peaks from experiment at 1150, 1360

and $1158\,\text{cm}^{-1}$ [139]. These Raman features are not observed in the ZnO not doped with nitrogen. In particular these peaks are observed when NO gas is used [118,136]. The local vibration modes calculated at 1019 and $1392\,\text{cm}^{-1}$ are stretching vibrations, and are expected to be Raman active.

$(NO_4)_O$ and $(NO_3)_i$ centres in ZnO present a rather appealing possible explanation for the production of p-type ZnO using N-O based doping precursors. The calculated structures show that nitrate groups are stable in the lattice, and combined with the formation energies can be viewed a preferentially adopting the anion state.

Conclusive assignment of the presence of these acceptors may be found from the characteristic vibrational modes that these complexes give rise to.

5.3.10 N_O–Zn_O complexes

N_O is a single acceptor and, as reviewed in section 5.3.1, Zn_O is a double donor [77]. The combination of these centres would therefore be expected to act as a single donor, so if they can be formed on the basis of their formation energy, then they may represent a source of compensation of any other N-related shallow acceptors that may be formed. This centre was previously considered theoretically [20], where it was found to be a shallow donor, easily formed (i.e. has a low formation energy) but is relatively weakly bound at $1.52\,\text{eV}$. The ease of formation and the shallow donor properties have obvious potential significance for the as-grown n-type material.

Structure Details

Fig. 5.29 shows the relaxed structure of the lowest energy $N_O Zn_O$ complex found, which is in good agreement with a previous theoretical study of this complex [20]. The Zn_O–N bond distance is calculated to be 1.97Å, which is close to the value calculated for the Zn_i–N bond distance at 2.03Å in $(N_O$–$Zn_i)$ (section 5.3.5). The Zn_O–Zn bond distances are calculated to be between 2.3–2.6Å which is in good agreement with another calculation of 2.4–2.8Å [77].

The interaction between the two component parts can be viewed as leading to
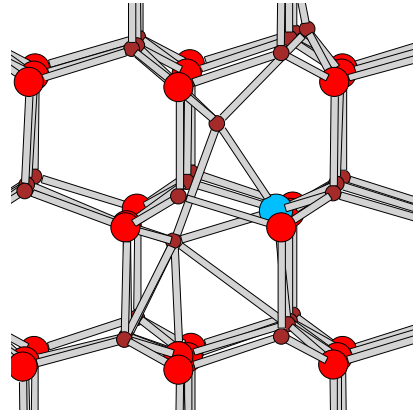
Figure 5.29: Schematic of the structure of $N_O Zn_O$ in ZnO. Colours and axis are as in Fig. 5.1.

only a perturbation to their geometry, and to a reasonable degree the structure of the complex can be seen as a simple combination of the parts.

Electrical levels

Isolated-N_O behaves as a deep single acceptor, and isolated Zn_O behaves as a shallow double donor. Therefore it would be expected that the $N_O Zn_O$ would behave as a single donor, and indeed this is what is found in the current study, as well as previously [20].
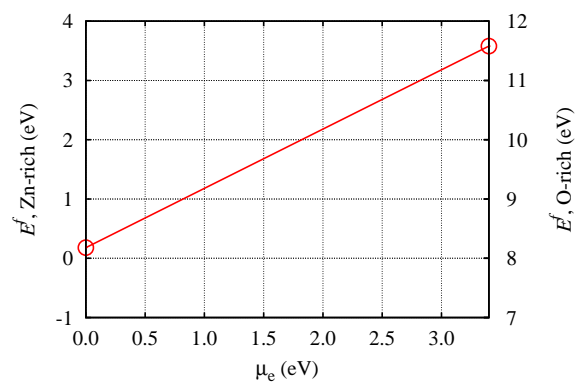
Figure 5.30: Plot of E^f *vs.* μ_e for N_O–Zn_O defects in ZnO calculated using the 192 atom supercell.
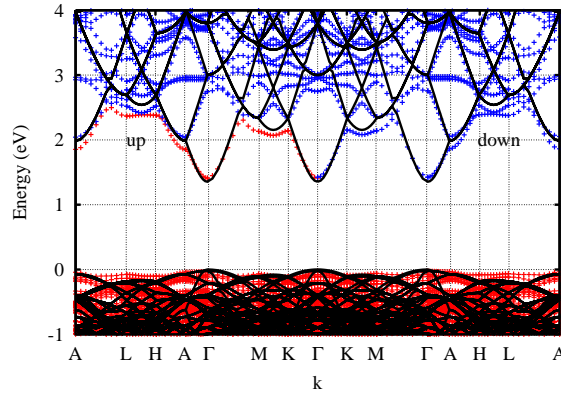
Figure 5.31: Plot of the band structure of N_O–Zn_O in the neutral charge state. Symbols, lines and scales are as in figure 5.3.

Fig. 5.30 shows a plot of the formation energy as a function of μ_e using (Eq. 3.9) for N_O–Zn_O. For the whole band-gap the only thermodynamically stable charge state is +1, *i.e.* the donor level in the conduction-band minimum. The electrical properties of the complex are further illustrated by the electronic structure as plotted in Fig. 5.31, which shows the band-structure along high-symmetry direction in the Brillouin-Zone. There are no bands within the band-gap, and in this neutral charge state there is a single electron in the conduction band.

Noting that the formation energy is relatively small in p-type, Zn-rich conditions, under such conditions the N_O–Zn_O complex is a reasonable candidate for an electrically compensating defect.

5.4 Nitrogen associated with the zinc lattice

A common theme in the structures determined for N associated with the oxygen sub-lattice is the preference for the formation of structures where covalent bonds are made, particularly in the formation of N–O bonds. This being the case it may be anticipated that group-V impurities should favour substitution at Zn sites where they will immediately neighbour oxygen. For example, some theoretical and experimental

research indicates that most of arsenic and antimony substitutions are at a Zn site rather than an O-site [21, 140]. Following this observation, the structure, electronic and vibrational properties of N associated with the Zn site were calculated and are presented in the following sections.

5.4.1 Nitrogen substituting at a Zn site, N_{Zn}

Based upon an ionic picture, substitution of Zn by N may appear a surprising suggestion. Nitrogen has three more valence electrons than Zn, so it might be predicted that N_{Zn} should act as a triple donor when substituting for Zn. However, some care has to be taken in such an interpretation. Under the model that N forms covalent bonds with its neighbours, one would have to examine the ion states not of the atoms, but of the ion-groups, such as is the case for $(N_2)_O$.

Structure Details

The relaxed structure for N substituting for Zn is shown schematically in Fig. 5.32. The nitrogen atom is bonded with two oxygen in the basal plane to make a (NO_2) molecule substituting for a O–Zn–O group.
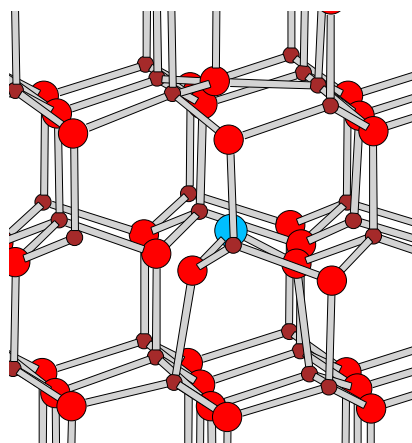
Figure 5.32: Schematic of the structure of N_{Zn} in ZnO. Colours and axis are as in Fig. 5.1.

The bond distance for the nitrite molecule component of N_{Zn} was calculated to be 1.4Å, which is in good agreement with the experimental value of 1.4Å for a N-O single bond [137], yielding support for the model of the formation of covalent interactions.

Electrical levels

The host atoms removed contain one more O atom than Zn, and to a first approximation one would expect the O–Zn–O group to have a net double-donor property. Since the nitrite ion is electronegative occurring in the negative charge state, the combination of this covalent group with the native double-donor may be expected to result in a single rather than a triple donor. By calculating the formation energy (Eq. 3.9) for N_{Zn} in ZnO as a function of charge state and μ_e, that can estimate the nature and energy of the electrical levels of N_{Zn}. The results are summarised in Fig. 5.33, which indicates that there is a single donor level located around $E_v + 1.5\,\text{eV}$ and possibly a single acceptor level around $E_v + 2.7\,\text{eV}$. The donor level is far too deep for room temperature n-type doping. The confidence in the location of the acceptor level which is well above the theoretical conduction band minimum, is perhaps improved by examination of the band-structure.
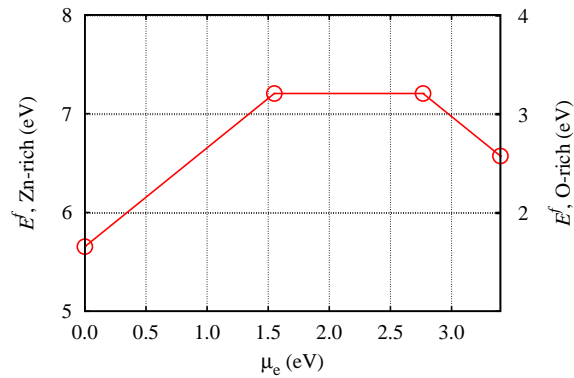
Figure 5.33: Plot of E^f *vs.* μ_e for N_{Zn} in ZnO calculated using the 192 atom supercell.

The band-structure of the neutral defect, Fig. 5.34, shows a localised state (as
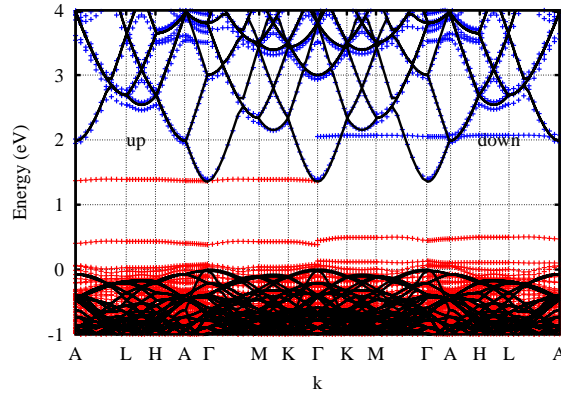
Figure 5.34: Plot of band structure of N_{Zn} in ZnO, in the neutral charge state. The zero of energy is set to be the valance band top for bulk ZnO. Symbols, lines and scales are as in figure 5.3.

indicated by the weak energy dependence upon k) around $E_v + 1.5\,\mathrm{eV}$. These two bands are derived from p_π^* states on the NO_2 ion in combination with orbitals on the nearby under-co-ordinated oxygen atoms. while the empty levels are derived from almost entirely from orbitals on the under-co-ordinated O atoms in the lattice.

In contrast to the N_O centre, it is found in this study that N_{Zn} shows no tendency to form pairs. This is likely a consequence of a strong Coulomb repulsion between these centres, and indeed by increasing the distance between two N_{Zn} in the same simulation cell, the energy is reduced. Where they lie on adjacent sites, based upon the current calculations there is no evidence that the N_{Zn} centres form covalent interactions to overcome the Coulomb repulsion, which is opposite to the case of the $(N_O)_2$ reconstruction into a strongly bound N_2 molecule and a native defect, V_O.

Since nitrogen substitution on a Zn site single donor, and focusing upon the aim of producing p-type ZnO, one might expect it may be converted into an acceptor by formation of a complex with components with sufficient acceptor activity.

5.4.2 N_{Zn} complexes with V_{Zn}

It is known both theoretically and experimentally that zinc vacancies form relatively shallow acceptor levels. In section 4.2.4 it was shown that AIMPRO calculations yield acceptors levels with $(-/0)$ and $(-2/-1)$ transitions at $0.11\,eV$ and $0.55\,eV$ above the valance band top, respectively, in good agreement with other theoretical calculations [27,84,86]. V_{Zn} has very high formation energies in p-type ZnO, but it is possible that an interaction with a nearby N_{Zn} centre may stabilise it energetically.

Structure Details

Since N_{Zn} is a single donor, it is possible it will be converted to become an shallow acceptor by combining it with double acceptor vacant Zn site [24,27,84,85]. In such an event, the complex would be made up from ionised forms of both centres, and the stability of the $(N_{Zn}-V_{Zn})$ complex is thus expected to be favourably influenced by an attractive Coulomb interaction. There are many possible $(N_{Zn}-V_{Zn})$ orientations determined by the location of V_{Zn} relative to N_{Zn}, all of which are found in this study to be at least meta-stable. Of the structures examined, in the neutral charge state there are configurations where the N atom is bonded to either one or two oxygen neighbours which are indistinguishable in energy. Other orientations have energies up to around $0.3\,eV$ higher. It is therefore especially difficult to be confident that the true ground state structure has been determined in this case.

Nevertheless, the most stable structure found is shown in Fig. 5.35, which has a calculated binding energy of $1.63\,eV$for the negative charge state and $1.9\,eV$ for the neutral charge state relative to isolated constituents via the reaction

$$N_{Zn}^{1+} + V_{Zn}^{2-} \longrightarrow (N_{Zn}V_{Zn})^{1-} \tag{5.7}$$

$$N_{Zn}^{1+} + V_{Zn}^{1-} \longrightarrow (N_{Zn}V_{Zn})^{0} \tag{5.8}$$

The N–O bond length was calculated at 1.17Å in the -1 charge state where the acceptor level is occupied, which is in good agreement with typical values for N–O double bonds [137].
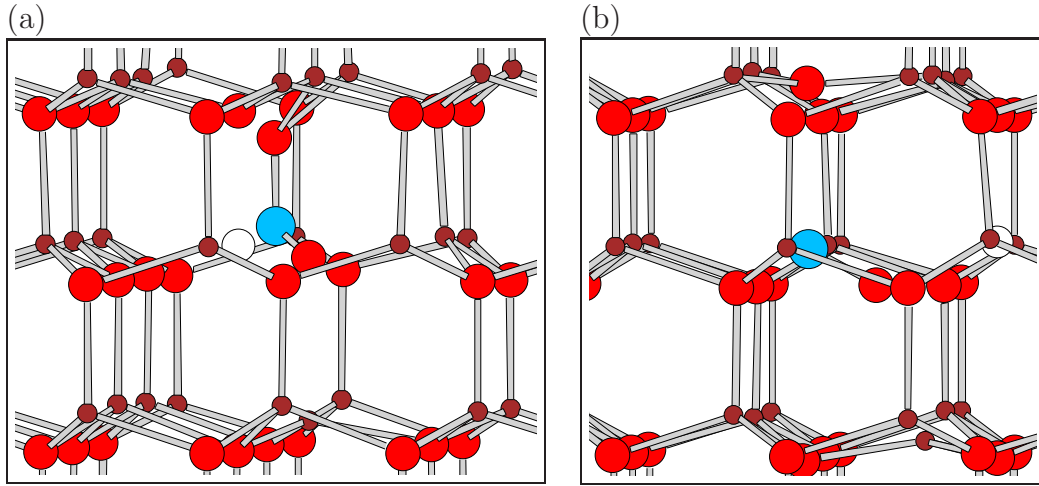
Figure 5.35: Schematic structure of (a) The energetically most stable $(N_{Zn}-V_{Zn})$ (b) The metastable structure complexes. Colours and axis are as in Fig. 5.1.
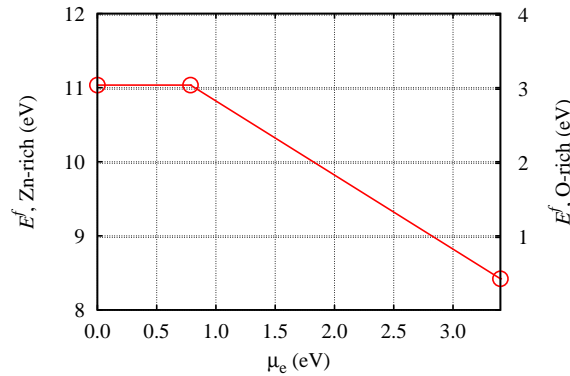
Figure 5.36: Plot of E^f *vs.* μ_e for $(N_{Zn}-V_{Zn})$ defects in ZnO calculated using the 192 atom supercell.

Electrical levels

Fig. 5.36 shows a plot of the μ_e-dependent formation energies (Eq.3.9) of $(N_{Zn}-V_{Zn})$ in ZnO for the various charge states of the stable acceptor system. This yields states in the band-gap, the $(-/0)$ level being calculated at around $E_v + 1.0\,eV$, which is much too deep to result in effective p-type conduction.

CHAPTER 5. NITROGEN
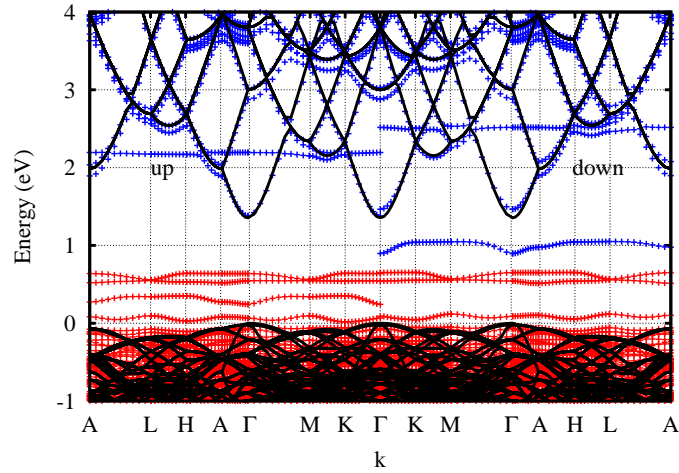
Figure 5.37: Plot of band structure of (N_{Zn}–V_{Zn}) in ZnO. Symbols, lines and scales are as defined in figure 5.3.

The acceptor properties are further illustrated in Fig. 5.37, which shows the bandstructure along high-symmetry directions in the Brillouin-Zone. The empty state between 2–3 eV is derived from π^* orbital localised on the NO_2 molecule, which is a similar result comparing to the $(NO)_O$ and $(NO_2)_O$ centres (sections 5.3.6 and 5.3.7). The filled states in the region of 0–1 eV are derived from the oxygen vacancy components left by the covalent bonding of two host O atoms to the N dopant. Again, parallels in the electronic structure can be drawn with N_O–V_O (section 5.3.4).

It is concluded that a simple combination of the N_{Zn} donor and V_{Zn} double acceptor does not yield a shallow acceptor level but is relatively stable and may, if present in sufficient quantities, contribute to optical emission due to the numerous localised states, both occupied and empty, in the band-gap

5.4.3 N_{Zn} complexes with O_i and $(NO)_{Zn}$

Oxygen interstitials (O_i) are double acceptors at the octahedral site, and act as donors when they interact with a host site to form an O_2 molecule (section 4.2.3). There are two main structures found for the combination of such an interstitial with N_{Zn}. First,

the non-bonded interstitial oxygen form may combine with the shallow donor, N_{Zn}, forming a single acceptor species. Alternatively it may chemically combine with the nitrogen and form a N–O bond, thus producing an NO molecule on a Zn site.

The molecular substitution is a potentially important contribution for a separate reason. Many experiments use species for nitrogen doping involves N–O bonds, such as NO and NO_2, and the resulting ZnO films may be activated to produce p-type carriers [16,18,31,103,103]. The suspicion might be that N-O bonds survive incorporation into the growing films, or even that the molecules themselves form interstitial dopants. The insertion of a nitric oxide anion (NO^-) into the lattice might result in substitution, either at the oxygen site as discussed in section 5.3.6, or at a zinc site, $(NO)_{Zn}$. It is the latter that is examined in this section.

Structure Details

The most stable form of defect arising from N_{Zn} and O_i in the neutral charge state is the substitution of the Zn site by NO (figure 5.38(a)). However, another configuration was also found where the NO molecule is displaced to chemically react with a nearby O site, forming a complex which may be described as $(NO_2)_{Zn}$–V_O (figure 5.38(a)). These structures are indistinguishable on the grounds of total energies. A third structure might be imagined where the N_{Zn} and O_i components are not directly bonded, so that you generate a N_{Zn}–O_i, oct pair. This was found to be energetically unfavourable and is therefore not considered further.

Relaxation of such starting configurations was found to result in two chemically distinct structures with different total energies and different potential impact upon electrical conductivity.

The N-O bond lengths are calculated to be 1.2Å and 1.4Å for the NO_2 based structure (Fig. 5.38(a)), which are typical of experimental values for N–O double and single bonds, respectively [137]. In contrast, for the NO molecular configuration, the bond lengths are calculated to be 1.15Å and 1.11Å for Figs. 5.38(b) and (c) respectively, which are slightly shorter than expected for a N–O double bond [137],
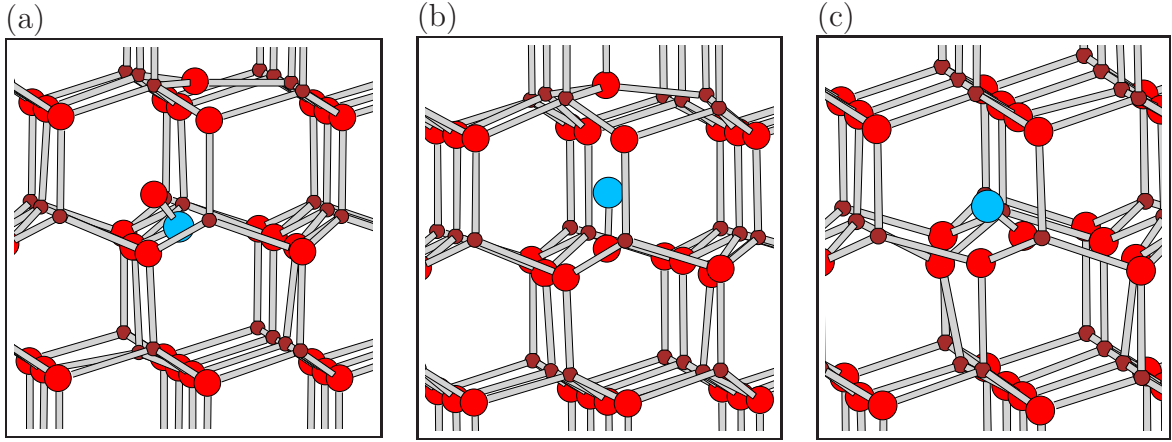
Figure 5.38: Plot of the structures of neutral (N_{Zn}–O_i) in ZnO. (a) $(NO_2)_{Zn}$–V_O (b) $(NO)_{Zn}$ with NO aligned along the c-axis, and (c) $(NO)_{Zn}$ in its equilibrium orientation. Colours and axis are as in Fig. 5.1.

but in agreement with the bond-length of gas-phase NO species (1.15Å).

In the current set of calculations, the total energies of the three configurations in the negative charge is indistinguishable, which may be viewed as somewhat surprising, especially comparing $(NO)_{Zn}$ and $(NO_2)_{Zn}$–V_O. where the number of N–O bonds differ. The binding energy of the $(NO)_{Zn}$ complex relative to separate $(NO)_i$ and zinc vacancy V_{Zn} centres is 2.2 eV for both reaction

$$(NO)_{Zn}^{-1} \longrightarrow (NO)_i^{1+} + V_{Zn}^{2-} - 2.2\,\text{eV}, \tag{5.9}$$

$$(NO)_{Zn}^{0} \longrightarrow (NO)_i^{1+} + V_{Zn}^{1-} - 2.2\,\text{eV}, \tag{5.10}$$
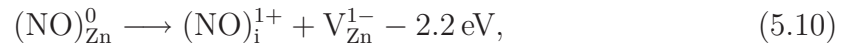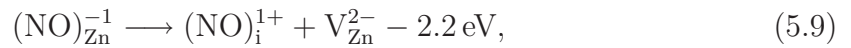
and this relatively modest binding perhaps suggests that high temperature anneals may result in the movement of nitrogen incorporated into the ZnO at a Zn site during growth, consistent with changes in electrical properties under such treatments [95, 103, 138]. Dissociation Into N_{Zn} and O_i components corresponds to a higher energy process.
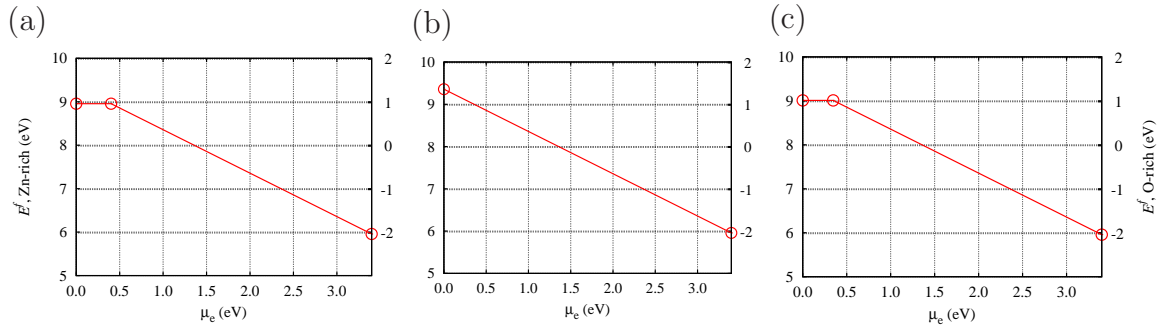
Figure 5.39: Plot of E^f vs. μ_e for $(NO)_{Zn}$ in ZnO calculated using the 192 atom supercell. (a)–(c) correspond to the structures in figure 5.38.

Electrical levels

As with the preceding defect, the electrical levels of $(NO)_{Zn}$ have been determined using the μ_e-dependent formation energies. Fig. 5.39 shows a plot of this data, which yields relatively shallow acceptor levels at around $E_v + 0.3\,\text{eV}$ for both NO and NO_2 based geometries. The axially aligned NO system is not stable in the neutral charge state.
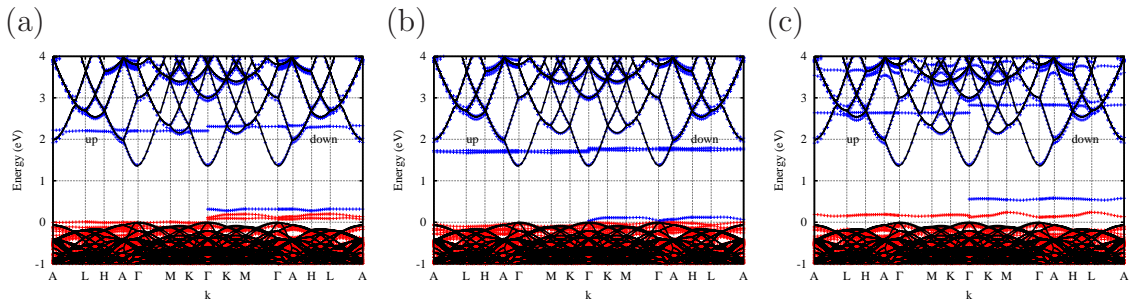
Figure 5.40: Plot of band structure of $(NO)_{Zn}$ in ZnO. (a), (b) and (c) correspond to structures (a), (b) and (c) in figure 5.38. Symbols, lines and scales are as defined in figure 5.3.

The acceptor properties of $(NO)_{Zn}$ are further illustrated in Fig. 5.40, which shows the band-structure along high-symmetry directions in the Brillouin-Zone, and it is in this data that the differences between the NO and NO_2 connectivities is perhaps more

clear. There are empty levels above the top of band-gap which are related to the NO_2 and NO molecules located at around $E_v + 2.2\,eV$, $E_v + 1.8\,eV$ and $E_v + 2.6\,eV$ for the structure in Fig. 5.38(a)–(c), respectively. Levels close to the valence band top in the case of the Fig. 5.38(a) and Fig. 5.38(c) structures are associated with anti-bonding combinations between orbitals on the NO_2 or NO molecule with the three or four oxygen atoms surrounding the molecule.

Combining the evidence from the formation energies and the band-structures, it may be concluded that both NO and NO_2 molecules supplied to make $(NO)_{Zn}$ might be produce relatively shallow acceptor species where associated with the zinc sub-lattice. Indeed, these structures might shed some light on experimental production of p-type ZnO with nitrogen using NO and NO_2 molecules as source species [18,87,103].

Vibrational Modes

Amongst the local modes of $(NO)_{Zn}$, the vibrational frequencies is calculated to be 1669 and $1767\,cm^{-1}$ for the neutral and negative charge states respectively, these are in relatively good agreement with experimental values from Raman scattering measured at 1710 and $1800\,cm^{-1}$, resulting from the incorporation of nitrogen in ZnO [129]. The $1800\,cm^{-1}$ peak, seen in p-type material, is noteworthy because it has high amplitude and small line width [129], consistent with a molecular vibrational state weakly coupled with the lattice.

5.4.4 N_{Zn} with two O_i, and $(NO_2)_{Zn}$

Extending the last section by an additional oxygen atom, one might envisage the insertion of an NO_2 ion into the lattice, potentially resulting in $(NO_2)_{Zn}$, or following the results in section 5.4.3, further react with the oxygen host to form a nitrate ion $(NO_3)_O$ at sites originally occupied by a Zn–O pair. A superficial view of the chemistry by which such species might be formed may be via reactions of the type
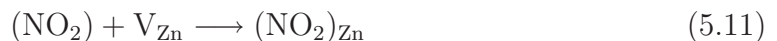
$$(NO_2) + V_{Zn} \longrightarrow (NO_2)_{Zn} \qquad (5.11)$$

and

$$(NO_2) + V_{Zn} \longrightarrow (NO_3)_{ZnO} \tag{5.12}$$

Structure Details

As with previous molecular groups, the structures composed from the addition of a single nitrogen atom and two additional oxygen atoms to ZnO were obtained in two ways. The first is simple insertion of the an NO_2 molecule into the lattice at a zinc site to make $(NO_2)_{Zn}$ with different orientations. The second was the decoration of the structure obtained for NO_3 as described shared over a Zn–O pair.

Following relaxation, there are chemically distinct structures obtained. The most stable structure is shown in Fig. 5.41, where the nitrogen atom in NO_2 forms a bond to the neighbouring host oxygen atom to make a nitrate ion, $(NO_3)_{ZnO}$. Other orientations of this structure are also found, but as much as $0.4\,eV$ higher in energy. In addition, a NO_2 molecule at the zinc site not bonded to the lattice is possible, but $3\,eV$ higher in energy, and there is also a form where a peroxide bond is created rather than a N–O, which is around $1.5\,eV$ higher in energy.
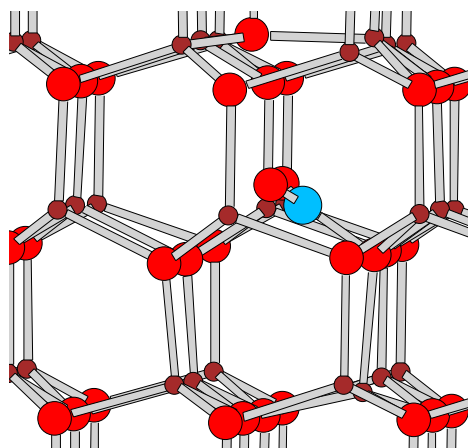
Figure 5.41: Schematic representation of the structure of $(NO_3)_{ZnO}$. Colours and axis are as in Fig. 5.1.

The N–O bond lengths are calculated to be one of 1.38Å and two of 1.21Å for the

overall negative charge state, which is in excellent agreement with typical values of N–O single and double bonds, respectively [137].

The binding energy of the complex relative to separate $(NO_2)_i$ and V_{Zn} centres is calculated to be $2.1\,eV$ and $2.4\,eV$ for the negative and neutral charge state, respectively via the reactions:

$$(NO_2)_i^+ + V_{Zn}^{-2} \longrightarrow (N_{Zn}O_{i2})^- \tag{5.13}$$

$$(NO_2)_i^+ + V_{Zn}^{-1} \longrightarrow (N_{Zn}O_{i2})^0 \tag{5.14}$$
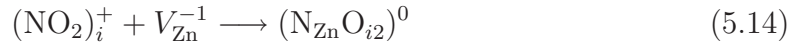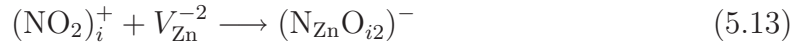
Such binding energies would render this structure unstable at very high temperatures, but may be sufficient to allow production during growth.

Electrical levels

Fig. 5.42 shows a plot of the μ_e-dependent formation energies (Eq. 3.9) of $(NO_2)_{Zn}$ in ZnO.
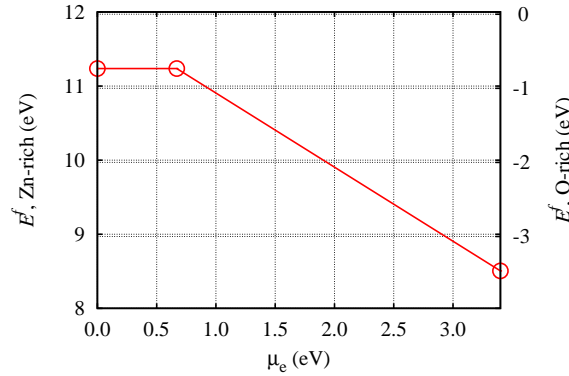
Figure 5.42: Plot of E^f *vs.* μ_e for $(NO_3)_O$-V_{Zn} in ZnO calculated using the 192 atom supercell.

Based upon the formation energies, there is a deep acceptor level, $(-/0)$, calculated at around $E_v + 0.6\,eV$. An acceptor level at this energy would be far too deep to lead to effective p-type doping. However, given the uncertainty in the precise location of

the acceptor level, and the chemical stability of the defect, this type of molecular doping perhaps warrants further investigation.
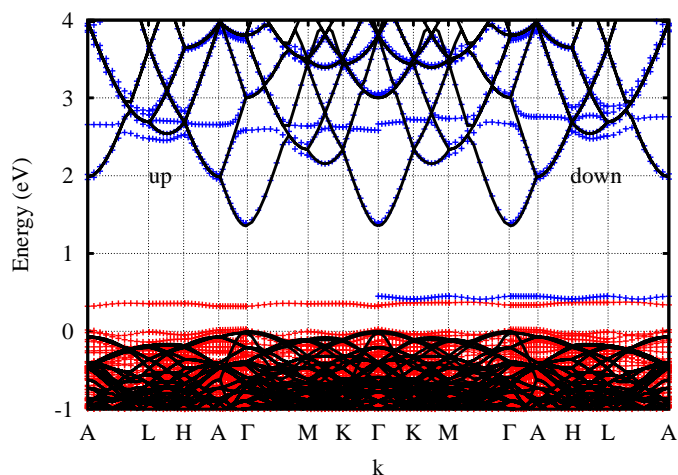
Figure 5.43: Plot of band structure of $(NO_2)_{Zn}$ in ZnO. Symbols, lines and scales are as defined in figure 5.3

The acceptor properties of $(NO_2)_{Zn}$ are further illustrated in Fig. 5.43, which shows the band-structure along high-symmetry directions in the Brillouin-Zone. The empty state around 2.6 eV is related to π^* orbitals of the NO_2 molecule. The filled state which is located at around $E_v + 0.5$ eV related to a strongly perturbed oxygen neighbour (that approximately above the molecular group along the c-axis in figure 5.41). The empty state which is located at round $E_v + 0.6$ eV above the valence-band is mostly associated with the remaining oxygen neighbours, but with some anti-bonding character with respect to the N-O bonds. The electrical levels of this centre, based upon the localisation of the gap levels on the oxygen neighbours rather than the NO_3 group, may perhaps be correlated with a modified acceptor level of V_{Zn}.

Based upon a preferential reaction leading to the formation of $(NO_3)_{ZnO}$, the combination of the formation energies in Fig. 5.42 and the band-structure of Fig. 5.43 illustrates that the substitution of Zn by NO_2 leads to relatively deep acceptor levels, with the states accepting the electron being localised on the the molecule rather than being associated with the valence band.

CHAPTER 5. NITROGEN

Another point that may be taken from the formation energies, is that by comparison with previous formation energy plots, it seems that $(NO_3)_{ZnO}$ has a very low formation energy in oxygen rich ZnO, with the neutral charge state being nearly $2\,eV$ lower that that of the $(NO)_{Zn}$ system. Combining the acceptor properties with the low formation energy may also point to NO_2 molecules contributing to p-type doping [18, 87, 103] provided that the materials are grown in the oxygen-rich limit.

5.4.5 N$_2$ substitution at a Zn site

V_{Zn} has a relatively high formation energy in p-type ZnO, but it is possible to reduce this with the addition of a nitrogen molecule. Although it more typically produces n-type material [126], experiment has indicated that the doping of ZnO using N_2 molecules *can* result in the production of p-type carriers. [11]. Given the very strong N–N interaction in the molecule, it may be anticipated that they may be incorporated directly in the growth surface to form species including $(N_2)_{Zn}$, especially where the material is produced in the oxygen-rich limit.

Structure Details

This is a simple insertion of the N_2 molecule into the lattice at a vacant Zn site. The relaxed structure obtained for an N_2 molecule substituting for Zn is shown in Fig. 5.44.

For the relaxed, neutral charge state, the N_2 molecule is found not to bond with neighbouring host oxygen atoms when the effective electron spin is unity, $S = 1$, as shown in Fig. 5.44(b), while for the $S = 0$ electronic configuration, the N_2 molecule becomes chemically bonded with two host oxygen atoms as shown in Fig. 5.44(a).

The chemical nature of the bonding is confirmed by the N–N bond lengths which are calculated to be 1.23Å in $S = 0$ Fig. 5.44(a) for neutral charge state, consistent with a N–N double bond, while the N–N bond length is calculated to be 1.11Å in Fig. 5.44(b) which is in good agreement with the experimental value of 1.10Å for the triple bond of free N–N molecule. The N–N bond is also 1.11Å for the -2 charge
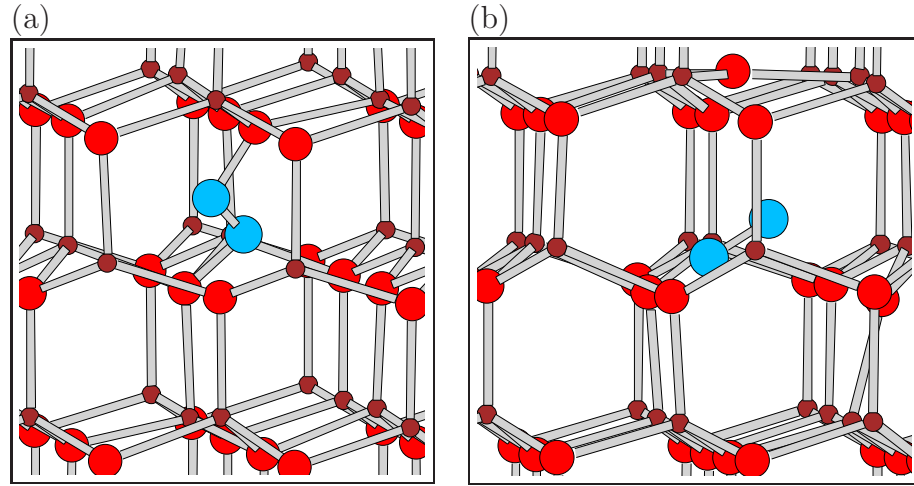
Figure 5.44: Schematic of the structure of neutral $(N_2)_{Zn}$ in ZnO for (a) $S = 0$, and (b) $S = 1$. Colours and axis are as in Fig. 5.1.

state, where one might consider the defect to be made up from a neutral N_2 molecule in a V_{Zn} in the -2 charge state.

Electrical levels

Fig. 5.45 shows a plot of the formation energies (Eq. 3.9) of $(N_2)_{Zn}$ in ZnO as a function of charge and electron spin state and μ_e.

The formation energies yield several electrical levels in the band-gap. Where the molecule is chemically bonded to the two host oxygen atoms the $(-2/0)$ acceptor level calculated at around $E_v + 1.3\,eV$, and the $(0/+1)$ donor level calculated at around $E_v + 0.3\,eV$. For $S \neq 0$, there is a $(-2/-1)$ acceptor level calculated at around $E_v + 1.0\,\text{eV}$ and a $(-1/0)$ level around $E_v + 0.2\,\text{eV}$, which closely match the electrical levels of V_{Zn}.

The acceptor levels of $(N_2)_{Zn}$ are further illustrated in Fig. 5.46 which shows the band-structure along a high-symmetry direction in the Brillouin-Zone (BZ).

In the configuration where there is an O–N–N–O linkage, there are two occupied bands in the vicinity of the valence band top, corresponding to a p-orbital on the two oxygen neighbours to the N_2 molecule that are not involved in the O–N–N–O
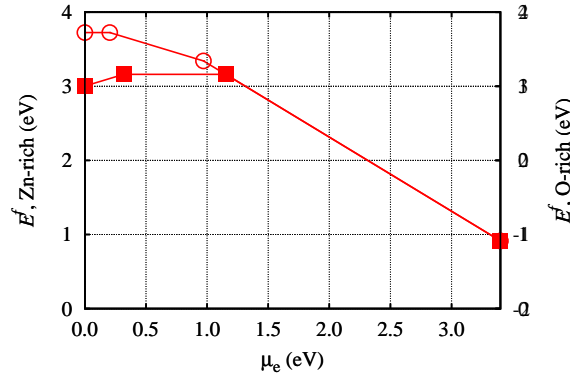
Figure 5.45: Plot of E^f *vs.* μ_e for (a) $(N_2)_{Zn}$(■) where N is bonded to the neighbouring O in the neutral charge state, $S = 0$ (b) $(N_2)_{Zn}$ (O) where the N_2 molecule is not bonded, being the $S = 1$ spin state in the neutral configuration. In the -2 charge state the structures are the same, with no bonds to the neighbouring O. All calculations are using the 192 atom supercell.

(a)   (b)
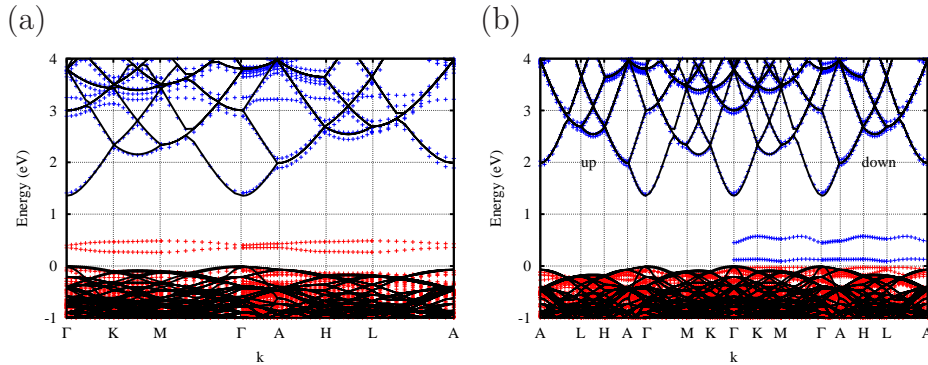
Figure 5.46: Plot of band structure of $(N_2)_{Zn}$ in the neutral charge state for (a) $S = 0$, and (b) $S = 1$. Symbols, lines and scales are as in figure 5.3.

linkage. In the non-bonded form (i.e. where there are no O–N bonds formed) there are only empty, spin-down bands in the gap. These empty bands correspond mostly to p-orbitals on the neighbouring oxygen atoms, but are weakly in an anti-bonding combination with orbitals on the N_2 molecule.

Although the $S = 1$ configuration in the neutral charge state is metastable, it is of

some interest. In ODMR experiments [106], there is evidence of an $S = 1$ centre that is not seen in standard EPR. This leads to the possibility during the optical excitation of the sample, there is a population of the metastable, but magnetically active state, which is being detected.

Vibrational Modes

Since the $(N_2)_{Zn}$ structure is based upon simple molecular groups, it may be fruitful to determine the vibrational frequencies that may be compared with experimental data.

Table 5.2: The vibrational modes of the ground state structures of $(N_2)_{Zn}$ in the three thermodynamically stable charge and effective spin states (cm^{-1}).

Defect			
$(N_2)_{Zn}, S = 0$	832	910	1537
$(N_2)_{Zn}, S = 1$	-	537	2167
$(N_2)_{Zn}^{+1}, S = 1/2$	851	867	1434
$(N_2)_{Zn}^{-2}, S = 0$	-	-	2214

The key modes of vibration of the $(N_2)_{Zn}$ defect are listed in Table 5.2. For $(N_2)_{Zn}^{-2}$, the modes are shifted to higher frequency, and are close to the vibrational mode for $(N_2)_O^{+2}$ (section 5.3.3). The highest frequency is in broad agreement with the experimental value of $2357\,cm^{-1}$ for free N_2 molecules. Such characteristic modes would act as a clear indication of their presence in N-doped ZnO.

The incorporation of nitrogen in ZnO as NO and NNO complexes the vibrational line at $974\,cm^{-1}$, $1150\,cm^{-1}$, and $1511\,cm^{-1}$ might be related to the stretching vibration of N–O or NNO [136].

5.5 Interstitial Nitrogen Molecules N$_2$ in ZnO

The final defect presented in this chapter is that made up from the insertion of a N$_2$ molecule directly into the interstitial spaces in the host ZnO lattice. Since this is not associated with either the oxygen or zinc sub-lattices, the discussion of this centre is given its own section.

A N$_2$ molecule can be incorporated directly into the growth surface to form a N$_2$ interstitial. When N$_2$ molecules are used as the nitrogen doping source the solubility of nitrogen is observed to increase greatly under O-rich conditions [19, 97–100]. Due to the evidence of N$_2$ molecules being present in the material from EPR studies [105], the possibility of an N$_2$ interstitial in ZnO was considered.

Structure Details

Fig. 5.47 shows the relaxed found structure for a N$_2$ molecule interstitial in the ZnO lattice.
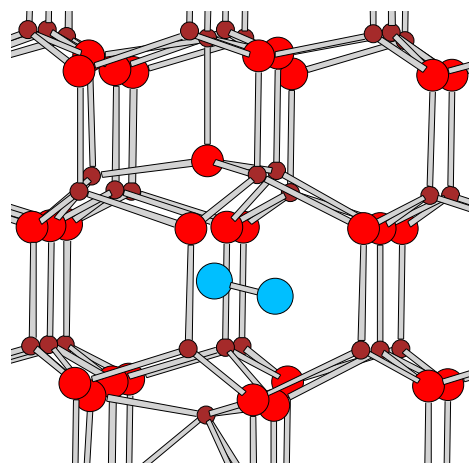
Figure 5.47: Plot of atomic structure of N$_2$ molecule interstitial ZnO, Colours and axes are as in Fig. 5.1.

There are many metastable structures, the energy difference between some of which is small, but the most stable structure shown is similar to that found in previous theoretical studies [28]. Here the nitrogen molecule breaks a Zn-O bond in the c-axis,

CHAPTER 5. NITROGEN

pushing the O and Zn atoms significantly from their equilibrium positions. The nitrogen molecule bond is found to be 1.12Å, which is in good agreement with experimental value of 1.1Å for N$_2$ gas, indicating that the nitrogen molecule is not chemically changed by insertion into the Zn–O bond.

Electrical levels

Fig. 5.48 shows a plot of the formation energies (Eq. 3.9) of the interstitial N$_2$ molecule in ZnO.
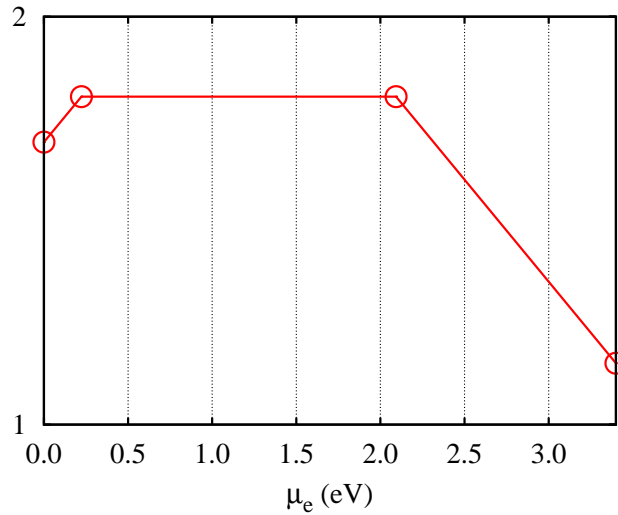
Figure 5.48: Plot of E^f *vs.* μ_e for N$_2$ interstitial in ZnO calculated using the 192 atom supercell.

This yields a localised state in the band gap; the nitrogen molecule produces a deep donor level around $E_v + 0.4$ eV, and an acceptor level around $E_v + 1.5$ eV, derived from π^* orbitals on the N$_2$ molecule. This suggests that interstitial N$_2$ is thermodynamically stable in neutral, $+1$, and -1 charge states.

The band-structure (Fig. 5.49) for the interstitial N$_2$ molecules shows a filled band around 0.4 eV above the valence band top. This state is related to a perturbed oxygen neighbour (that approximately above the N$_2$ molecule along c-axis in Fig. 5.47).
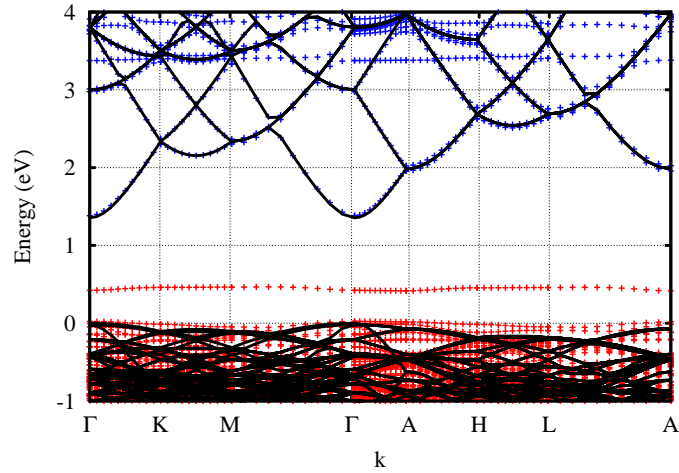
Figure 5.49: Plot of band structure of (N_2) interstitial in ZnO. Symbols, lines and scales are as defined in figure 5.3

5.6 Discussion and Conclusions

Of the nitrogen-containing centres discussed in this chapter, many act as deep donor and/or acceptor, and others are possible acceptors for the p-type conductivity observed in experiment. To establish a model of the equilibrium behaviour of N-doped ZnO, the total formation energies were compared as a function of the growth conditions (O-rich *vs.* Zn-rich, as described in section(5.3, 5.4) and the electron chemical potential.

5.6.1 Structures by association with sub-lattice

One way to divide the defects, as has been adopted in the structure of this chapter, is by the sub-lattice that the defect might be most closely associated with.

The oxygen sub-lattice

For the O-sub-lattice under extreme O-rich conditions, Fig. 5.50(a), the formation energies show that the species that may be described as either $(NO_{n-1})_i$ or $(NO_n)_O$ group are highly favourable. Amongst these stable structures, there are possible

(a)

(b)

Figure 5.50: Plot of E^f per N atom *vs.* μ_e for key N-containing defects associated with the oxygen sub-lattice in ZnO, calculations using the 192 atom supercell. $N_O(*)$, $(NO_4)_O(+)$, $(NO_3)_O(X)$, $(NO_2)_O(\nabla)$, $(NO)_O(O)$, N_O-V_O (●), $(N_O$-$Zn_O)(▲)$, N_O-$Zn_i(\triangle)$, $(N_2)_O(\blacksquare)$, $(N_O)_2(\square)$ (a) Oxygen-rich conditions and (b) zinc-rich conditions.

candidates for acceptor complexes where $n = 4$ are favoured for must values of μ_e. However in p-type material, and specifically where $\mu_e < 1\,\text{eV}$ in the oxygen-rich limit, the $(NO_3)_O$ deep donor is favoured, so in equilibrium a combination of the two species

$(NO_4)_O$ and $(NO_3)_O$ might be expected to form.

Although it cannot be guaranteed that there is not another, lower energy defect complex associated with the oxygen sub-lattice (e.g. one based on structures containing other chemical species), it seems reasonable based upon the known chemical stability of nitrate ions that under O-rich conditions $(NO_4)_O$ or $(NO_3)_i$ are particularly low in energy, and it is worth noting that the formation energies yields the precise location of the acceptor level to be $E_v + 200\,\text{meV}$. Encouragingly, experimentally, p-type N-doped ZnO has been reported under O-rich conditions achieved by annealing in an oxygen atmosphere with an acceptor level located around $200\,\text{meV}$ above the valence band [14, 107–110, 139].

To support the view that N–O bond formation is a plausible route to p-type materials, a general view formed from the interpretation of XPS data is that in p-type material, group-V elements such as Sb are predominantly bonded to oxygen [87]. In addition, it should be emphasised that p-type material from N-doping is almost exclusively obtained using sources that involve N–O bonds [16, 18, 31, 103, 103, 138].

Therefore, at this interim point in the discussion, $(NO_3)_i$ must be viewed as a strong candidate for the formation of p-type ZnO.

Turning to Zn-rich material, Fig. 5.50(b), species described as $(NO_n)_O$ are less favourable than other structures. There are energetically favourable donor structures such as $(N_O–Zn_O)$ and those that can be characterised as V_O-related, being $(N_2)_O$ and the form of $(N_O)_2$ that is structurally $((N_2)_O–V_O)$. For n-type material the favoured structures are all based upon N_O.

Again the lack of energetically stable acceptor levels in the vicinity of the valence band has connections with observation. Experimentally, n-type N-doped ZnO has been reported under Zn rich conditions. Noting that $(N_O–Zn_O)$ under these conditions is very stable and a shallow donor a number of potential formation routes may be imagined. One might involve the formation of V_O in the vicinity of N_O, both of which are low energy defects in Zn-rich conditions. If Zn_i are formed in such material, since the diffuse readily, it seems reasonable to expect them to combine with V_O to form

anti-sites, and hence contribute to n-type conduction.

However, in the zinc-rich limit, under equilibrium conditions, the formation energies suggest that a mixture of shallow donors and deep acceptors would be formed. Therefore, a kinetic argument, perhaps based upon reactions such as that above, may explain the n-type conductivity in this material.

The zinc sub-lattice

For Zn-sub-lattice and under O-rich condition Fig. 5.51(a) shows that the $(NO_n)_{Zn}$ group are highly favourable and the possible acceptor complexes are favoured for must values of μ_e. In p-type material under O-rich conditions $(NO_3)_{ZnO}$ is lowest in energy, and given the uncertainty in the precise location of the acceptor level, it must be viewed as a candidate for the formation of p-type ZnO.

For Zn-rich material the $(NO_3)_{ZnO}$ is less favourable than the donor structure, which could be incorporated directly with the ZnO thin films to make n-type ZnO.

In summary, the (NO_n) centres in ZnO present a rather appealing possible explanation for the production of p-type ZnO using N–O based doping precursors. The calculated structures show that the (NO_n) groups are stable in the lattice, and combined with the formation energies can be viewed preferentially adopting ZnO.

5.6.2   Analysis for most stable structures

Next, the energies will be compared over both sub-lattices, focusing upon those defect structures that are most stable in O- and Zn-rich conditions.

Figure 5.52 shows a plot of the formation energies of those defect structures within $4\,\text{eV}$ of the most stable defect form including charge state. Both limits show clear trends in the equilibrium form of nitrogen.

In O-rich conditions, the stable forms of N-containing centres can all be identified as being a nitrate species, but located in different environments in the lattice. In particular, for an electron chemical potential around the valence band top, the most favourable form is a nitrate group substituting for oxygen in the positive charge state.

(a)

(b)
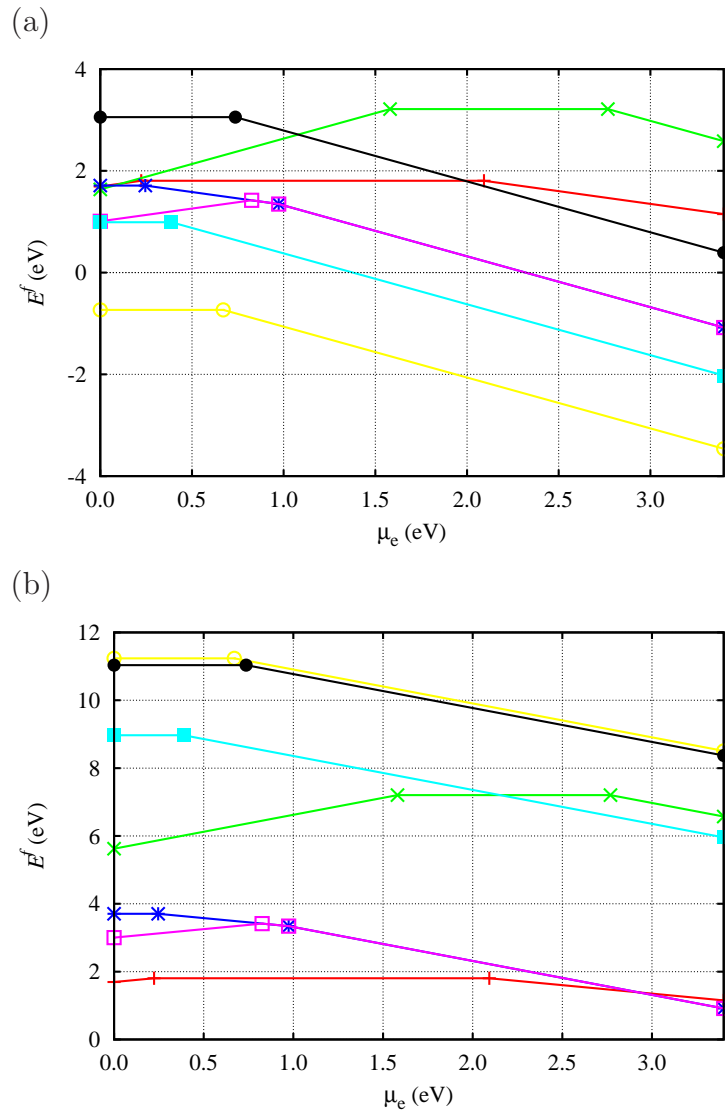
Figure 5.51: Plot of E^f per V atom *vs.* μ_e for key N-containing defects associated with the zinc sub-lattice in ZnO, calculations using the 192 atom supercell: $(N_2)_i(+)$, $N_{Zn}(X)$, $(N_2)_{Zn}(*)S = 1$, $(N_2)_{Zn}(\square)S = 0$, $(NO_2)_{ZnO}(\blacksquare)$, $(NO_3)_{ZnO}(O)$, N_{Zn}-$V_{Zn}(\bullet)$. (a) Oxygen-rich conditions and (b) zinc-rich conditions.

Under conditions where μ_e is in the upper part of the band-gap, substitution of a Zn-O pair by a nitrate group is favoured, closely followed by a nitrate group in an interstitial location (equivalent to $(NO_4)_O$). This reflects a general trend that where oxygen is

CHAPTER 5. NITROGEN

(a)

(b)
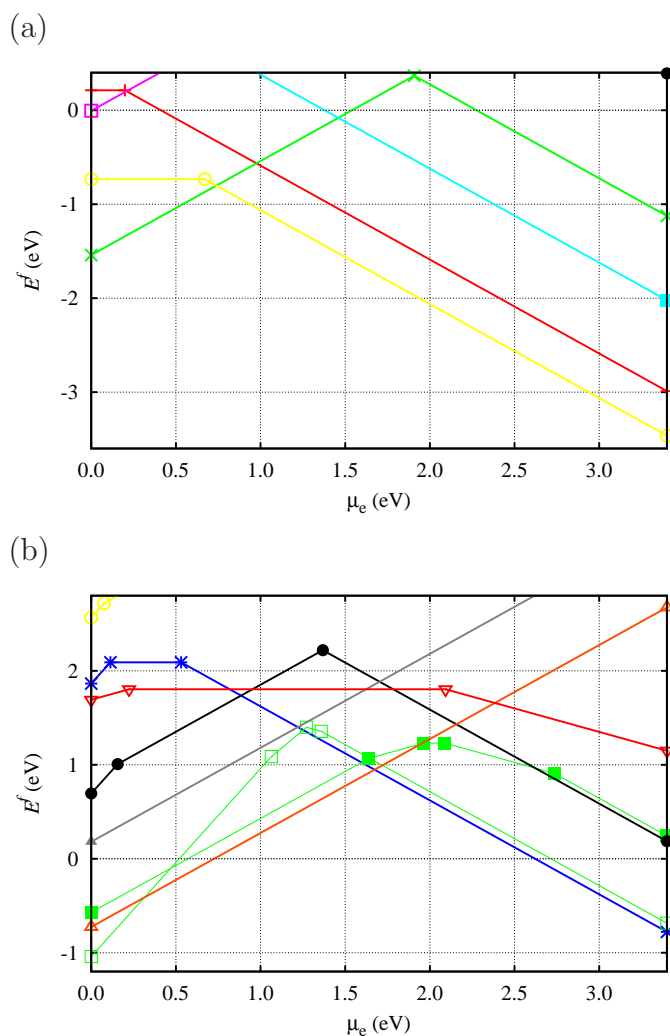
Figure 5.52: Plot of E^f per N atom *vs.* μ_e for key N-containing the most stable defects in ZnO calculations using the 192 atom supercell: $(N_O)Zn_i(\triangle)$, $(N_2)_O(\blacksquare)$, $(N_2)_OV_O(\square)$, $(N_O)Zn_O(\blacktriangle)$, $(N_O)V_O(\bullet)$, $(N_2)_i(\triangledown)$, $(N_O)(*)$, $(NO_2)_O(\square)$, $(NO_2)_{ZnO}(\blacksquare)$, $(NO_3)_O(X)$, $(NO_4)_O(+)$, $(NO_3)_{ZnO}(O)$. (a) Oxygen-rich conditions and (b) zinc-rich conditions.

in abundance, the favourability in energy terms of covalent bond formation is a key factor. It is also worthy of note that acceptor species, such as $(NO_3)_i/(NO_4)_O$, are relatively stable in absolute terms, and that perhaps surprisingly, defects associated with the O-lattice are favoured.

In Zn-rich conditions, the low energy species are also mostly associated with the O-lattice. Several forms of defect based upon N_O are present in the low-energy range: N_O acceptors are favoured in n-type material, whereas in p-type material, N_2 on the oxygen site (including the form generated by the combination of neighbouring N_O centres), section 5.3.2, 5.3.3 plus N_O–Zn_i are favoured.

This shows a mixed chemical picture: the N_2 based systems are related to the very strong covalent interactions in the molecule, but the N_O–Zn_i and N_O centres in n-type material are more reasonably described by an ionic picture. Overall, it is clear that in Zn-rich conditions, amongst the defect centres examined in this work there are no clear candidates for acceptors, but there are good candidates for donors.

One might then combine these descriptions to reflect upon the experimental observations. It is a general trend that to form p-type material, O-rich conditions are required, whereas in the Zn-rich limit, n-type conduction is seen. The calculations showing favourability for nitrate groups in O-rich conditions may therefore offer some explanation for this growth condition dependence.

5.6.3 Comparison between N-O and N-N based doping species

The final division of the data relates to the form of nitrogen used in the source species. Broadly speaking, one can divide N-species into those with N–N bonds, and those without. The latter typically has the form of a N-O containing species such as NO_2. If one accepts that the energy required to break the N–N bond in the molecule is unlikely to be available during many growth procedures, it may be worth reflecting upon the relative formation energies of the defects produced containing N–N bonds compared to those N–O bonds. This is done in figure 5.53. In figure 5.53(a) it can be seen that under O-rich conditions, growth species containing N–O bonds, if they survive the incorporation into the ZnO film, may be anticipated to form the nitrate acceptor structures reviewed above. Under the same conditions, but with a N–N source (figure 5.53(b)) there are no candidates for acceptors.

Under Zn-rich conditions, plotted in figure 5.53(c) and (d), the results for both
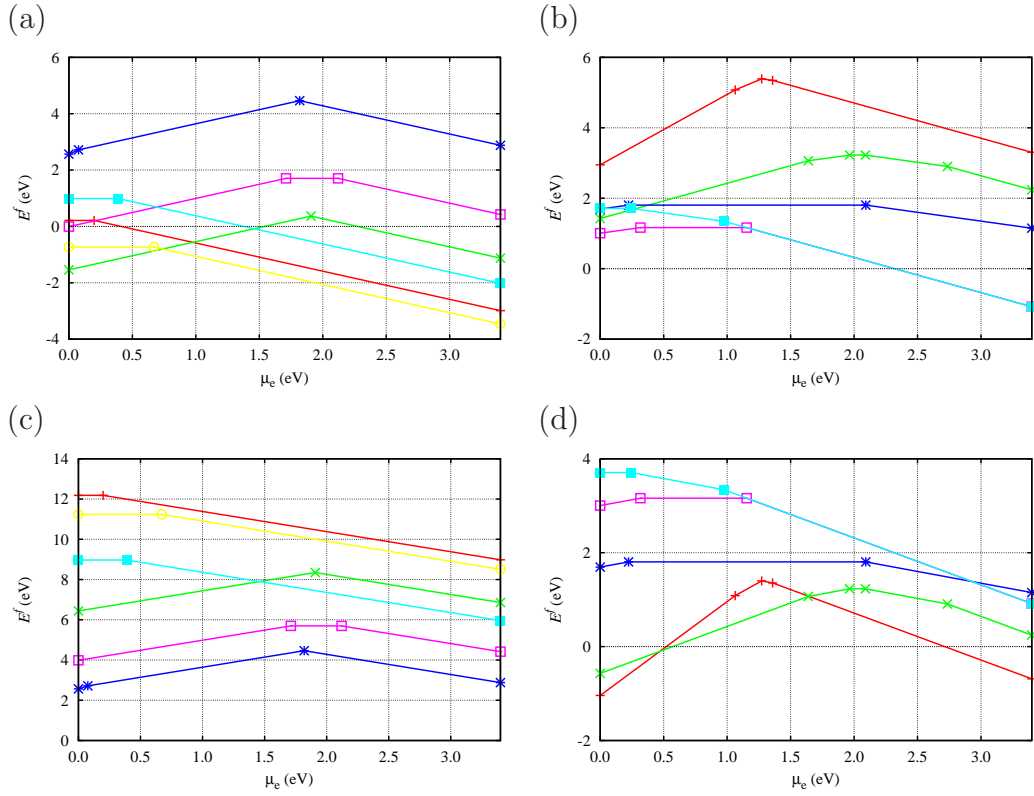
Figure 5.53: Plot of E^f per N atom *vs.* μ_e for (a,c) $(NO)_n$ defects and (b,d) NN defects in ZnO. Calculations using the 192 atom supercell: (a,c) $(NO_3)_{ZnO}(O)$, $(NO_4)_O(+)$, $(NO_3)_O(X)$, $(NO)_{Zn}(\blacksquare)$, $(NO_2)_O(\square)$, $(NO)_O(*)$, (b,d) $(N_2)_O V_O(+)$, $(N_2)_O(X)$, $(N_2)_i(*)$, $(N_2)_{Zn}(\square)$ $S=0$ (O–N–N–O) structure, $(N_2)_{Zn}(\blacksquare)$ $S=1$ (N–N) structure, (a,b) Oxygen-rich conditions and (c,d) zinc-rich conditions.

N–O and N–N sources both show a more favourable energy where the structures are deep donors.

Overall, the calculations show some support for the view that N_2 source species are not likely to generate the desired p-type conductivity.

In summary, the calculation of the energetics and electrical activity of a wide range of defect structures obtained by the insertion of one or two N atoms within the ZnO

lattice gives some clear guidance to the manufacture of p-type ZnO:

- The use of O-rich growth conditions tends to favour the formation of NO_n molecular groups, which are a plausible source of acceptor centres (e.g. $(NO_3)_i$).

- Zn-rich growth conditions tend to favour the formation of N-containing defects which act as donors, with N_O–Zn_i being a notable shallow example.

- The use of N_2 as a source of N during growth is likely to result in the formation of deep donor and deep acceptor species such as $(N_2)_{Zn}$ and $(N_2)_O$.

However, there remain several key challenges in the use of DFT calculations in the determination of the species present in N-doped ZnO. Perhaps the most notable issue relates to the uncertainties in the formation energies due to the functional (future application of screened-exchange is an important task), and the contribution from the periodic boundary condition in the charge states.

Furthermore, for conclusive determination of defect structures present in real materials, unambiguous determination of, for example, spectroscopic data is highly desirable. For example, although there are many vibrational modes tentatively linked to nitrogen, they are not a diagnostic tool in isolation as several defects may well give rise to vibrational frequencies that are indistinguishable to within the accuracy of the calculation. Perhaps a better form of identification may come with the calculation of hyperfine interactions with nitrogen nucleus in EPR experiments, which are planned to be performed in the near future.

Chapter 6

Phosphorus Doping ZnO

6.1 Introduction

Since ZnO exhibits n-type conductivity even without intentional doping, part of difficulty in to obtaining p-type conductivity is due carrier compensation [130].

A potential route is doping with group-V elements, although theoretical studies signified a difficulty to explain the p-type activity. Nevertheless, high hole carrier concentrations have been achieved using P, As and Sb [92, 93, 96, 141–143].

The conductivity, mobility and charge carrier type is known to depend strongly upon growth conditions including temperature and whether the conditions are zinc or oxygen rich. For example, phosphorus-doped ZnO exhibiting n-type conduction as-grown is converted to p-type by annealing at 600°C in an oxygen atmosphere, [104] and as-grown p-type material is favoured in growth involving higher oxygen partial pressure [144].

Quantum-chemical simulations have greatly informed on the potential of candidate dopants to produce p-type ZnO. Some calculations indicate that group-V doping may work [93, 96, 142, 143, 145, 146]. However, experimentally doping with phosphorus can both produce p-type material or enhance n-type behaviour in as-deposited films, indicating the potential for formation of donor states. This is contrary to the expectation of acceptor-defect formation via substitution on the oxygen site [146]. In addition,

according to the first-principles density-functional calculations, the phosphorus defect substitutes for an O site P_O it is a deep acceptor [13, 25, 29, 35].

Where p-type conduction is achieved, one possible shallow acceptor is derived from the triple-donor configuration of P substituting for zinc combined with two zinc-vacancies, [25, 145] since each V_{Zn} is a double acceptor [145]. Such a centre would naturally be most favourable in oxygen-rich (zinc-lean) conditions, and suppressed in zinc-rich conditions, leading to a plausible explanation for the efficacy of phosphorus-based p-type doping based on these centres. For group-V elements there is independent experimental evidence that they are more likely to be associated with substitution on the zinc sub-lattice rather than the oxygen sub-lattice, and are more likely to for P–O than P–Zn bonds [21–23, 140].

Another native defect yielding a double-acceptor level is interstitial oxygen [26, 27, 79], O_i. This defect also acts as a donor as O_i may either be in a non-bonded anion state, or chemically react with the lattice where is forms an O_2 molecule on the O-site depending on charge state. The formation energy of O_i is calculated [27, 79] to be comparable or lower than that of V_{Zn}, so it may then be expected to be of importance, especially in oxygen rich conditions.

This chapter will explain the mechanism of interaction that occurs within the film, and will explain why there is success in producing p-type material in some cases and failure in others. This study show that six-fold coordination with oxygen is considerably more favourable than structures such as P_{Zn}-2V_{Zn}.

6.2   Results

6.2.1   Phosphorus substituting for oxygen

Relaxation of P on the O-site (P_O) has been examined. The structure obtained for neutral P_O is shown in Fig. 6.1(a). The P atom remains on-site and is approximately tetrahedral with four P–Zn bonds of 2.23–2.27Å, in excellent agreement with previous calculations [25]. Since P has one fewer valence electron than the oxygen atom it

replaces, it is expected that P_O will be an acceptor, and indeed this is what is found. The negatively charged state closely resembles the neutral in structure, but with slightly shorter P–Zn bonds of 2.17–2.20Å, also in excellent agreement with previous calculations [13]. The charge-dependent formation energies (Fig. 6.2(a)) indicate a $(-/0)$ acceptor level around $E_v + 1.0\,\text{eV}$, far too deep for p-type doping, and in line with previous theory [13, 25, 29, 35].
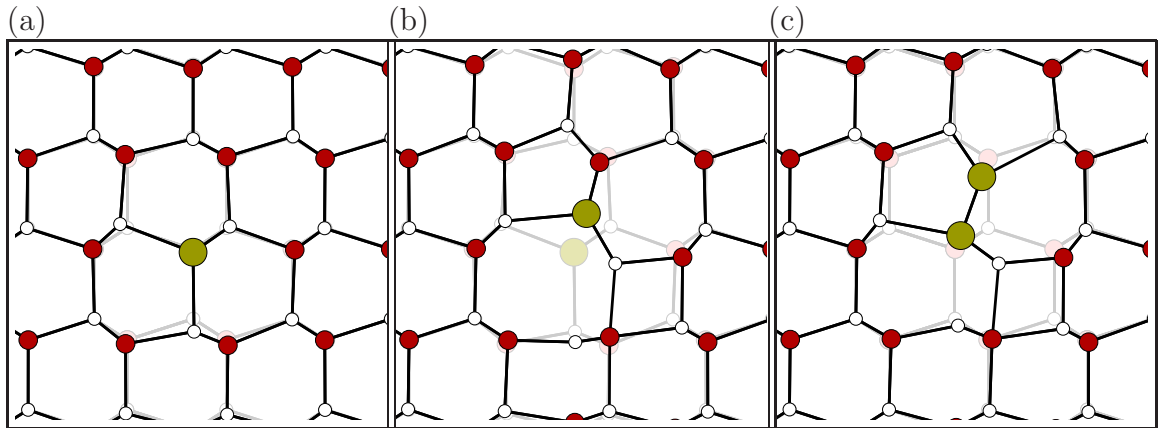
Figure 6.1: Projections onto $(1\bar{1}00)$ of the structure of P_O in (a) the neutral charge state and (b) the positive charge state, AX structure. (c) shows the lowest energy orientation of the reconstructed P_O-pair. Small, medium, and large circles represent Zn, O, and P atoms, respectively. In (a) and (c) the host-lattice is shown in the background as a reference, whereas in (b) the on-site structure is shown in the background to help show the sense of the reconstruction. The c-axis is in the vertical direction in the projections.

The acceptor level of P_O is further illustrated in Fig. 6.3(a), which shows the band-structure along high-symmetry directions in the (BZ).

In addition, and similar to N_O (AX) 5.3.1, P_O may act as a donor, as it can undergo a chemical reaction with a neighbouring oxygen atom, forming the structure shown schematically in Fig. 6.1(b), the so-called AX centre [13].

Indeed, in this form the calculations suggest that P_O may donate *two* electrons. As ZnO is a hexagonal material, there are three distinct types of second-neighbour
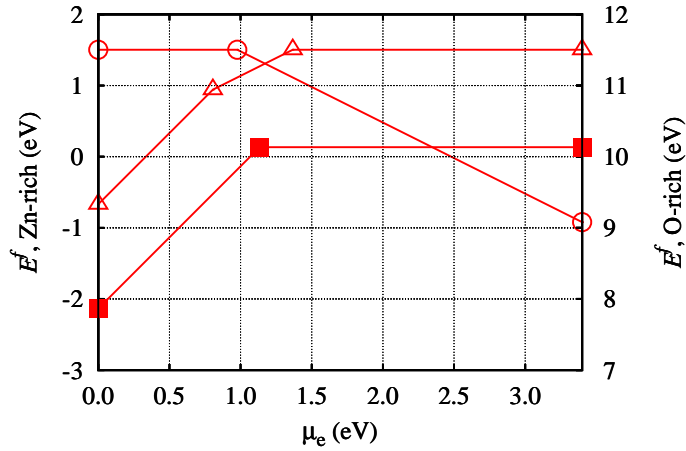
Figure 6.2: Plot of E^f *vs.* μ_e for key P-containing defects in ZnO calculated using the 192 atom supercell: P_O (O), AX^{+1} ($\triangle$) $(P_O)_2$ ($\blacksquare$).

sites by symmetry. The orientation for the AX^{+1} structure which is found to be lowest in energy differs from that previously suggested [124], which is found is meta-stable and 0.5 eV higher in energy. In addition, there is a meta-stable, on-site form similar to Fig. 6.1(a) in the positive charge state which is around 1.0 eV higher in energy than AX^{+1}. The AX structure is metastable in the neutral charge state, but has a formation energy around 2.6 eV *higher* than that of the on-site form. In all charge states, where present, the substantial structural re-arrangement can be viewed as the formation of a P=O molecular fragment within the ZnO lattice, and the band-gap levels are highly characteristic of π^*-interactions between these two atoms.

The existence of the AX form introduces the possibility of a $(-/+)$ transition from the on-site negative charge state to the AX positively charged configuration. Fig. 6.2 shows a plot including the formation energies (Eq. 3.9) of the AX centre. This yields a level around $E_v + 1.3$ eV. A second donor level is found at $E_v + 0.9$ eV, which can be understood as further depopulation of a π^* combination of orbitals on the P=O pair. The donor levels of AX is further illustrated in Fig. 6.3(b), which shows the band-structure along a high-symmetry directions in the (BZ).

This picture is extended when we examine the possibility of P_O forming pairs.

(a)
(b)
(c)
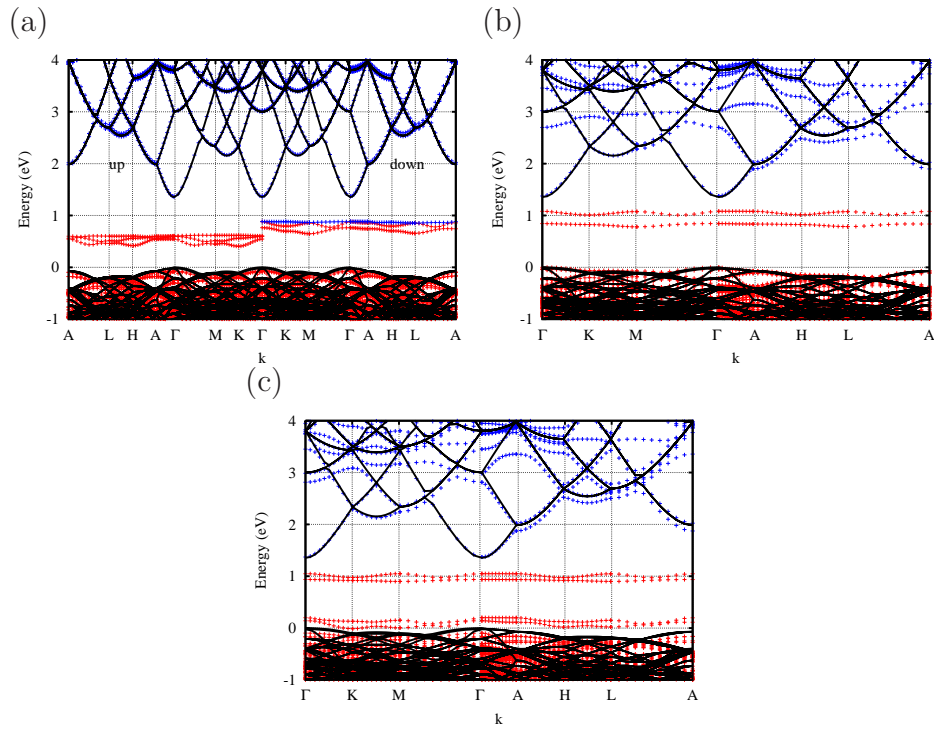
Figure 6.3: Plot of band structure for (a) P_O (b) AX^{+1} (c) $(P_O)_2$ in w-ZnO, where the zero of energy is set to be the valance band top for bulk ZnO. Red and blue cross indicates filled and empty bands, respectively

There are a number of P pairs starting configurations reflecting the anisotropy of the lattice. Where P_O pairs are in the nearest-neighbour configuration, there is a *spontaneous* reconstruction between the P atoms to form a P_2 molecule, with the more energetically favourable orientation combining O-sites in different basal planes, as shown in Fig. 6.1(c). The P–P bond length is calculated to be 2.1Å for the neutral charge state, which is in good agreement with the experimental value of 1.9Å for P_2 molecule in the gas phase [147]. This significantly reduces the formation energy (Fig. 6.2) for substitution onto the oxygen lattice, the formation energy *per P atom* being 1.3 eV lower for the pair as compared with isolated P_O centres. It is clear that P_O-pairs have a structure which strongly resembles the P_O AX centre.

One might expect P_O-pairs to preferentially adopt a different structure if they become negatively charged, since individually P_O centres in the negative charge state are

close to tetrahedral and on-site. Perhaps surprisingly, the reconstruction between P atoms is *not* lost upon charging with additional electrons, and from this it is concluded that the energy gained in the formation of the P–P bond destabilises the neighbouring on-site P_O-pairs, *even if they are negatively charged*, and the electrons are moved into the host conduction band. Thus, the nearest-neighbour P_O-pairs cannot act as acceptors. There are $(0/+)$ and $(+/2+)$ levels in the band-gap, estimated at $E_v + 1.1$ eV and $E_v + 0.7$ eV, respectively (Fig. 6.2(c)). The donor levels of AX are further illustrated in Fig. 6.3(c), which shows the band-structure along high-symmetry directions in the (BZ). In equilibrium, therefore, if P_O are significant in the manufacture of p-type ZnO, they will have to compete with the formation of $(P_O)_2$ double-donors.

The formation of P–O reconstructions in the positive charge state of P_O, and the P–P bond in neighbouring P_O-pairs reflects the impact that the formation of strong, covalent bonds has upon the total energies. The following section will show that this is a driving factor in a wide range of P-containing centres associated with both the oxygen and zinc lattices.

6.2.2 Interstitial P

The possibility for phosphorus to lie in an interstitial site (P_i) has been examined. Since it is found that such defects spontaneously react with the oxygen in the lattice, interstitial P can be thought of as being associated with the oxygen lattice, so they are examined here.

There is a significant number of metastable P_i structures, separated by small differences in total energy, but chemically distinct with differing numbers and orientation of P–O (and P–Zn) bonds. In general they are characterised by the phosphorus being covalently bonded to one, two, or three host oxygen atoms, and two characteristic structures that are found illustrated in Fig. 6.4.

Fig. 6.5 shows a plot including the formation energies (Eq. 3.9) of P_i in w-ZnO. This yields a *triple donor*, with a $(+1/ + 3)$ transition around $E_v + 1.8$ eV. The localisation of the band-gap levels of P_i suggest that it can be characterised as a

(a) (b)
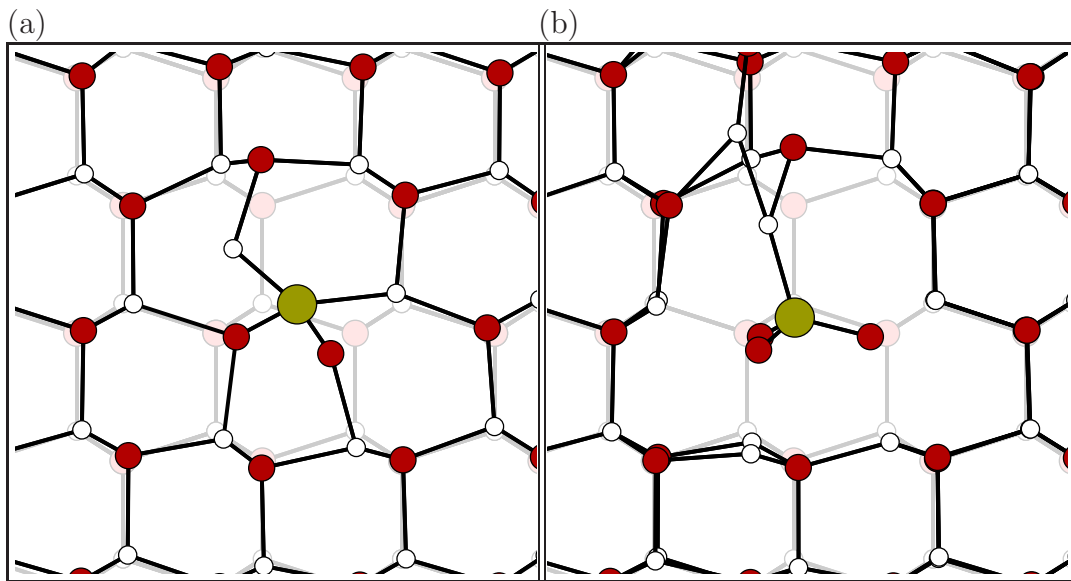
Figure 6.4: Schematic of the most stable P_i structure. Colours and axes are as in Fig. 6.1.
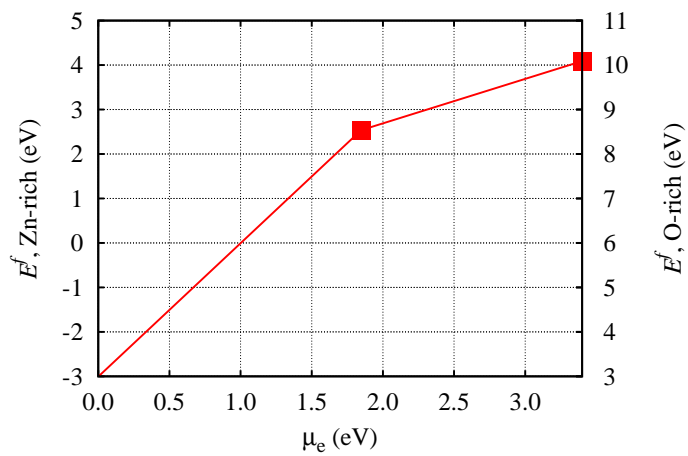
Figure 6.5: Plot of E^f *vs.* μ_e for P_i defect in ZnO. calculated using the 192 atom supercell.

molecular ion, in this case PO_2 and PO_3.

The donor level of the P_i structure is further illustrated in Fig. 6.6, which shows the band-structure along a high symmetry direction in the (BZ).

CHAPTER 6. PHOSPHORUS DOPING ZNO
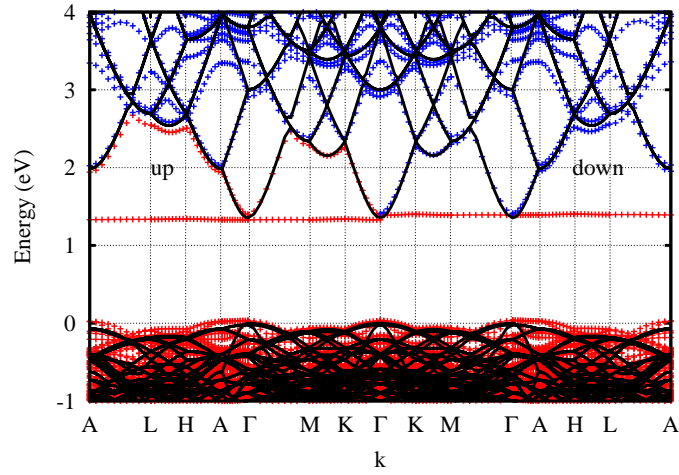
Figure 6.6: Plot of band structure for P_i in w-ZnO, where the zero of energy is set to be the valance band top for bulk ZnO. The red and blue crosses indicate filled and empty bands, respectively

Fig. 6.7 shows the energy barrier for diffusion of P_i, which includes many stages, such as bond-rotations, and inter-conversion between PO_2 and P=O molecular fragments. The details of the path are less important than the rate-limiting barrier, which is about $1\,\text{eV}$. This must be an upper limit to the net barrier height (there may be other, lower energy routes) so at growth temperatures, where such a barrier would be easily overcome, P_i is a relatively mobile species.

The formation energy of P_i has been calculated to be between 4.8–$5.9\,\text{eV}$, (the range of values arising due to the dependence of μ_P upon μ_O), so that even in the most favourable growth conditions the likelihood of formation of this centre is rather low.

In addition, during the simulations of P_i we observed *spontaneous* reactions of the type $P_i \rightarrow P_{Zn} + Zn_i$. Using the formation energies of P_i and the reaction products separated from each other, the loss of P_i and formation of Zn_i in the neutral charge state has been calculated and involves no significant gain or loss in energy.

The substitution of oxygen by a P_2 molecule can be thought of as P_O capturing a phosphorus interstitial, and such centres have been proposed as possessing a low
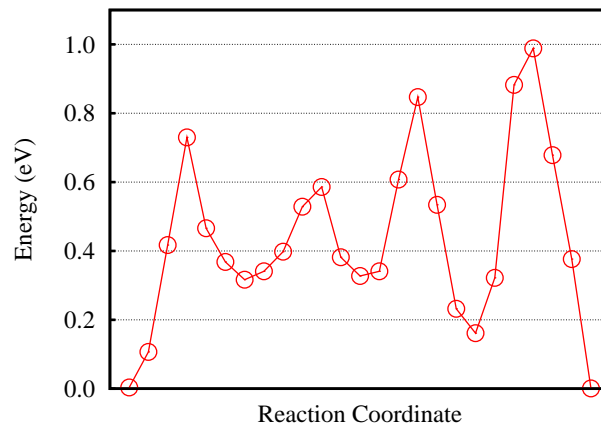
Figure 6.7: NEB calculated migration barrier for interstitial phosphorus in ZnO.
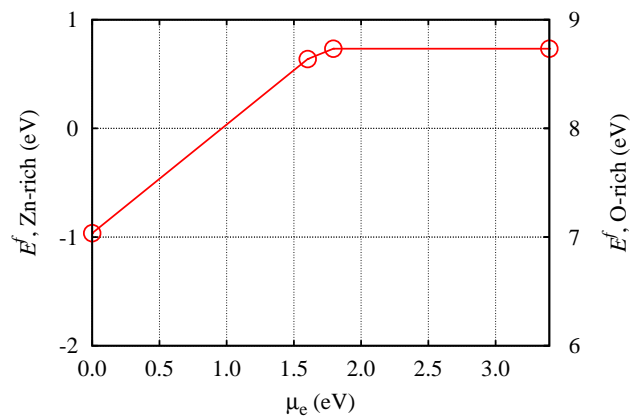
Figure 6.8: Plot of E^f vs. μ_e for $(P_2)_O$ defect in ZnO. calculated using the 192 atom supercell.

formation-energy previously [25] in p-type material.

Fig. 6.8 shows the plot of the formation energies (Eq. 3.9) of $(P_2)_O$ in w-ZnO. $(P_2)_O$ is competitive in energy in p-type material, but is never the most stable form of P-centre associated with the oxygen sub-lattice as shall be shown in (Sec. 6.2.6).

6.2.3   Phosphate ion on the oxygen lattice

The structure and chemistry of P_i is suggestive of a class of defects which are P-containing molecules substituting for O, $(PO_n)_O$. For $n = 4$, this represents a phosphate ion at the oxygen site. The structure is shown schematically in Fig. 6.9.
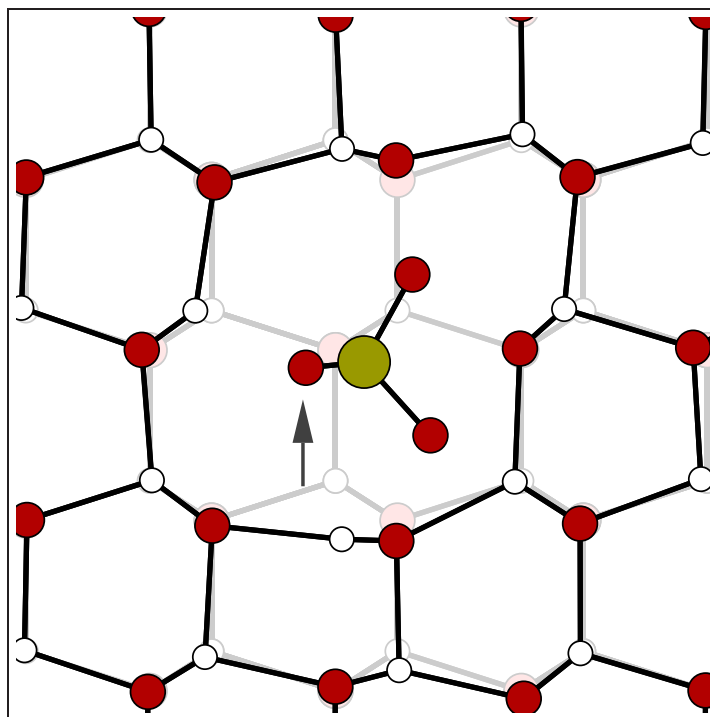
Figure 6.9: Schematic of a phosphate ion at an oxygen site. Symbols are as in in Fig. 6.1, and arrow indicates where one of the O-atoms in the phosphate ion eclipses another.

The phosphate group normally adopts a -3 oxidation state, rather than the -2 oxidation state of the oxygen ion it replaces. This leads to a deficit of charge at this defect site, and it acts as an effective acceptor. Fig. 6.10 shows a plot of the formation energies (Eq. 3.9) for $(PO_4)_O$. This yields a shallow acceptor level, around $E_v + 0.10\,\text{eV}$. This level is in excellent agreement with one interpretation of bound-exciton photoluminescence from P-doped ZnO, suggestive of an acceptor level between $\sim$90–120 meV above the valance band E_v [148,149]. These phosphorus-doped ZnO thin films
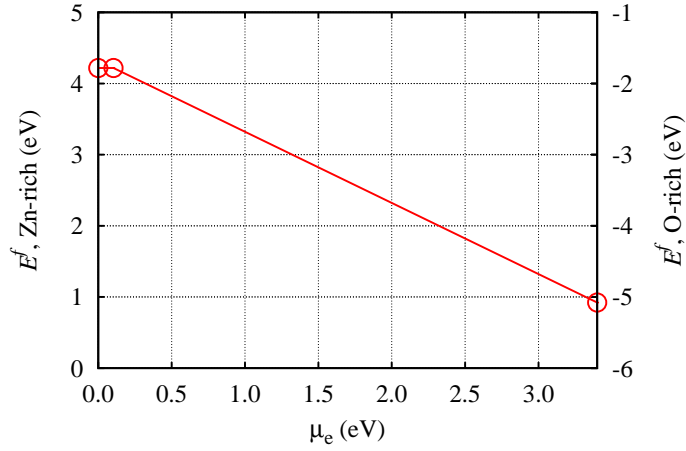
Figure 6.10: Plot of E^f *vs.* μ_e for a phosphate ion at an oxygen site. The energy is calculated using the 192 atom supercell.

showed a good p-type conductivity with a hole carrier concentration of $5.3 \times 10^{-18} \text{cm}^{-3}$ at room temperature. The acceptor level of the structure is further illustrated in Fig. 6.11, which shows the band-structure along high symmetry directions in the (BZ). Note the empty band close to the valance band top for the neutral charge state is indicating a shallow acceptor level, and the charge-state dependent formation energies indicate a level at $E_v + 0.10\,\text{eV}$.

This defect contains additional oxygen atoms relative to the host, and is therefore clearly a centre that will be favoured energetically under oxygen-rich growth conditions. The absolute formation energy of this shallow acceptor in the oxygen-rich limit is found to be highly favourable in comparison to other acceptor structures.

The intermediates (in terms of increasing oxygen content) between P_i and $(PO_4)_O$ all act as donors, but are energetically less favourable than the phosphate ion in oxygen-rich conditions. However, there is a strong theme in terms of the structures. For example, in the $(PO_3)_O$ centre, phosphorus forms an additional bond to a neighbouring O-site, and can be considered to be a phosphate ion distributed over two host O-sites. Since the phosphate ion normally adopts a -3 charge state, which in this case is substituting for two O^{-2} ions, it is easy to see why $(PO_3)_O$ acts as a single
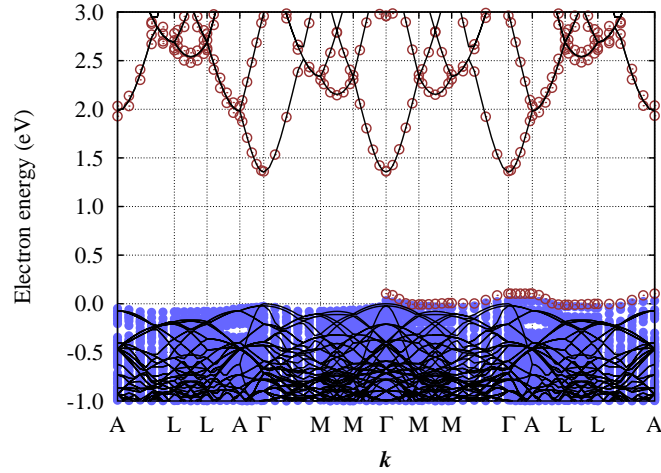
Figure 6.11: (a) Schematic of the Kohn-Sham band-structure for $(PO_4)_O$ this centre. Black lines represent the host bands of a defect free cell of the same size. Filled and empty circles show occupied and unoccupied bands of $(PO_4)_O$, with the bands to the right of centre being the spin-down states, and to the left spin-up. Only bands in the vicinity of the band-gap are shown, and the bands are set such that the valence band top is at zero.

donor.
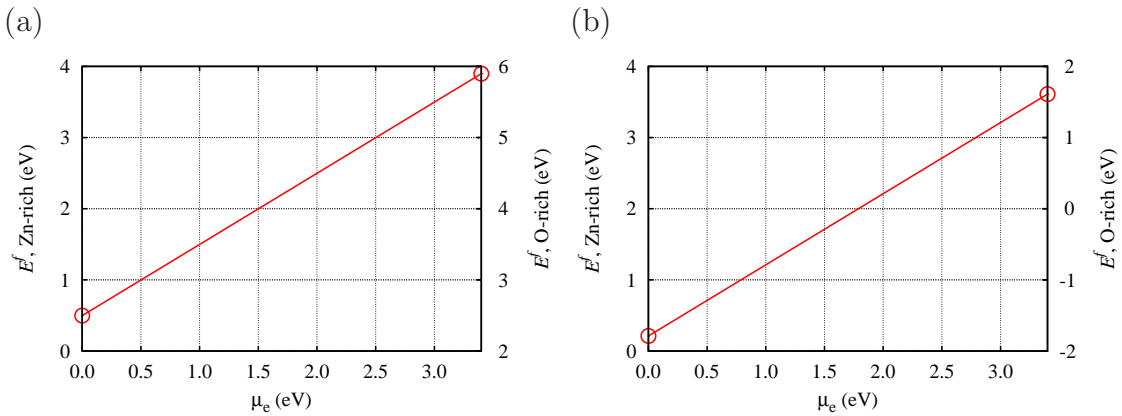
Figure 6.12: Plot of E^f vs. μ_e for (a) $(PO_2)_O$ and (b) $(PO_3)_O$ in w-ZnO. The energy is calculated using the 192 atom supercell.

$(PO_n)_O$ centres are included in Fig. 6.12 for $(PO_2)_O$ and $(PO_3)_O$ defects associated with the oxygen sub-lattice, and in the oxygen rich limit, these centres are highly favourable on the basis of formation energy. This point will be returned to in Sec. 6.2.6.

6.2.4 Phosphorus substituting for zinc

If phosphorus impurities favour bonding with oxygen atoms over Zn atoms, phosphorus might be expected to substitute at Zn site. These centres, with the exceptions highlighted here, have received relatively little attention in the literature, but it shall be shown that they are probably of greater relevance than P on the oxygen lattice.

(a)　　　　　　　　　　　　(b)
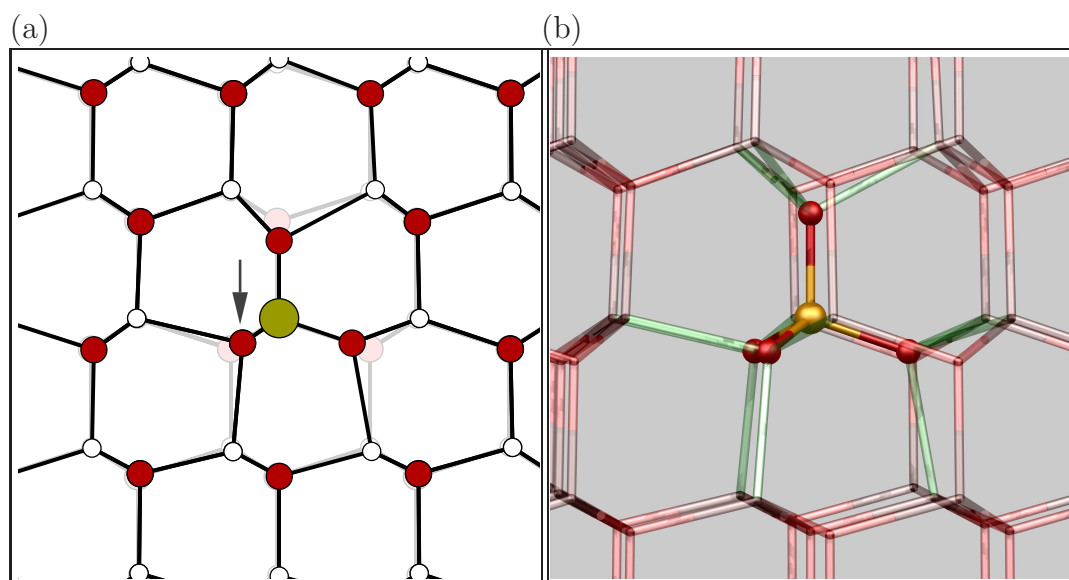
Figure 6.13: Schematic of the P_{Zn} defect in ZnO. Colours and axes are as in Fig. 6.1. The arrow in (a) shows the oxygen site which eclipses the fourth site in the PO_4 group.

Since phosphorus has three more valence electrons than Zn, P_{Zn} is expected to be a triple donor. The relaxed geometry, shown schematically in Fig. 6.13 indicates a significant dilation of the surrounding Zn–O bonds, and it is more realistic to describe the P_{Zn} as PO_4 inside a cavity bordered immediately by 12 Zn^{+2} sites. As noted above, the phosphate group normally exists in the -3 oxidation state, and the twelve

Zn atoms surrounding PO_4 readily provide these electrons. However, since each Zn-neighbour has 1/2 an electron to donate, there are a further three electrons to be accounted for. In our calculations these go to the host conduction band, so that in effect the phosphate group in ZnO is a shallow triple donor (Fig. 6.14).
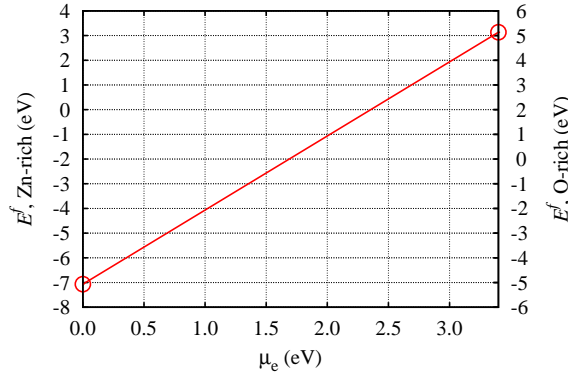
Figure 6.14: Plot of E^f vs. μ_e for P_{Zn} in w-Zn. The energy is calculated using the 192 atom supercell.

The $(0/+1)$ and $(+1/+2)$ levels lie above the conduction-band minimum, and only the $+3$ charge state is thermodynamically stable. Thus, as previously suggested [25], it is found that P_{Zn} is expected to lead to n-type conduction.

The donor level of the structure is further illustrated in Fig. 6.15, which shows the band-structure along high symmetry directions in the (BZ).

As with P_O, to support the use of a 192-atom cell P_{Zn} is also simulated in a 400 atom cell ($5 \times 5 \times 4$ primitive unit cells). The formation energy and electrical levels are in close agreement between these cells, from which it is concluded that the 192-atom supercell is adequate.

6.2.5 P_{Zn} complexes with V_{Zn} and O_i

As P_{Zn} is a triple donor, it is expected to be a single donor when in complexes with V_{Zn} or O_i which both have the capacity to act as double acceptors. The analysis
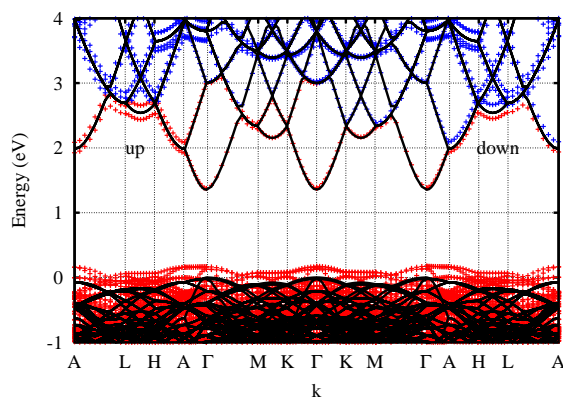
Figure 6.15: Schematic of the Kohn-Sham band-structure for P_{Zn}. Black lines represent the host bands of a defect free cell of the same size. Filled and empty circles show occupied and unoccupied bands of P_{Zn}, with the bands to the right of centre being the spin-down states, and to the left spin-up.

confirms this, with the donor levels of both $P_{Zn}V_{Zn}$ and $P_{Zn}O_i$ complexes predicted to lie above E_c (Δ) and ($\circ$) in Fig. 6.17).
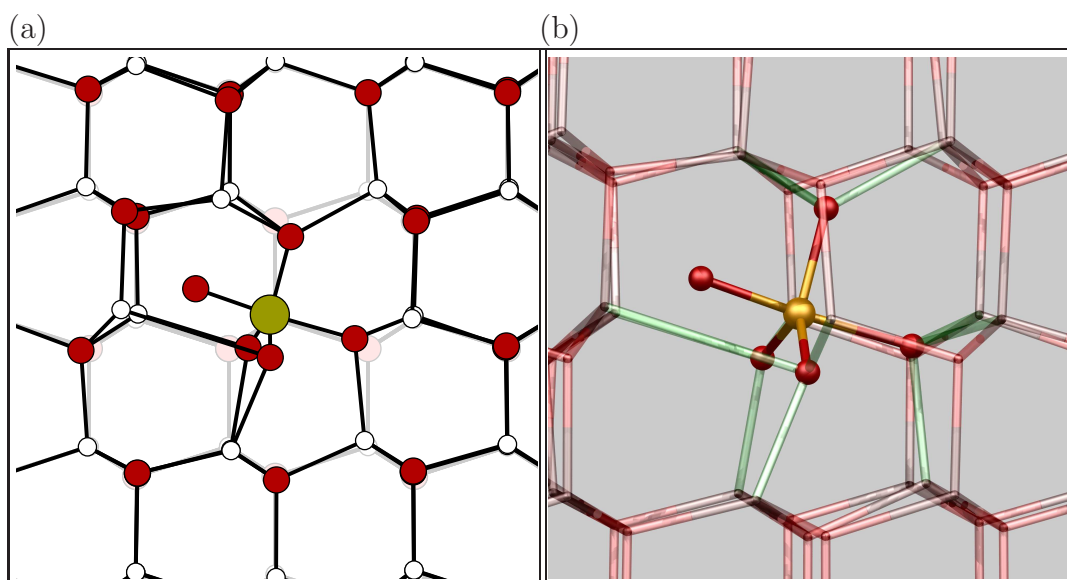
Figure 6.16: Schematic of the $P_{Zn}O_i$ defect in ZnO. Colours and axes are as in Fig. 6.1.
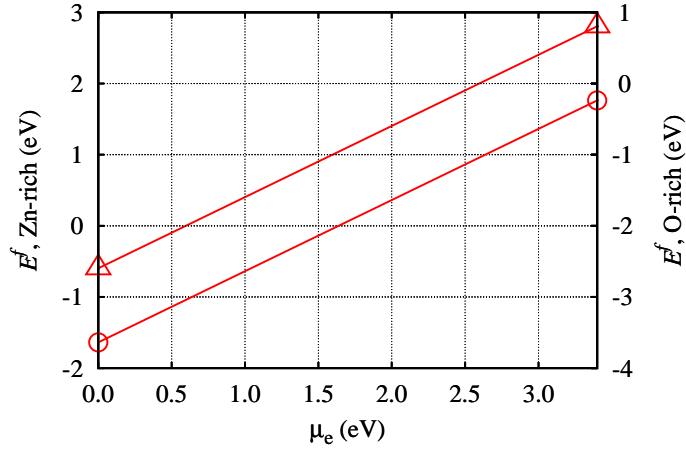
Figure 6.17: Plot of E^f *vs.* μ_e for $P_{Zn}V_{Zn}$ (Δ), $P_{Zn}O_i$ (O).The energy is calculated using the 192 atom supercell.

Fig. 6.17 also shows that $P_{Zn}O_i$ is thermodynamically more stable than $P_{Zn}V_{Zn}$ independent of whether the material is in the oxygen-rich or zinc-rich regimes[1]. $P_{Zn}O_i$ [Fig. 6.16] can be described as P_{Zn} in *five-fold coordination* with oxygen, *i.e.* somewhat akin to a phosphorane, further indicating the significance of the stabilising effect in the formation of P–O bonds.

Since $P_{Zn}O_i$ and $P_{Zn}V_{Zn}$ are single donors, they may in turn be converted into acceptors by the addition of V_{Zn} or O_i centre. Such a procedure results in three types of p-type structure.

The first is the well established complex with two V_{Zn} sites [25, 145], P_{Zn}-2V_{Zn}. This is stabilised by the attractive Coulomb interaction between the components. Due to the number of components and the anisotropy of the lattice, there are many possible P_{Zn}-2V_{Zn} orientations determined by the V_{Zn} positions relative to P_{Zn}. The most stable structure which found is shown in Fig. 6.18, but in other orientations where the vacancies are in the nearest shell of Zn-neighbours to the P-site, the total energies vary by just 100s of meV. The structure which is found to be most stable

---

[1]Since the composition of these centres differs by one Zn and one O atom, the difference in the formation energies is independent of μ_O
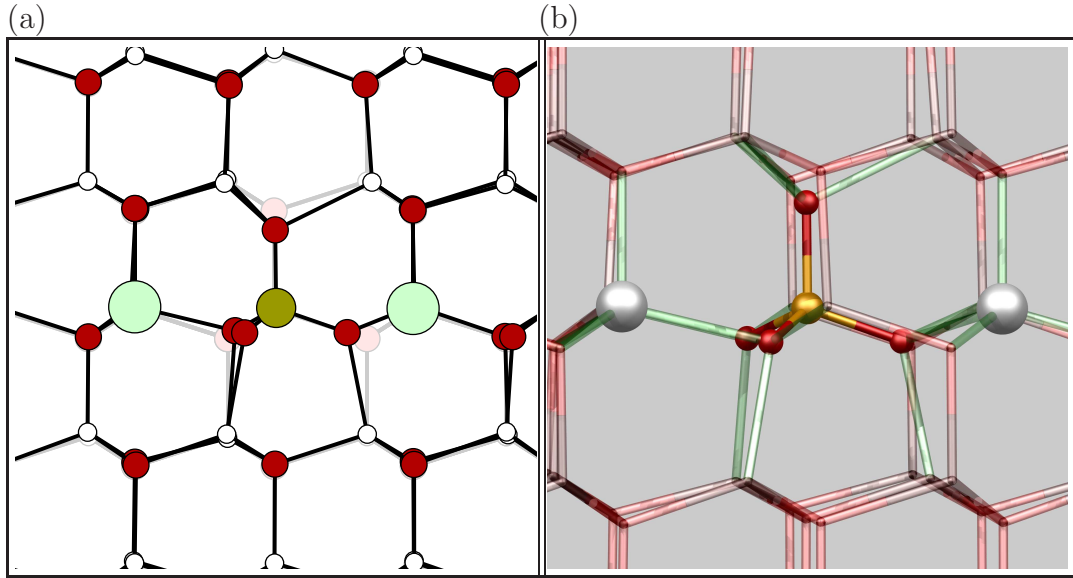
Figure 6.18: Schematic of the P_{Zn}-$2V_{Zn}$ defect in ZnO. Colours and axes are as in Fig. 6.1. The two Large circles indicate V_{Zn} sites

is 35 meV lower than that previously suggested using smaller simulation cells [25]. Calculation of the binding energy of the complex relative to separate P_{Zn} and V_{Zn} centres is 3.7 eV for all species in the neutral charge state, and 1.3 eV for the reaction

$$(P_{Zn}V_{Zn})^+ + (V_{Zn})^{-2} \rightarrow P_{Zn}V_{Zn}^-. \tag{6.1}$$

Both values are in good agreement with previous calculations [25, 150].

The formation energies for the various charge states of the most stable orientation are plotted in Fig. 6.19, showing that the acceptor level lies around $E_v + 0.5$ eV, which is in good agreement with previous calculations [25]. Although there is some uncertainty in this estimate, such a deep level would not result in efficient p-type doping, and these centres are therefore predicted to be less effective that $(PO_4)_O$.

The acceptor level of the structure is further illustrated in Fig. 6.20, which shows the band-structure along high symmetry directions in the (BZ). Note the empty band of the band-structure is identical to the result of the location of the empty level in formation energy. The localised states in the band-gap are associated with the anti-bonding combinations between a P=O molecule and the nearest-neighbour oxygen
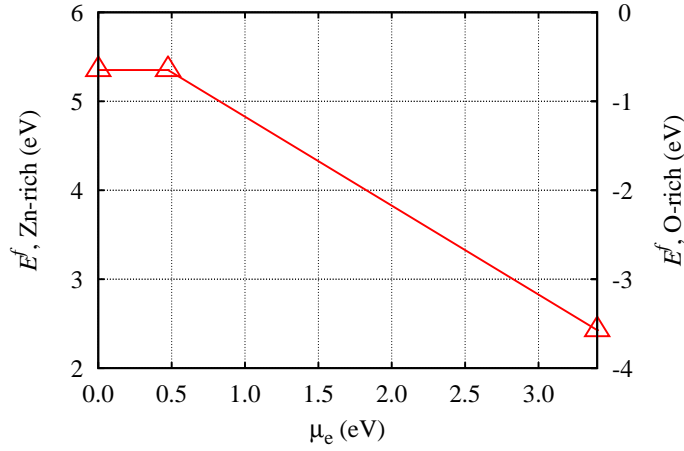
Figure 6.19: Plot of E^f *vs.* μ_e for P_{Zn}-$2V_{Zn}$ defects associated with the zinc sub-lattice in ZnO calculated using the 192 atom supercell.
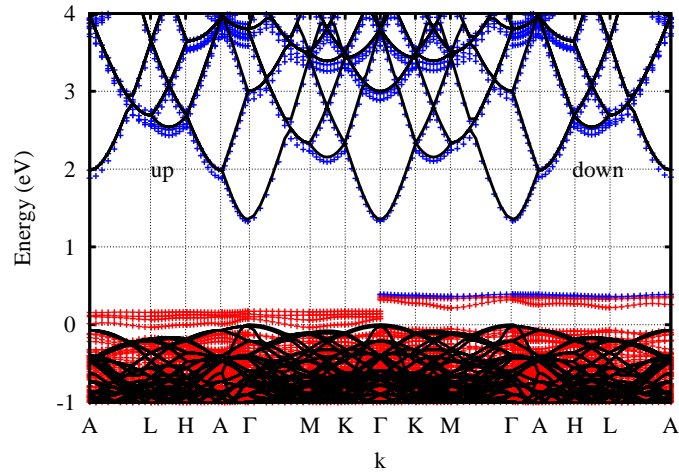
Figure 6.20: Schematic of the Kohn-Sham band-structure for P_{Zn}-$2V_{Zn}$. Black lines represent the host bands of a defect free cell of the same size. Filled and empty circles show occupied and unoccupied bands of P_{Zn}-$2V_{Zn}$, with the bands to the right of centre being the spin-down states, and to the left spin-up.

atoms in the *c*-plane. The association of the gap state particularly with the O-atoms in the *c*-plane most probably arises due to the relative distance between PO_4 ion and

those O-atoms in this plane, compared to the under-co-ordinated O-atoms directed more along the c-axis.

The second complex configuration is $P_{Zn}V_{Zn}O_i$. Among the stable structures, one is where phosphorus is bounded to five oxygen neighbours, somewhat similar to the structure illustrated in Fig. 6.16, but with one neighbouring Zn vacancy. However, an alternative structure where the O_i component becomes detached from the P centre resulting in a phosphate structure P_{Zn} in close proximity with V_{Zn} and O_i is around 0.4 eV lower in energy in both the neutral and negative charge states. This difference in energy is nearly independent of charge state, with all low-energy structures that have been examined resulting in a deep acceptor level (Fig. 6.21).
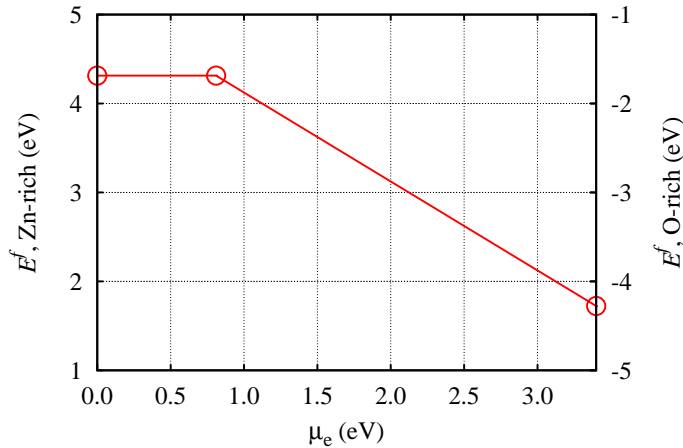
Figure 6.21: Plot of E^f *vs.* μ_e for P_{Zn}-$V_{Zn}O_i$ defects associated with the zinc sub-lattice in ZnO calculated using the 192 atom supercell.

The acceptor level of the structure is further illustrated in Fig. 6.22, which shows the band-structure along high symmetry directions in the (BZ).

Note the empty band of the band-structure is identical to the result of the location of the empty level in formation energy. In addition, the localised state in Fig. 6.22 is similar to all band-structures, where the P=O molecule substituting at Zn-site.

Since $P_{Zn}O_i$ is more stable than $P_{Zn}V_{Zn}$, one might anticipate that $P_{Zn}V_{Zn}O_i$ will be more stable than P_{Zn}-$2V_{Zn}$, and this is precisely what is found. The formation
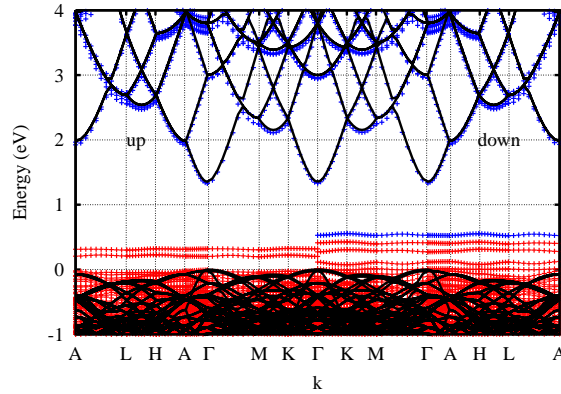
Figure 6.22: Schematic of the Kohn-Sham band-structure for P_{Zn}-$V_{Zn}O_i$. Black lines represent the host bands of a defect free cell of the same size. Filled and empty circles show occupied and unoccupied bands of P_{Zn}-$V_{Zn}O_i$, with the bands to the right of centre being the spin-down states, and to the left spin-up.

energies in the neutral charge state in Fig. 6.21 and Fig. 6.19 illustrate this difference, which is independent of μ_O and estimated at $1.0\,eV$.

The final configuration is P_{Zn}-$2O_i$. By examination of the relaxed geometry it is clear that it is more realistic to describe the system not as P_{Zn}-$2O_i$, but as a PO_6 molecular group in a cage surrounded by 12 Zn sites, as illustrated in Fig. 6.23.

The calculations show that this is the most stable structure for the candidates which have examined for p-type ZnO with phosphorus. In addition, due to the relative formation energies of V_{Zn} and O_i, it has a favourable binding energy of $2.4\,eV$ per O_i under a reaction resulting in dissociation into $P_{Zn}O_i$ and O_i species in the neutral charge state. As with P_{Zn}-$2V_{Zn}$ and $P_{Zn}V_{Zn}O_i$, the calculated acceptor level is relatively deep.

Fig. 6.24 shows plots of the formation energies Eq. 3.9 for P_{Zn}-$2O_i$. This yields a deep acceptor level, around $E_v + 0.6\,eV$.

The acceptor level of the structure is further illustrated in Fig. 6.25, which shows the band-structure along high symmetry directions in the (BZ). Note the empty band

(a) (b)
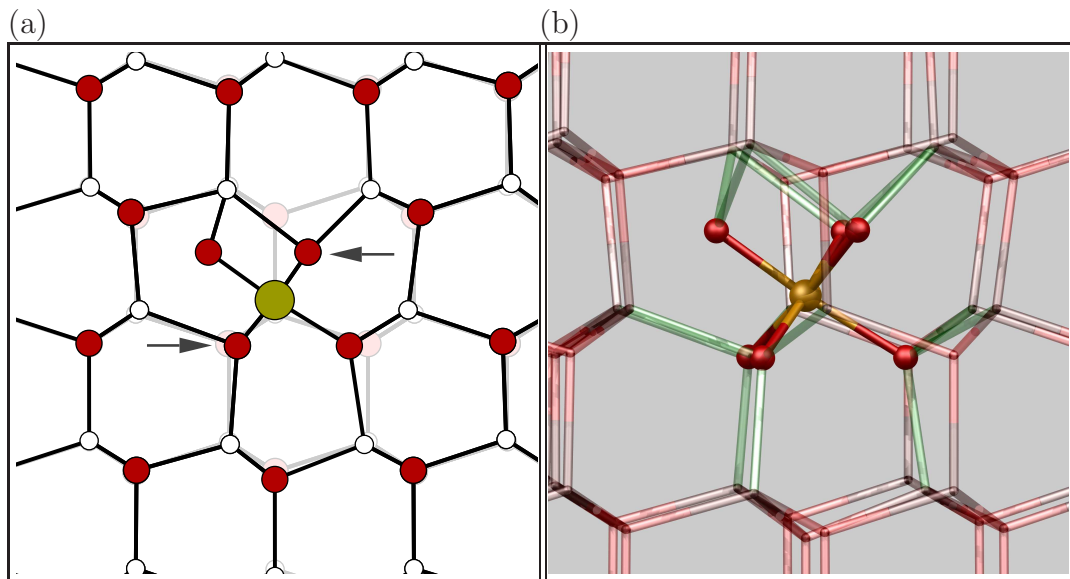
Figure 6.23: Schematic of the P_{Zn}-$2O_i$ defect in ZnO. Colours and axes are as in Fig. 6.1. The arrows in (a) show the sites where O-atoms bonded to P are eclipsed.
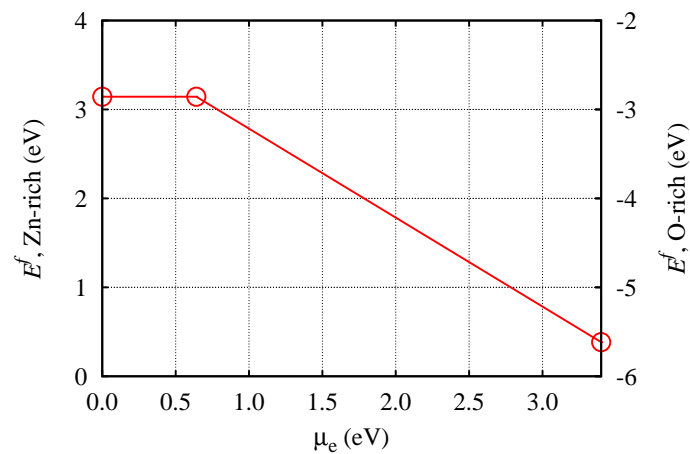
Figure 6.24: Plot of E^f $vs.$ μ_e for P_{Zn}-$2O_i$ defects associated with the zinc sub-lattice in ZnO calculated using the 192 atom supercell.

of the band-structure is identical to the result of the location of the empty level in formation energy. In addition, the localised state in Fig. 6.25 is similar to all band-

structures, where the P=O molecule substitutes at the Zn-site.
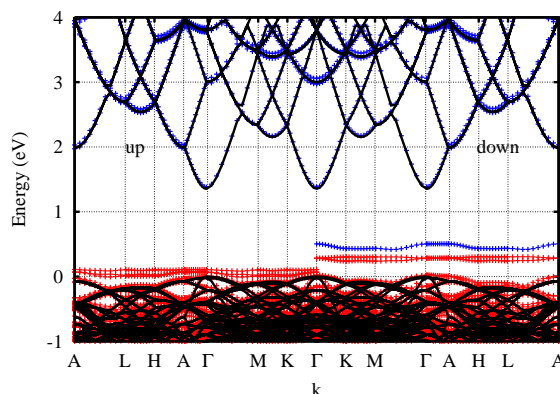
Figure 6.25: Schematic of the Kohn-Sham band-structure for P_{Zn}-$2O_i$. Black lines represent the host bands of a defect free cell of the same size. Filled and empty circles show occupied and unoccupied bands of P_{Zn}-$2O_i$, with the bands to the right of centre being the spin-down states, and to the left spin-up.

However, again the methodology leads to appreciable uncertainty in the precise location of the acceptor level, and whether or not any of these complexes may lead to p-type conductivity remains to be established.

It is perhaps worth noting that five-fold (phosphoranes) and six-fold coordinated phosphorus compounds have been reported both experimentally and theoretically [151, 152]. Indeed, the P-O bond-lengths and angles in the point-defects above are close to the experimental values for P co-ordinated with five oxygen atoms in organic compounds [153], providing some additional confidence in the chemically sound nature of the structures obtained.

6.2.6 Discussion and chemical trends

Of the phosphorus-containing centres discussed in this chapter, many act as shallow donors, and others possible acceptors. To establish a model of the equilibrium behaviour of P-doped ZnO, we compare their total formation energies as a function of

the growth conditions (O-rich *vs.* Zn-rich) and the electron chemical potential.

In O-rich conditions, Fig. 6.26, substitution of P onto the Zn-lattice is highly favourable and the possible acceptor complexes are favoured for most values of μ_e. However in p-type material, P_{Zn} is favoured, so in equilibrium a combination of the two species would form. A key result is that under O-rich conditions it is not P_{Zn}-$2V_{Zn}$ but P_{Zn}-$2O_i$ that is lowest in energy, and given the uncertainty in the precise location of the acceptor level, it must be viewed as a candidate for the formation of p-type ZnO.

Experimentally, p-type P-doped ZnO has been reported with an acceptor level located between 90–127 meV above the valence band [148, 149]. In XPS, the general view is that in p-type material the group-V elements are bonded to oxygen [87]. However, XANES data [154] might be suggestive of P on the O-site, as the data is interpreted as P existing in the -3 oxidation state in p-type material, possibly consistent with P_O.

For Zn-rich material the P_{Zn}-$2O_i$ is less favourable than donor structures, with the uptake of P expected to be dominated by the incorporation of P_{Zn}.

What is the origin of the stability of these configurations? The formation of PO_n, $n =$ 1–6, molecular fragments in the highly stable configurations reflects the relative strength of the bonding between P and O, relative to P and Zn. Despite the relative cost in formation of O_i, the formation of P–O bonds significantly stabilises them. Indeed, the formation of octahedrally bonded P and As is established under high-pressures in minerals. [152, 155–158].

Combining the most stable forms of P-containing centres, Fig. 6.26 shows that in both oxygen and zinc rich conditions, there is a definite driving force for the formation of complexes where P–O bonds are formed. The phosphate ion on either lattice is low in energy, and can move the Fermi-level towards either the valence band top or the conduction band minimum. Additional oxygen atoms can be introduced in the presence of P, such as the highly stable P_{Zn}-$2O_i$ centre. Under no conditions are P–Zn bonds favoured (such as might occur in P_O).

(a)

(b)
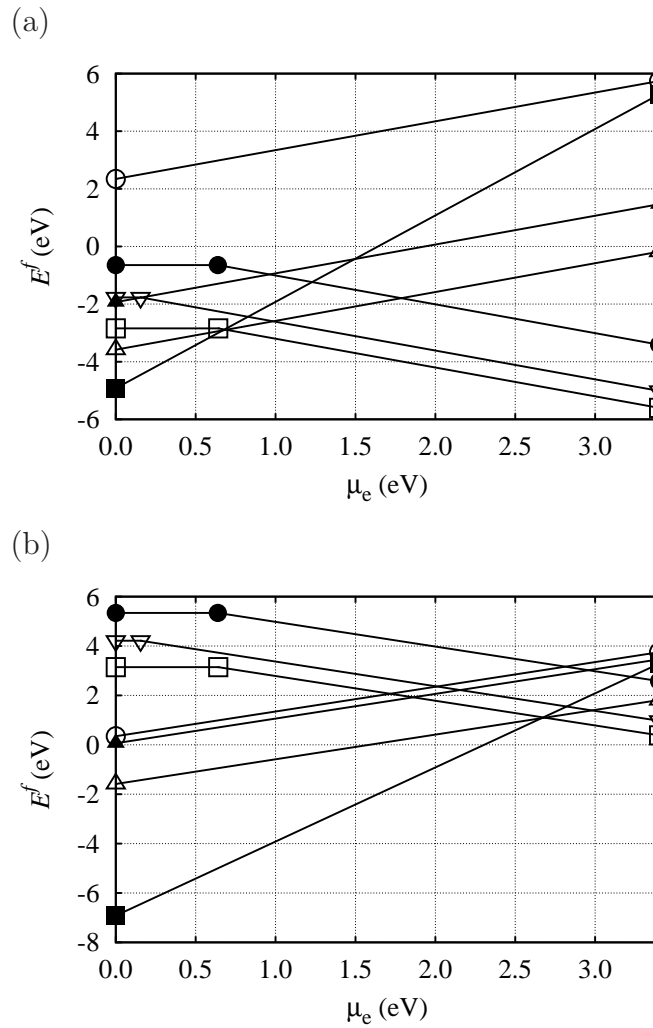
Figure 6.26: Plot of E^f *vs.* μ_e for key P-containing defects in ZnO calculated using the 192 atom supercell: P_{Zn} ($\blacksquare$), P_{Zn}-$2O_i$ ($\square$), P_{Zn}-$2V_{Zn}$ ($\bullet$), $P_{Zn}O_i$ ($\triangle$) (PO)$_O$ (O), (PO$_3$)$_O$ ($\blacktriangle$), and (PO$_4$)$_O$ ($\triangledown$). (a) Oxygen-rich conditions and (b) zinc-rich conditions.

Guided by the results for P, the other group-V elements were also examined the relative energies of candidate acceptor species based upon As and Sb. The general trends are mostly *independent of chemical species* and in fact similarities are found in the formation of six-fold coordination for chalcogens substituting for Zn. Table 6.1 summarises these results. The generality of O_i-based centres being energetically favoured

CHAPTER 6.   PHOSPHORUS DOPING ZNO

Table 6.1: Formation energies per impurity in neutral charge state under O-rich conditions for selected group-V and group-VI impurities in complexes with V_{Zn} and O_i in ZnO, calculated relative to X_{Zn}–$(O_i)_2$ (eV).

| | Impurity species, X | | | | |
Defect	P	As	Sb	S	Se
X_{Zn}	4.2	3.0	3.1	3.8	4.1
X_{Zn}–V_{Zn}	2.2	2.7	2.8	3.4	2.8
X_{Zn}–O_i	1.2	1.4	1.4	1.7	1.1
X_{Zn}–$(V_{Zn})_2$	2.2	3.0	1.7	3.4	4.7
X_{Zn}–V_{Zn}-O_i	1.6	1.7	1.8	2.2	2.5
$(XO_4)_O$	0.9	3.6	3.6	0.5	3.6

is clear, and has widespread implications for understanding the properties these impurities.

Of particular importance is the thermal stability of the acceptor complexes. It has been determined that O_i is more mobile than V_{Zn} in ZnO [27, 159], having activation energies of 0.8 eV or less and 1.4 eV, respectively. Taking the activation for dissociation of complexes of P_{Zn} with V_{Zn} or O_i to be the sums of the binding energy and migration barriers for the native component, a simplistic model would lead to the reversal of p-type doping, to be achieved at a lower temperature for O_i-based acceptors than for V_{Zn}-based centres. In addition, once P_{Zn}-$2O_i$ dissociates into $P_{Zn}O_i$+O_i, the resultant components favour n-type material due to the amphoteric behaviour of O_i. Then the type-dependence upon growth temperature in P-doped films [160,161] might be understood as the conversion of P_{Zn}-$2O_i$ acceptors into $P_{Zn}O_i$, O_i and P_{Zn}-related donors.

The stabilising effect of the formation of X–O bonds is also seen in the low formation energies of $(PO_4)_O^n$ shallow acceptors and $(SO_4)_O^{n+1}$ iso-electronic centres. In

contrast, this type of structure centred upon As, Sb, or Se dopants are high in energy in comparison to the corresponding $X\text{–}(O_i)_2$ complexes. However, in these cases there is a substantial perturbation to the immediate neighbours, resulting in the displacement of a neighbouring Zn atom. A small change in initial conditions for these complexes produces a $X_{\text{Zn}}(O_i)_2$ defect with a ZnO formula unit displaced into an interstitial location, which reduces the relative energies listed in Table 6.1 by around $1\,\text{eV}$. The balance of the formation energy is the cost of the formation of the self-interstitials. This may be viewed as further evidence that the production of acceptors in As and Sb doped materials might be correlated with the formation of six-fold oxygen-coordinated dopants.

6.3 Summary

In summary, the overwhelming trend is for the group-V elements P, As, and Sb to adopt forms with multiple oxygen bonds, which result in both donor and acceptor configuration depending upon whether the material is under oxygen-rich or zinc-rich conditions.

The previously favoured structure of group-V acceptors involving native defects has been revised: the involvement of pairs of V_{Zn} in the formation of acceptor centres is energetically less favourable that the decoration with additional oxygen interstitials. However, the thermodynamic principle that acceptor species appear to be more likely to be formed in oxygen-rich conditions remains, since $P_{\text{Zn}}\text{-}2V_{\text{Zn}}$ and $P_{\text{Zn}}\text{-}2O_i$ depend upon μ_{O} in the same way.

Among the favoured structures, the formation of co-ordinations between the dopants and more than four oxygen atoms may be resolvable experimentally, and we suggest that octahedral XO_5 and XO_6 structures are likely to have a wider impact: since the formation of these structures is largely driven by the strength of the impurity-oxygen bonds, doping of metal-oxides such as the high-κ dielectrics including TiO_2 and HfO_2, and ferroelectric materials such as $BaTiO_3$ and $PbTiO_3$ with group-V and group-VI

species is likely to result in these configurations.

Part III

Conclusions

Chapter 7

Summary

7.1 Conclusions on Doping of ZnO

The aim of this work was to investigate the mechanism of p-type ZnO with group-V elements. There are two distinct areas that must be covered in the study: the stability of doping (formation energies), and the type of conductivity. The studies of ZnO yielded a number of important results. The conclusions of this chapter are a recap of chapter 4-6.

It has been shown through the quantum-mechanically based modelling that doping of ZnO with group-V elements is indeed a possible route to for the formation of p-type material. Indeed, this must be the case since the experimental observations are unambiguous in this respect.

However, the accepted structures responsible for the hole-conduction must, in some important ways, be revised based upon the modelling presented in this thesis.

It is important to accept first that the growing body of evidence from theory is that, in the case of N, simple "traditional substitution" based doping is not the correct model. This requires some qualification however. XPS has been frequently used as a basis for placing the most common site for N as being on the oxygen site, based upon the XPS-peak coinciding with that of zinc-nitride, meaning that the N-atoms are bonded to Zn. Such arguments, although persuasive, are not conclusive, since the

peak-energy is not **uniquely** associated with one particular chemical environment.

If the nitrogen-related acceptor is not nitrogen substituting for oxygen, then the modelling performed for this study suggests that a plausible model might be a nitrogen based molecular ion, internally bonded with strong, covalent bonds. The nitrate anion is one particular model that is favourable for three main reasons. First, theoretically it is a shallow acceptor. Second, the energy required to form these acceptors is highly favourable. Finally, such centres are favoured in oxygen-rich conditions, in line with the observation of p-type material grown under these conditions.

This picture is extended beyond the case of N, more generally in the group-V elements. Covalently bonded molecular groups are energetically favoured, and several plausible candidates have been obtained for P, As and Sb. Such structures are energetically favoured over the widely publicised candidate made up from zinc-vacancies complexed with the group-V element on the Zn-site. For example attaching two oxygen interstitials to P on the zinc site is more favourable than P_{Zn}–$(V_{Zn})_2$ by more than $2\,eV$. It is also important to note that this formation energy difference is *independent of the oxygen chemical potential* and so is unaffected by whether the material is grown in O-rich or Zn-rich conditions. Another intriguing possibility is that phosphate ions may substitute for oxygen and also give rise to p-type conductivity. This is also more stable than P_{Zn}–$(V_{Zn})_2$.

Although the calculated electrical levels need to be confirmed, on the basis that the formation of specific covalently bonded ions are a potential route to the formation of p-type ZnO, two clear recommendations may be presented. First, it is clear that the favourable species are most likely to form in oxygen rich material, so growth should be performed under these conditions. Second, it may be possible to enhance the probability of forming, for example, nitrite based acceptors by deliberate introduction of the appropriate molecular groups during growth.

7.2 Future calculations

Although it is possible to draw many conclusions from the currently available data, there are some areas where uncertainties can be addressed by using a modified methodology. Of these areas, perhaps the two most significant ones are the underestimate of the band-gap (or more precisely the error in the band-structure), and the second is the role of the periodic boundary conditions in the energies of charged defects.

The first of these problems can be tackled using the screened-exchange (SX) approach [57]. This is currently being implemented in the software. The SX method recovers the band-gap so that it agrees closely with experiment. For defects such as $(NO_2)_O$ (figure 5.21) where there are molecular states that cross the host conduction band, the opening of the band-gap may have an impact in terms of both the energy and electrical properties.

For the periodic boundary conditions, one possible solution is to simulate point defects in very large supercells as the periodic interactions decay in line with a power law for the inverse of the distance. Recent methodological developments [58] in the software will allow for the *routine* simulation of 1000's of atoms, reducing the absolute error arising from the periodic boundary conditions.

Finally, although the vibrational modes presented in this thesis are a useful tool in the correlation between experiment and theory, there are others which might also be of value. In particular, the paramagnetic centres, such as neutral single acceptors, should give rise to characteristic hyperfine interactions between the group-V nucleus and the unpaired electron spin. These calculations will also be performed in the near future, and in the case of nitrogen, compared with available experimental data.

Bibliography

[1] D. M. Bagnal, Y. F. Chen, Z. Chen, Zhu, T. Yao, S. Koyama, M. Y. Shen, and T. Goto, Appl. Phys. Lett. **70**, 2230 (1997).

[2] Z. K. Tang, G. K. L. Wong, P. Yu, M. Kawasaki, A. Ohtomo, H. Koinuma, and Y. Segawa, Appl. Phys. Lett. **72**, 464 (1998).

[3] D. K. Hwang, S. H. Kang, J. H. Lim, E. J. Yang, J. Y. Oh, J. H. Yang, and S. J. Park, Appl. Phys. Lett. **86**, 222101 (2005).

[4] M. Willander, O. Nur, Q. X. Zhao, L. L. Yang, M. Lorenz, B. Q. Cao, J. Zuniga Perez, C. Czekalla, G. Zimmermann, M. Grundmann, A. Bakin, A. Behrends, M. Al-Suleiman, A. El-Shaer, A. Che Mofor, B. Postels, A. Waag, N. Boukos, A. Travlos, H. S. Kwack, J. Guinard, and D. Le Si Dang, Nucl. Technol. **20**, 332001 (2009).

[5] K. Ellmer and J. Hinze, J. Appl. Phys. **80**, 2433 (2000).

[6] S. B. Zhang, S.-H. Wei, and A. Zunger, Phys. Rev. B **63**, 075205 (2001).

[7] C. G. Van de Walle, Phys. Rev. Lett. **85**, 1012 (2000).

[8] A. Janotti, G. Chris, and C. G. Van de Walle, Nature Mater. **6**, 44 (2007).

[9] Y. Yan and S. T. Zhang, S. B. Pantelides, Phys. Rev. B **86**, 5723 (2001).

[10] J. M. Bian, X. M. Li, C. Y. Zhang, W. D. Yu, and X. D. Gao, Appl. Phys. Lett. **85**, 4070 (2004).

[11] D. C. Look, D. C. Reynolds, C. W. Litton, R. L. Jones, D. B. Eason, and G. Cantwell, Appl. Phys. Lett. **80**, 1830 (2002).

[12] A. Kobayashi, O. F. Sankey, and J. D. Dow, Phys. Rev. B **28**, 946 (1983).

[13] C. H. Park, S. B. Zhang, and S.-H. Wei, Phys. Rev. B **66**, 073202 (2002).

[14] J. L. Lyons, A. Janotti, and C. G. Van de Walle, Appl. Phys. Lett. **95**, 252105 (2009).

[15] Stephan. Lany and Alex. Zunger, Phys. Rev. B **81**, 205209 (2010).

[16] I. V. Rogozin, Thin Solid Films **4**, 4318 (2008).

[17] W. Mu, L. Kerr, and N. Leyarovska, Chem. Phys. Lett. **469**, 318 (2009).

[18] H. W. Liang, Y. M. Lu, D. Z. Shen, Y. C. Liu, J. F. Yan, C. X. Shan, B. H. Li, Z. Z. Zhang, J. Y. Zhang, and X. W. Fan, Phys. Status Solidi A **202**, 1060 (2005).

[19] P. Niki S. Yamada A. Matsubara K. Nakahara K. Tanabe T. Takasu H. Iwata, K. Fons, J. Cryst. Growth **214**, 50 (2000).

[20] E. C. lee, Y. S. Kim, Y. G. Jin, and K. J. Chang, Phys. Rev. B **64**, 085120 (2001).

[21] U. Wahl, E. Rita, J. G. Correia, Marques A. C., E. Alves, and J. C. Soares, Phys. Rev. Lett. **95**, 215503 (2005).

[22] J. M. Qui, B. Yao, Y. Yan, J. Y. Zhang, X. P. Lia, Z. Z. Zhang, and B. H. Li, Appl. Phys. Lett. **95**, 022101 (2009).

[23] D. E. Pugel, R. D. Vispute, S. S. Hullavarad, T. Venkatesan, and B. Varughese, J. Appl. Phys. **101**, 063538 (2007).

[24] S. Limpijumnong, S. B. Zhang, Su-Huai. Wei, and C. H. Park, Phys. Rev. Lett. **92**, 1555041 (2004).

[25] W.-J. Lee, J. Kang, and K. J. Chang, Phys. Rev. B **73**, 024117 (2006).

[26] J. Hu and B. C. Pan, J. Chem. Phys. **129**, 154706 (2008).

[27] A. Janotti and C. G. Van de Walle, Phys. Rev. B **76**, 165202 (2007).

[28] N. H. Nickel and M. A. Gluba, Phys. Rev. Lett. **103**, 145501 (2009).

[29] R-Y. Tian and Y-J. Zhao, J. Appl. Phys. **106**, 043707 (2009).

[30] S. Limpijumnong, X. Li, S-H. Wei, and S. B. Zhang, Appl. Phys. Lett. **86**, 211910 (2005).

[31] Y. Yan, S. B. Zhang, and S. T. Pantelides, Phys. Rev. Lett. **86**, 5723 (2001).

[32] W. Körner and C. Elsässer, Phys. Rev. B **81**, 085324 (2010).

[33] K. Li, Y. Yan, H. Wang, Y. S. Zhan, Q. Mohammed, and H Jin, Phys. Lett. A **374**, 628 (2010).

[34] Z. G. Yu, H. Gong, and P. Wu, Chem. of Materials **17**, 852 (2005).

[35] Z. G. Yu, H. Gong, and P. Wu, Appl. Phys. Lett. **86**, 212105 (2005).

[36] K. Senthilkumar, M. Tokunaga, H. Okamoto, O. Senthilkumar, and Y. Fujita, Appl. Phys. Lett. **97**, 091907 (2010).

[37] M. Born and J. R. Oppenheimer, Ann. Phys. **84**, 457 (1927).

[38] P. Hohenberg and W. Kohn, Phys. Rev. **136**, 864 (1964).

[39] W. Kohn, Rev. Mod. Phys. **71**, 1253 (1999).

[40] W. Kohn and L. J. Sham, Phys. Rev. **140**, A1133 (1965).

[41] P. Hohenberg and W. Kohn, Phys. Rev. **136**, B864 (1964).

BIBLIOGRAPHY

[42] J. R. smith, Phys. Rev. Lett. **24**, 1023 (1970).

[43] N. W. Ashcroft and N. D. Mermin, *Solid State Physics*, international ed. (Saunders College, Philadelphia, 1976).

[44] U. von Barth and L. Hedin, J. Phys. C **5**, 1629 (1972).

[45] J. P. Perdew and A. Zunger, Phys. Rev. B **23**, 5048 (1981).

[46] S. J. Vosko, L. Wilk, and M. Nusair, Chinese J. Phys. **58**, 1200 (1980).

[47] J. P. Perdew and Y. Wang, Phys. Rev. B **45**, 13244 (1992).

[48] D. M. Ceperley and B. J. Alder, Phys. Rev. Lett. **45**, 566 (1980).

[49] J. P. Perdew, K. Burke, and Y. Wang, Phys. Rev. Lett. **77**, 3865 (1996).

[50] D. C. Patton, D. V. Porezag, and M. R. Pederson, Phys. Rev. B **55**, 7454 (2007).

[51] J. P. Goss, M. J. Shaw, and P. R. Briddon, in *Theory of Defects in Semiconductors*, Vol. 104 of *Topics in Applied Physics*, edited by David A. Drabold and Stefan K. Estreicher (Springer, Berlin/Heidelberg, 2007), pp. 69–94.

[52] A. Baldereschi, Phys. Rev. B **7**, 5212 (1973).

[53] D. J. Chadi and M. L. Cohen, Phys. Rev. B **7**, 692 (1973).

[54] D. J. Chadi and martin L. Cohen, Phys. Rev. B **8**, 5747 (1973).

[55] H. J. Monkhorst and J. D. Pack, Phys. Rev. B **13**, 5188 (1976).

[56] N. Troullier and J. L. Martins, Phys. Rev. B **43**, 1993 (1991).

[57] S. J. Clark and J. Robertson, Phys. Status Solidi B **248**, 537 (2011).

[58] M. J. Rayson and P. R. Briddon, Phys. Rev. B **80**, 205104 (2009).

[59] G. Kresse and J. Furthmuller, Phys. Rev. B **54**, 11169 (1996).

BIBLIOGRAPHY

[60] P. R. Briddon and R. Jones, Phys. Status Solidi B **217**, 131 (2000).

[61] E. Polak, *Computational methods in optimisation: a unified apporach* (Academic Press, Berkley, California, 1971).

[62] W. Press, *Numerical Recipes in Fortrann 77* (Cambrdge University Press, Cambridge, UK, 1996).

[63] G. Mills and H. Jonsson, Phys. Rev. Lett. **72**, 1124 (1994).

[64] G. Mills, H. Jonsson, and G. Schenter, Surface Sci. **66**, 305 (1995).

[65] G. Henkelman, B. P. Uberuaga, and H. Jónsson, J. Chem. Phys. **113**, 9901 (2000).

[66] G. Henkelman and H. Jónsson, J. Chem. Phys. **113**, 9978 (2000).

[67] *Handbook of chemistry and physics*, 73 ed., edited by D. R. Lide (CRC, Boca Raton, FL, 1992).

[68] S. Lany and A. Zunger, Phys. Rev. B **78**, 235104 (2008).

[69] N. S. Han, H. S. Shim, J. H. Seo, S. Y. Kim, S. M. Park, and J. K. Song, J. Appl. Phys. **107**, 084306 (2010).

[70] D. C. Look, J. W. Hemsky, and J. R. Sizelove, Phys. Rev. Lett. **82**, 2552 (1999).

[71] L. S. Vlasenko, G. D. Watkins, and R. Helbig, Phys. Rev. B **71**, 115205 (2005).

[72] T. Kondela, J. Gregus, M. Zahoran, and T. Roch, Mater. Sci. Eng. **15**, 012041 (2010).

[73] K. Vanheusden, C. H. Seager, W. L. Warren, D. R. Tallant, and J. A. Voigt, Appl. Phys. Lett. **68**, 403 (1996).

[74] D. C. Reynods, D. C. Look, and B. Jogai, J. Appl. Phys. **89**, 6189 (2001).

[75] S. Limpijumnong and S. B. Zhang, Appl. Phys. Lett. **86**, 151910 (2005).

[76] E. C. lee and Y. G. Chang K. J. Kim, Y. S. Jin, Physica B **308**, 912 (2001).

[77] A. Janotti and C. G. Van de Walle, J. Cryst. Growth **287**, 58 (2006).

[78] C. D. Pemmaraju, R. Hanafin, T. Archer, H. B. Braun, and S. Sanvito, Phys. Rev. B **78**, 054428 (2008).

[79] P. Erhart, K. Albe, and A. Klein, Phys. Rev. B **73**, 205203 (2006).

[80] Stephan. Lany and Alex. Zunger, Phys. Rev. Lett. **98**, 045501 (2007).

[81] F. Oba, I. Togo, A. Tanaka, J. Paier, and G. Kresse, Phys. Rev. B **77**, 245202 (2008).

[82] A. R. Hutson, Phys. Rev. **108**, 222 (1957).

[83] P. Erhart and K. Albe, Appl. Phys. Lett. **88**, 201918 (2006).

[84] A. F. Kohan, G. Ceder, D. Morgan, and C. G. Van de Walle, Phys. Rev. B **61**, 15019 (2000).

[85] M. G. Wardle, J. P. Goss, and P. R. Briddon, Phys. Rev. B **71**, 155205 (2005).

[86] M. G. Wardle, J. P. Goss, and P. R. Briddon, Phys. Rev. B **72**, 155108 (2005).

[87] X. Xu, Y. Shen, N. Xu, W. Hu, J. Lai, and J. Ying, Z. Wu, Vacuum **48**, 1306 (2010).

[88] K. Minegishi, Y. Koiwai, Y. Kikuchi, and K. Yano, Jpn. J. Appl. Phys. Part 2 **36**, L1453 (1997).

[89] W. Z. XU, Z. Z. Ye, Y. J. Zeng, L. P. Zhu, B. H. Zhao, L. Jiang, J. G. Lu, and H. P. He, Appl. Phys. Lett. **88**, 173506 (2006).

[90] X.-L. Guo, H. Tabata, and T. Kawai, J. Cryst. Growth **223**, 135 (2001).

[91] M-L. Tu, Y-K. Su, and C-Y. Ma, J. Appl. Phys. **100**, 053705 (2006).

[92] A. Tsukazaki, A. Ohtomo, T. Onuma, M. Ohtani, T. Makino, M. Sumiya, S. F. Ohtani, K. Chichibu, S. Fuke, Y. Segawa, H. Ohno, H. Koinuma, and M. Kawasaki, Nature Mater. **4**, 42 (2005).

[93] K.-K. Kim, H.-S. Kim, D.-K. Hwang, J.-H. Lim, and S.-J. Park, Appl. Phys. Lett. **83**, 63 (2003).

[94] Y. R. Ryu, S. Zhu, D. C. Look, J. M. Wrobel, H. M. Jeong, and H. W. White, J. Cryst. Growth **216**, 330 (2000).

[95] A. Allenic, W. Guo, Y.B. Chen, G.Y. Zhao, X.Q. Pana, Y. Che, Z.D. Hu, and B. Liu, J. Mater. Res. **22**, 2339 (2007).

[96] Y. R. Ryua, T. S. Lee, J. H. Leem, and H. W. White, Appl. Phys. Lett. **83**, 4032 (2003).

[97] J. Sann, A. Stehr, A. Hofstaetter, and D. M. Hofmann, Phys. Rev. B **76**, 195203 (2007).

[98] X Wanga, S. Yang, M. Wang, J. Li, X. Jiang, G. Du, X. Liu, and R.P.H. Chang, J. Cryst. Growth **226**, 123 (2001).

[99] K. Iwata, P. Fons, A. Yamada, K. Matsubara, and S. Niki, J. Cryst. Growth **209**, 526 (2000).

[100] S. Lautenschlaeger, S. Eisermann, B. K. Meyer, G. Callison, M. R. wagner, and A. Hoffmann, Phys. Status Solidi **3**, 16 (2009).

[101] J. Wang, E. Elamurugu, V. Sallet, F. Jomard, A. Lusson, A. M. Botelho do Rego, P. Barquinha, G. Goncalves, R. Martins, and E. Fortunato, Appl. Surf. Sci. **254**, 7178 (2008).

[102] J. B. Cui, M. A. Thomas, Y. C. Soo, H. Kandel, and T. P. Chen, J. Phys. D **42**, 155407 (2009).

[103] X. Li, Y. Yan, T. A. Gessert, C. DeHart, C. L. Perhins, D. Young, and T. J. Coutts, Solid State Commun. **6**, 56 (2003).

[104] W. Allenic, A.and Guo, Y. B. Chen, Y. Che, Z. D. Hu, B. Liu, and X. Q. Pan, J. Appl. Phys. **41**, 025103 (2008).

[105] N. Y. Garces, Lijun. Wang, N. C. Giles, and L. E. Halliburton, J. Appl. Phys. **94**, 519 (2003).

[106] W. E. Carlos, E. R. Glaser, and D. C. Look, Physica B **308-310**, 976 (2001).

[107] J. A. Aparicio and F. E. Fernandez, J. Mol. Struct. **10**, 46840 (2010).

[108] T. Monteiro, A. J. Neves, M. C. Carmo, M. J. Soares, M. peres, and J. Wang, J. Appl. Phys. **98**, 013502 (2005).

[109] B. K. Meyer, H. Alves, D. M. Hofmann, W. Kriegseis, D. Forster, F. Bertram, J. Christen, A. Hoffmann, M. Straßburg, M. Dworzak, U. Haboeck, and A. V. Rodina, Phys. Status Solidi B **241**, 231 (2004).

[110] B. T. Adekore, J. M. Pierce, R. F. Davis, D. W. Barlage, and J. F. Muth, J. Appl. Phys. **102**, 024908 (2007).

[111] K. Thonke, N. Gruber, Th. Teofilov, A. onfelder, R. Sch. Waag, and R. Sauer, Physica B **308**, 945 (2001).

[112] K. Thonke, M. Schirra, R. Schneider, A. Reiser, M. Prinz, G. M. Feneberg, R. Sauer, and J. Biskupek, Phys. Status Solidi **247**, 1464 (2010).

[113] D. Tainoff, B. Masenelli, P. Mëlinon, A. Belsky, G. Ledoux, D. Amans, and C. Dujardin, Phys. Rev. B **81**, 115304 (2010).

[114] M. Gomi, N. Oohira, K. Ozahi, and M. Koyano, J. Appl. Phys. **42**, 481 (2003).

[115] U. Ozgur, Y. L. Alivov, C. Liu, A. Teke, S. Reshchikov, M. A. Dogan, V. Avrutin, and H. Cho, S. J. Morkoc, J. Appl. Phys. **98**, 041301 (2005).

[116] S. Yamauchi, Y. Goto, and T. Hariu, J. Cryst. Growth **260**, 1 (2004).

[117] N. Tabet, M. Faiz, and A. Al-Oteibi, J. Electrochemical Soc. **163**, 15 (2008).

[118] L. L. Kerr, X. Li, M. Canepa, and A. J. Sommer, Thin Solid Films **515**, 5282 (2007).

[119] K. Tang, S. L. Gu, S. M. Zhu, J. G. Liu, H. Chen, J. D. Ye, R. Zhang, and Y. D. Zheng, Appl. Phys. Lett. **95**, 192106 (2009).

[120] C. W. Zou, X. D. Yan, J. Han, R. Q. Chen, W. Gao, and J. Mstson, Appl. Phys. Lett. **94**, 171903 (2009).

[121] M. Petravic, P.N.K. Deenapanray, V.A. Coleman, C. Jagadish, K.-J. Kim, B. Kim, K. Koike, S. Sasa, M. Inoue, and M. Yano, Surface Sci. **600**, L81 (2006).

[122] C. Lee, S. Y. Park, J. Lim, and H-W. Kim, Mater. Lett. **61**, 2495 (2007).

[123] P. Fons, H. Tampo, A. V. Kolobov, M. Ohkubo, J. Niki, S. Tominaga, R. Carboni, F. Boscherini, and S. Friedrich, Phys. Rev. Lett. **96**, 045504 (2006).

[124] C. H. Park, S. B. Zhang, and Su-Huai Wei, Phys. Rev. B **66**, 073202 (2002).

[125] A. Kaschner, U. Haboeck, Martin. Strassburg, Matthias. Strassburg, G. Kaczmarczyk, A. Hoffmann, C. Thomsen, A. Zeuner, H. R. Alves, D. M. Hoffmann, and Meyer B. K., Appl. Phys. Lett. **80**, 1909 (2002).

[126] J. Karamdela, C. F. Dee, and B. Y. Majlis, Appl. Surf. Sci. **256**, 6164 (2010).

[127] B-Ho. Cheong, C. H. Park, and K. J. Chang, Phys. Rev. B **51**, 10610 (1995).

[128] L. Li, C. X. Shan, B. H. Yao Li, B., J. Y. Zhang, D. X. Zhao, Z. Z. Zhang, D. Z. Shen, X. W. Fan, and Y. M. Lu, J. Phys. D **41**, 245402 (2008).

[129] B. M. Keyes, L. M. Gedvilas, and T. J. Li, X. Coutts, J. Cryst. Growth **281**, 297 (2005).

[130] S. B. Zhang, S.-H. Wei, and A. Zunger, Phys. Rev. B **63**, 75205 (2001).

[131] F. Oba, S. R. Nishitani, S. Isotani, and H. Adachi, J. Appl. Phys. **90**, 824 (2001).

[132] K. Tamura, T. Makino, A. Tsukazaki, M. Sumiya, S. Fuke, T. Furumochi, M. Lippmaa, C.H. Chia, Y. Segawa, H. Koinuma, and M. Kawasaki, Solid State Commun. **127**, 265 (2003).

[133] A. Zunger, Appl. Phys. Lett. **83**, 57 (2003).

[134] P. H. Kasal and R. M. Gaura, J. Phys. C **86**, 4257 (1982).

[135] W. A. Brown and D. A. King, J. Phys. Chem. B **104**, 2578 (2000).

[136] N. H. Nickel, F. Friedrich, J. F. RommeluÃÍre, and P. Galtier, Appl. Phys. Lett. **87**, 211905 (2005).

[137] H. Oberhammer, J. Mol. Struct. **605**, 1439 (2002).

[138] J. F. Rommeluere, L Svob, F. Jomard, G. Mimila-Arroyo, J. Amiri, V. Lusson, A. Sallet, O. Gorochov, P. Galtier, and Y. Marfaing, Phys. Status Solidi **1**, 904 (2003).

[139] N. Haneche, C. Lusson, A. Sartel, A. Marzouki, V. Sallet, M. Oueslati, F. Jomard, and P. Galtier, Phys. Status Solidi **247**, 1671 (2010).

[140] U. Wahl, J. G. Correia, T. Mendonca, and S. Decoster, Appl. Phys. Lett. **94**, 261901 (2009).

[141] Y. R. Ryua and T. S. Lee, Appl. Phys. Lett. **83**, 87 (2003).

[142] F. X. Xiu, Z. Yang, L. J. Mandalapu, D. T. Zhao, and J. L. Liu, Appl. Phys. Lett. **87**, 252101 (2005).

[143] F. X. Xiu, Z. Yang, L. J. Mandalapu, D. T. Zhao, and J. L. Liu, Appl. Phys. Lett. **87**, 252102 (2005).

[144] J. Xiong, G. amd Wilkinson, B. Mischuck, S. Tuzemen, K. B. Ucer, and R. T. Williams, Phys. Rev. Lett. **80**, 1195 (2002).

[145] S. Limpijumnong, S. B. Zhang, Su-Huai Wei, and C. H. Park, Phys. Rev. Lett. **92**, 155504 (2004).

[146] Y. W. Heo, K. Ip, S. J. Park, J. Pearton, S, and P. Norton, D, Appl. Phys. Lett. **78**, 53 (2004).

[147] V. Wazer and R. John, in *Phosphorus and its compounds*, 2nd ed. (Interscience, New York, 1958-1961).

[148] D. K. Hwang, S. H. kim, J. H. Lim, J. Y. Oh, J. H. Yang, S. J. Park, K. K. Kim, D. C. Look, and Y. S. Park, Appl. Phys. Lett. **86**, 151917 (2005).

[149] D. Yu, L. Hu, S. Qiao, H. Zhang, S-E. A. Len, Q. Len, L. K. Fu, X. Chen, and K. Sun, J. Phys. D **42**, 055110 (2009).

[150] R. Qin, J. Zheng, J. Lu, L. Wang, L. Lai, G. Luo, J. Zhou, H. Li, Z. Gao, G. Li, and W. N. Mei, J. Phys. Chem. C **113**, 9541 (2009).

[151] J. Dong, A. A. Kinkhabwala, and P. F. McMillan, Phys. Scr. **10**, 2319 (2004).

[152] F. Brunet, A-M. Flank, Itie J-P., T. Irifune, and P. Lagarde, Acta Metall. **92**, 989 (2007).

[153] N. V. Timosheva, A. Chandrasekaran, Roberta. O. Day, and Robert. R. Holmes, Inorg. Chem. **37**, 3862 (1998).

[154] V. Vaithianathan, K. Asokan, J. Y. Park, and S. S. Kim, Appl. Phys. A **94**, 995 (2009).

[155] W. Y. Ching and P. Rulis, Phys. Rev. B **77**, 125116 (2008).

[156] J. P. Porres, A. M. Saitta, A. Polina, Itie J. P., and M. Hanfland, Nature Mater. **6**, 698 (2007).

[157] S. D. Perez, J. Haines, U. Amador, E. Moran, and A. Vegas, Surface Sci. **62**, 1019 (2006).

[158] S. Sapochak Padmaperuma, A. B. Linda and Burrows E. Paul, Chem. of Materials **18**, 2389 (2006).

[159] P. Erhart and K. Albe, Phys. Rev. B **73**, 115207 (2006).

[160] B. Claflin, D. C. Look, S. J. Park, and G. Cantwell, J. Cryst. Growth **287**, 16 (2006).

[161] G. Hu and H. Gong, Acta Metall. **56**, 5066 (2008).

BIBLIOGRAPHY